

Apoptotic signalling and structural alterations in
autophagy-deficient murine skeletal muscle

by

Marie-France Paré

A thesis

presented to the University of Waterloo

in fulfillment of the

thesis requirement for the degree of

Master of Science

in

Kinesiology

Waterloo, Ontario, Canada, 2014

© Marie-France Paré 2014

Author's Declaration

I hereby declare that I am the sole author of this thesis. This is a true copy of the thesis, including any required final revisions, as accepted by my examiners.

I understand that my thesis may be made electronically available to the public.

Marie-France Paré

Abstract

Autophagy is a catabolic process by which the cell targets and degrades cytoplasmic materials, such as proteins and organelles. Autophagy is required for the control of muscle mass under catabolic conditions, but is also active basally to maintain myofibre homeostasis. The purpose of this thesis was to characterize the role of autophagy in the maintenance of skeletal muscle morphology and cellular health. A conditional muscle-specific *Atg7* knockdown mouse model was used to examine the morphological, apoptotic, proteolytic, and proteasomal response to autophagy deficiency in the glycolytic and oxidative skeletal muscle of 5-week and 15-week-old mice. While overt phenotypic differences were absent between the autophagy-deficient animals and the controls, structural alterations were observed at the fibre level indicating moderate damage. *Atg7* knockdown resulted in significant age-dependent accumulation of the autophagic markers LC3I ($p < 0.001$) and p62 ($p < 0.01$) in both oxidative and glycolytic muscle. Evidence of the upregulation of apoptosis was observed in the autophagy-null animals, including Bax expression ($p < 0.05$) and nuclear translocation of AIF to the nucleus ($p < 0.01$). The proteolytic activities of caspase-8 ($p = 0.06$) and calpain ($p < 0.05$) were also increased with autophagy knockdown. Reactive oxygen species (ROS) generation was not affected by *Atg7* knockdown, nor were markers of mitophagic degradation. Several of the apoptotic and mitophagic measures revealed differences between the observed age groups, highlighting a role for degradative and cell death processes in skeletal muscle growth and development. Together, these findings point towards moderate but accumulative damage in autophagy-ablated skeletal muscle. The present work contributes to the existing literature demonstrating the importance of autophagy in the maintenance of skeletal muscle health.

Acknowledgements

I would like to thank my supervisor, Dr. Joe Quadrilatero, and the members of my committee, Dr. Russ Tupling and Dr. Paul Spagnuolo, for their time and guidance. Their insights and expertise helped hone my research and writing skills and were valuable to the development of this project.

Through the relationships I shared with my labmates, I've learned an abundance of lab techniques, protocols, and research skills that have set the foundation for my academic career. Elliott McMillan has been at times a teacher, dictator, critic, and co-conspirator. This roller coaster ride of mentorship has formed me as a scientist. I owe thanks to Darin Bloemberg and Andrew Mitchell for their encouragement and their time taken teaching me a number of techniques. I am also extremely grateful for my fellow Master's students, Kira Vorobej and Troy Campbell, with whom I shared many trials and tribulations. Finally, I was fortunate to work with a number of undergraduate students. I would specifically like to thank Evan Earl and Erin Turner for their assistance in collecting data for this project.

During my time at the University of Waterloo, many other staff and faculty members have provided invaluable guidance, advice, and encouragement. I would like to thank Marg Burnett and Jing Ouyang for their technical guidance and support; Dawn McCutcheon, Nancy Gibson, Jean Flanagan, and Angela Wagler for their expert management of the animal colonies involved in my research; Dr. Eric Bombardier for sharing his wealth of experience; and Dr. Robin Duncan for her inspiration, encouragement, and advice.

Lastly, but most importantly, I owe a debt of gratitude to my family for their

unwavering and continuing support throughout my rather lengthy academic career. My parents Marg and François and my brother Stéphane's love and understanding have been indispensable. My partner Ryan was my safety net and the keeper of my sanity during my Masters. His patience and support keep me going, and his passion for science continues to inspire me.

Dedication

I would like to dedicate this thesis to women who are passionate about science:

The giants on whose shoulders I stood on; the faculty members who guided, mentored, and inspired me; the colleagues who struggled with me; the students I had the opportunity to teach; and the women who will come to this department after me.

Our work isn't finished.

Table of Contents

Author's Declaration	ii
Abstract	iii
Acknowledgements	iv
Dedication	vi
List of Figures	ix
List of Appendix Figures	x
List of Tables	xi
List of Abbreviations	xii
Introduction	1
<i>Autophagy</i>	<i>1</i>
<i>Apoptosis</i>	<i>5</i>
<i>Cross-talk between autophagy and apoptosis</i>	<i>6</i>
<i>The ubiquitin-proteasome system</i>	<i>7</i>
<i>The role of mitochondria in skeletal muscle degradation</i>	<i>8</i>
<i>Degradative processes in skeletal muscle</i>	<i>9</i>
Rationale	13
Purpose and objectives	14
Hypothesis	16
Methods	18
<i>The Cre-loxP system</i>	<i>18</i>
<i>Animals</i>	<i>18</i>
<i>Genotyping</i>	<i>19</i>
<i>Isolation of skeletal muscle</i>	<i>20</i>
<i>Histological and immunofluorescent analyses</i>	<i>20</i>
<i>Preparation of whole muscle lysates and muscle subcellular fractions</i>	<i>21</i>
<i>Immunoblot analyses</i>	<i>22</i>
<i>Enzyme and protease activity</i>	<i>23</i>
<i>Measurement of reactive oxygen species generation</i>	<i>24</i>

<i>Statistical analysis</i>	24
Results	26
<i>Generation of muscle-specific Atg7 knockdown animals</i>	26
<i>Morphological measures and histological observations</i>	28
<i>Autophagic and mitophagic protein expression</i>	36
<i>UPS signalling and proteolytic activity</i>	42
<i>Apoptotic protein expression and enzyme activity</i>	44
<i>Reactive oxygen species generation</i>	49
Discussion	50
<i>The role of autophagy in the maintenance of skeletal muscle morphology</i>	51
<i>The relationship between apoptosis and autophagy</i>	53
<i>The mitochondrial response to skeletal muscle-specific autophagy knockdown</i>	56
<i>Muscle-specific ubiquitin ligases as an alternative degradative pathway</i>	58
<i>Developmental modulation of skeletal muscle degradative pathways</i>	59
<i>Study limitations</i>	61
<i>Conclusion</i>	63
<i>Future directions</i>	62
References	64
Appendix	88

List of Figures

Figure 1	Overview of autophagosome formation and fusion with the lysosome.	p. 8
Figure 2	The Atg5-Atg12 and LC3-PE ubiquitin-like cascades share components	p. 10
Figure 3	Mitophagy degrades dysfunctional mitochondria	p. 16
Figure 4	Generation of <i>mAtg7^{-/-}</i> animals	p. 33
Figure 5	Total cross-sectional area of <i>mAtg7^{-/-}</i> muscle	p. 35
Figure 6	Representative immunohistochemical images of <i>mAtg7^{-/-}</i> soleus muscle	p. 37
Figure 7	Immunohistochemical analyses of <i>mAtg7^{-/-}</i> soleus muscle	p. 38
Figure 8	Representative immunohistochemical images of <i>mAtg7^{-/-}</i> EDL muscle	p. 36
Figure 9	Immunohistochemical analyses of <i>mAtg7^{-/-}</i> EDL muscle	p. 41
Figure 10	Analysis of H&E-stained cross-sections of <i>mAtg7^{-/-}</i> muscle	p. 42
Figure 11	Expression of autophagic markers in <i>mAtg7^{-/-}</i> muscle	p. 44
Figure 12	Expression of lysosomal markers in <i>mAtg7^{-/-}</i> muscle	p. 46
Figure 13	Expression of mitophagic markers in <i>mAtg7^{-/-}</i> muscle	p. 47
Figure 14	Expression of markers of the ubiquitin-proteasome system in <i>mAtg7^{-/-}</i> muscle subcellular fractions	p. 49
Figure 15	Expression of apoptotic markers in <i>mAtg7^{-/-}</i> muscle	p. 51
Figure 16	Expression of apoptotic markers in <i>mAtg7^{-/-}</i> muscle subcellular fractions	p. 52
Figure 17	Proteolytic enzyme activity in <i>mAtg7^{-/-}</i> muscle	p. 54
Figure 18	ROS generation in <i>mAtg7^{-/-}</i> muscle	p. 55

List of Appendix Figures

Appendix Figure 1	Use of <i>Flox/Flox</i> littermates as controls	p. 93
Appendix Figure 2	Immunohistological analyses of <i>Flox/Flox</i> control animals	p. 94
Appendix Figure 3	Validation of red and white muscle isolation procedure	p. 95
Appendix Figure 4	Skeletal muscle specificity of <i>Atg7</i> knockdown	p. 96
Appendix Figure 5	Use of extensor digitorum longus and soleus as representative white and red muscles	p. 97
Appendix Figure 6	<i>Atg7</i> knockdown in extensor digitorum longus and soleus	p. 98
Appendix Figure 7	Validity of the subcellular fractionation procedure	p. 99

List of Tables

Table 1	<i>Atg7 loxP</i> genotyping thermocycler protocols	p. 25
Table 2	Anthropomorphic characteristics of control and <i>mAtg7^{-/-}</i> animals	p. 34

List of Abbreviations

AIF	Apoptosis-inducing factor
ANT	Adenine nucleotide translocator
Apaf-1	Apoptotic protease activating factor 1
Atg	Autophagy-related gene
ATP	Adenosine triphosphate
AU	Arbitrary units
Bcl-2	B-cell lymphoma 2
BH	Bcl-2 homology
BNIP	BCL2 and adenovirus E1B 19 kDa-interacting protein 3
CSA	Cross-sectional area
Drp1	Dynamin-related protein 1
EDL	Extensor digitorum longus
ER	Endoplasmic reticulum
FoxO	Forkhead box O
H&E	Hematoxylin and eosin
IMM	Inner mitochondrial membrane
LAMP	Lysosomal-associated membrane proteins
LC3	Microtubule-associated protein 1 light chain 3
MAFbx	Muscle atrophy F-box
MHC	Myosin heavy chain
MuRF1	Muscle-specific ring finger-1
OMM	Outer mitochondrial membrane
PARL	Presenilin-associated rhomboid-like protein
PE	Phosphatidylethanolamine
PINK1	PTEN-induced putative protein kinase 1
PTEN	Phosphatase and tensin homolog
RG	Red gastrocnemius
ROS	Reactive oxygen species
RQ	Red quadriceps
SDS-PAGE	Sodium dodecyl sulfate polyacrylamide gel electrophoresis
SR	Sarcoplasmic reticulum
UPS	Ubiquitin proteasome system
VDAC	Voltage-dependent anion channel
Vps34	Vesicular protein sorting 34
WG	White gastrocnemius
WQ	White quadriceps

Introduction

Muscle mass is maintained through a balance between protein breakdown and synthesis [1]. This homeostatic balance is altered in skeletal muscle in a number of conditions including starvation, physical activity, disuse, and disease [1, 2]. In mammalian skeletal muscle, the breakdown of proteins is mediated by two proteolytic systems: the autophagy-lysosome system and the ubiquitin-proteasome pathway [1-3]. These systems work in conjunction with apoptotic programmed cell death to modulate the process of skeletal muscle atrophy [4].

Autophagy

Autophagy is a catabolic process by which the cell targets and degrades cytoplasmic materials, such as proteins and organelles [5]. This process is highly conserved and is critical for nutrient balance, cell differentiation, and remodeling [6]. Cellular materials to be degraded are sequestered in the autophagosome, a double-membrane vesicle, subsequently fusing with a lysosome where the contents are broken down by lysosomal proteases [7]. This process is specifically referred to as macro-autophagy, herein referred to as autophagy. Micro-autophagy and chaperone-mediated autophagy also degrade proteins in conjunction with the lysosome, but play a lesser role in overall protein turnover [7, 8]. Autophagy was thought to be a bulk, non-specific degradation process; however, increasing evidence suggests that specific cytoplasmic contents can be targeted for degradation [5].

Through yeast genetics research, a number of autophagy-related (abbreviated to *Atg*) genes have been characterized [9]. These genes are well conserved, and mammalian orthologs for most have been identified [5, 9]. Autophagy begins with the formation of an isolation membrane (phagophore), a process that is thought to be initiated at the endoplasmic reticulum (ER) membrane [7] (Figure 1). The isolation membrane is elongated through the addition of

further membrane components, shuttled by Atg9 [5, 10]. In mammals, the initiation of autophagosome formation requires the activity of Vps34 (vesicular protein sorting 34), a phosphatidylinositol-3-kinase [5]. Vps34 is involved in a variety of membrane sorting processes, but when complexed to Beclin-1 (Atg6) plays a key role in the elongation of the early autophagic membrane [7, 11]. Beclin-1 regulates the formation and fusion of the autophagosome through interactions with a number of signalling molecules [11]. Of note is Bcl-2, the anti-apoptotic BH protein (define BH protein) that blocks the interaction between Beclin-1 and Vps34, thereby inhibiting the induction of autophagosome formation [7, 12, 13].

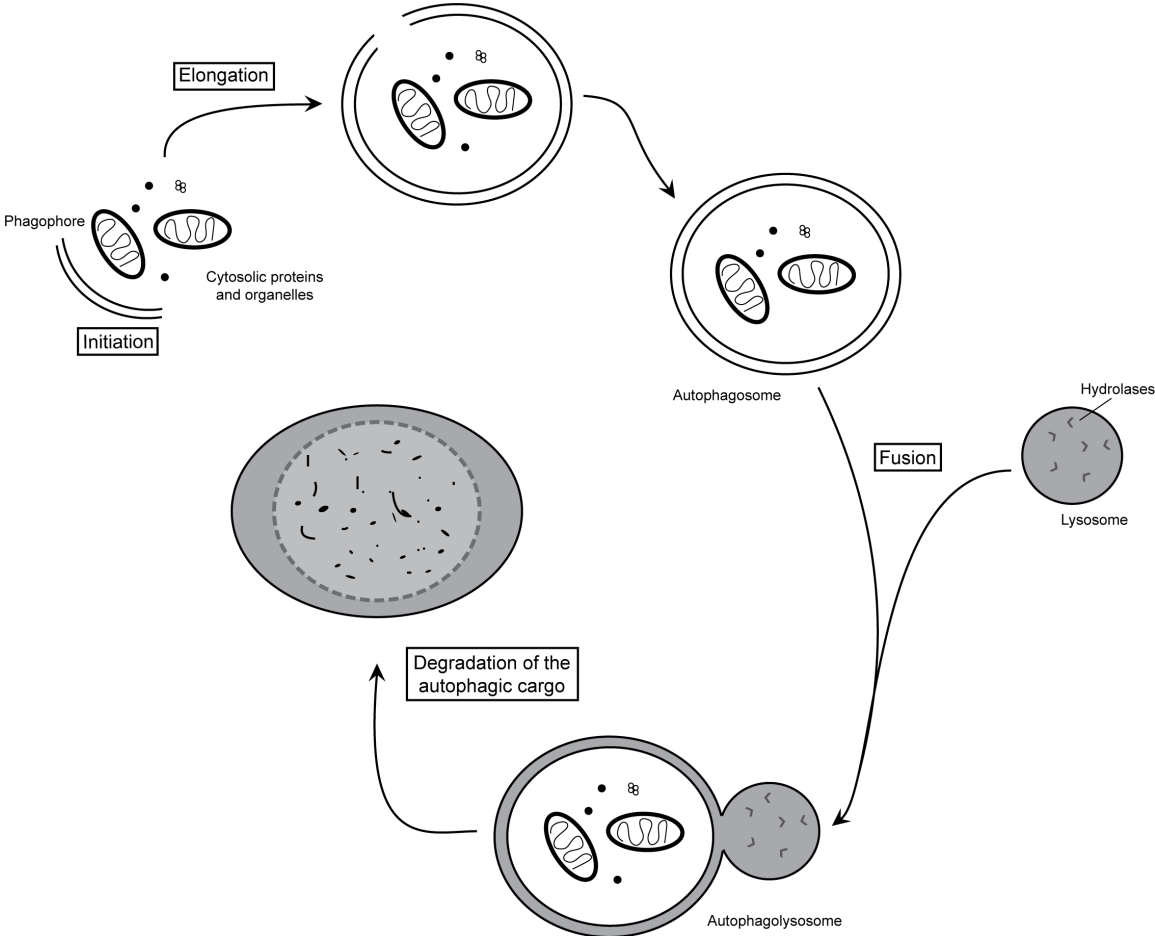
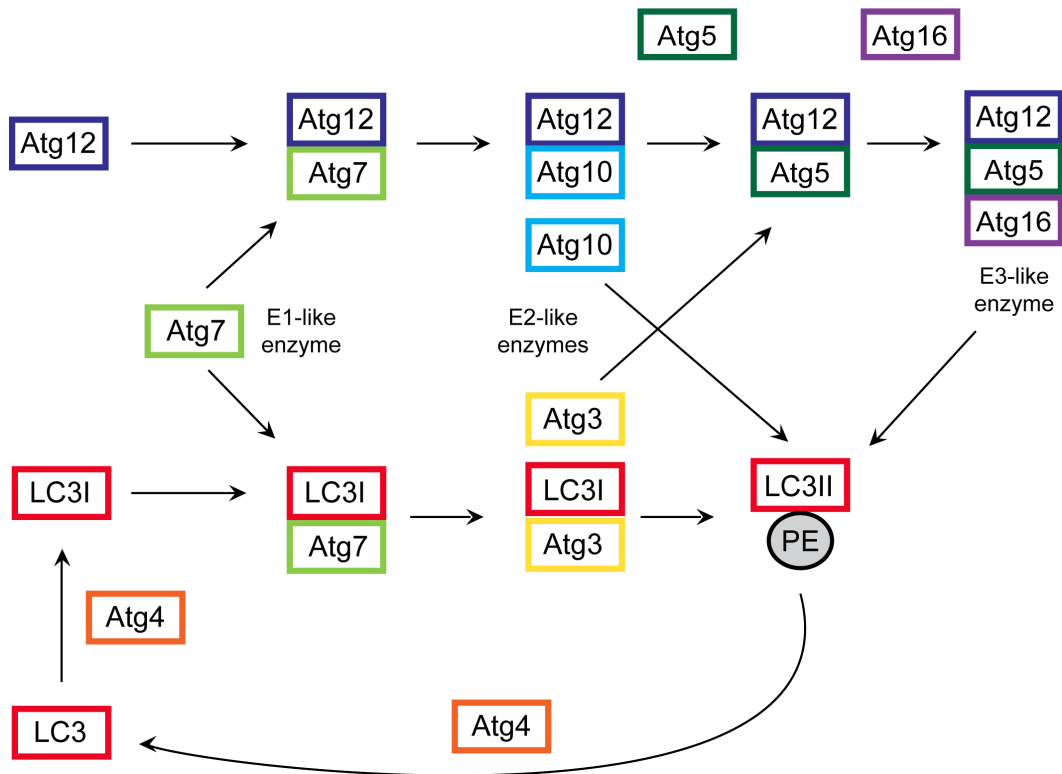


Figure 1. Overview of autophagosome formation and fusion with the lysosome. The autophagosome forms around the targeted cellular components and fuses with the lysosome. Lysosomal hydrolases are released, degrading the autophagic cargo. Adapted from Xie & Klionsky, 2007 [14].

Following initiation, signaling from two conjugation systems promotes elongation of the growing autophagosome [7, 15] (Figure 2). Atg12 is activated by the enzyme Atg7 then transferred to Atg10, after which it covalently binds to Atg5. This complex forms a conjugate with Atg16 to form a large tetramer [5, 8].

The second cascade associated with the growing autophagosome surrounds the protein microtubule-associated protein 1 light chain 3 (LC3). LC3I refers to the cytosolic, or unconjugated, form of LC3. LC3II is conjugated to the phosphatidylethanolamine (PE) residues of the growing autophagosome membrane through a reaction with Atg7 and Atg3 [5, 15]. This process requires association with the Atg5-Atg12/Atg16 tetramer [16]. While the Atg12-Atg5/Atg16 complex dissociates from the fully formed autophagosome, LC3II, the PE-conjugated form of LC3, remains as part of the autophagosome until its fusion with the lysosome [5]. At this point, LC3 molecules on the cytoplasmic side of the autophagolysosome can be delipidated by Atg4 and recycled [5, 15]. Because of the specific association of LC3 with the autophagosomal membrane, the ratio of LC3II to LC3I is considered an essential marker of autophagic flux [17].

Atg5-Atg12 Conjugation



LC3-PE Conjugation

Figure 2. The Atg5-Atg12 and LC3-PE ubiquitin-like cascades share components. Adapted from Ravikumar et al., 2010 [5].

Lysosomal-associated membrane proteins (LAMP) also play a role in the integration of the lysosomal and autophagosomal membranes [8]. Once the two vesicles are fused, lysosomal cathepsins and other lysosomal proteases degrade the autophagic cargo and inner membrane of the autophagosome [8, 9].

Proteins and organelles may be degraded through autophagy for a variety of reasons, but their delivery to the autophagosome always involves tagging with the small protein ubiquitin, a process termed ubiquitination [18]. Ubiquitinated proteins destined for the autophagosome are bound by the ubiquitin-associated domain of the protein p62, which itself

is recruited by LC3 through its LC3-interacting region [19, 20]. p62 is then degraded with the contents of the autophagosome upon lysosomal digestion; as such, accumulation of p62 is a characteristic marker of impaired autophagy [21].

Apoptosis

Apoptosis is a highly conserved process of programmed cell death that is required for normal tissue development and homeostasis [22, 23]. Apoptosis can be triggered by intracellular mechanisms mediated by a cascade of caspases, proteolytic enzymes that target aspartic acid residues. Once cleaved and activated from their inactive procaspase form, initiator caspases (caspase-8, -9, and -12) cleave executioner caspases (caspase-3, -6, or -7), thus amplifying the apoptotic signal [24, 25]. Executioner caspases cleave targets such as cytoskeletal proteins and DNA repair enzymes, resulting in structural and genomic breakdown, ultimately leading to cell death [26].

ER stress, such as that caused by an accumulation of misfolded proteins, can also trigger cell death by apoptosis. In these cases, the release of excess calcium from the ER activates calcium-dependent proteases known as calpains that in turn, activate procaspase 12 [22, 27]. In skeletal muscle, the pumps and channels involved in the movement of calcium in and out of the sarcoplasmic reticulum (SR) during contraction are also involved in apoptotic signaling [28].

Mitochondria play a key role in intracellular initiation of apoptosis [29]. A variety of cell stressors can result in the loss of mitochondrial membrane potential and the subsequent segregation of damaged mitochondria through fission [30]. In response to apoptotic stimuli, pro-apoptotic members of the Bcl-2 family Bax and Bak undergo a conformational change causing them to insert in the outer mitochondrial membrane, forming a pore [31, 32].

Cytochrome *c* is released from the mitochondria through this pore [33]. Anti-apoptotic members of the Bcl-2 family of proteins, Bcl-2 and Bcl-X_L, inhibit apoptosis by blocking the release of mitochondrial contents [22, 34, 35]. Cytochrome *c* initiates the formation of the apoptosome with the apoptotic protease activating factor 1 (Apaf-1) and caspase-9, resulting in the activation of the initiator caspase [23, 25].

Apoptosis can also be initiated independently of caspases. Apoptosis-inducing factor (AIF) is a mitochondrial flavoprotein located in the intermembrane space, where it plays a role in oxidative phosphorylation [36, 37]. Following apoptotic stimulus, the mitochondrial membrane is permeabilized and AIF is cleaved from its inner mitochondrial membrane (IMM) anchor, released into the cytosol through Bax/Bak pores, and translocated into the nucleus where it causes chromatin condensation and DNA cleavage [37, 38]. This mechanism is calcium-dependent; in fact, calpains are a major processor of AIF [37]. Furthermore, stressors such as oxidative damage render mitochondrial AIF more vulnerable to cleavage from the IMM [39, 40].

Cross-talk between autophagy and apoptosis

Extensive research has shown that autophagy and apoptosis are not mutually exclusive pathways, but share several upstream regulators and key effectors [41]. Many findings support the hypothesis that autophagy antagonizes apoptosis by removing damaged cell components and cycling nutrients, processes promoting cell survival [41, 42]. Cells undergoing nutrient starvation require autophagic clearance in order to avoid apoptosis [43], a process that may be modulated by Bcl-2 [44]. Conversely, there is evidence that autophagy and apoptosis work jointly to maintain homeostasis, specifically through the interaction of autophagic initiator Beclin-1 and the anti-apoptotic Bcl-2 family of proteins [11, 45]. In this model, the two

processes also have the potential to cooperate to induce cell death [41]. In a similar fashion, autophagic degradation can also lead to cell death, a phenomenon termed “autophagic cell death” [46]. This cell death process has been observed in cultured cells with impaired apoptotic pathways [47, 48], and may play a role in tumour cell responses to cytotoxic treatments [46]. Controversy on the physiological relevance of autophagic cell death continues as it has only been defined *in vivo* in cells lacking key apoptotic effectors [49-51].

The ubiquitin-proteasome system

The ubiquitin-proteasome system (UPS) is responsible for the ATP-dependent degradation of damaged, denatured, or unnecessary proteins and polypeptides, as well as the removal of subunits in the regulation of larger protein complexes [52]. This process is characterized by tagging with ubiquitin [53]. Similarly to the autophagosome-elongating conjugation systems characterized in autophagic degradation, three enzymes coordinate the addition of ubiquitin molecules to target proteins, beginning with E1 ubiquitin-activating enzymes [54]. Subsequently, ubiquitin is transferred to an E2 ubiquitin-conjugating enzyme and bound to a target protein by E3 ubiquitin ligases [53, 54]. This process of activation, conjugation, and ligation is repeated until a minimum of four ubiquitin molecules are covalently bound to the target protein [53]. The polyubiquitin chain tags proteins for degradation by the 26S proteasome, a large protease complex consists of a 19S regulatory particle responsible for the binding and unfolding of target proteins and the 20S proteolytic core [55-57].

The proteasome is a key effector of muscle degradation, and is spatially associated with myofibrils [52]. More precisely, muscle-specific E3 enzymes target sarcomeric structural proteins [58-60], as well as key protein synthesis and muscle differentiation factors [61]. The

most widely examined are muscle-specific ring finger-1 (MuRF1) and muscle atrophy F-box (MAFbx). Often termed ‘atrogenes’, these proteins were initially found to be upregulated in murine muscle undergoing atrophy due to starvation or disuse [58, 62], and were more recently shown to play a role in a variety of disease-related models of atrophy [53, 63].

The role of mitochondria in skeletal muscle degradation

Several proteins mediating the selective autophagy of mitochondria, or mitophagy, have been characterized in yeast, but a similar depth of understanding remains to be achieved in higher eukaryotes [64]. By removing dysfunctional mitochondria and altering the mitochondrial network, this process may protect the cell from mitochondrial-mediated damage and apoptosis [64, 65]. As in traditional autophagy, mitochondria targeted for degradation are tagged and directed to the autophagosome [66]. Damaged or dysfunctional mitochondria are isolated from the mitochondrial network through fission and tagged for degradation (Figure 3) [67, 68]. A recently elucidated mechanism involves PTEN-induced putative protein kinase 1 (PINK1) and Parkin, proteins first characterized in Parkinson’s disease [65, 69]. In healthy mitochondria, PINK1 is rapidly processed and cleaved at the OMM by the mitochondrial protease presenilin-associated rhomboid-like protein (PARL), after which it is degraded by the proteasome [70, 71]. Loss of mitochondrial membrane potential results in the accumulation of PINK1 on the OMM [72], which in turn induces the translocation of Parkin to the mitochondria from the cytosol [73, 74]. In its role as an ubiquitin ligase, Parkin ubiquitinates mitochondrial proteins, tagging the organelle for degradation by the core autophagic machinery [69, 75]. In an *in vivo* model, Parkin was shown to co-localize with LC3 [76]. The specific interactions between mitophagic markers and key autophagosome components are currently under investigation by multiple groups, but definitive relationships have yet to be

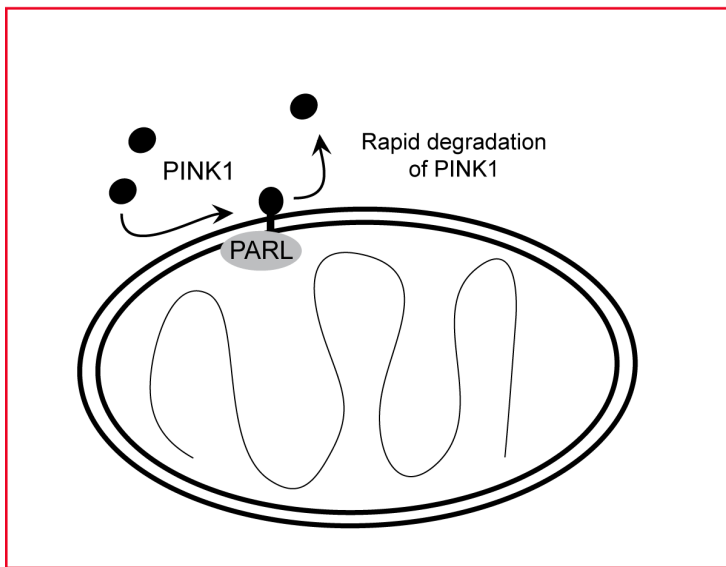
established. PINK1 and Parkin are known to interact directly with each other [77, 78], possibly through the phosphorylation of Parkin by PINK1 [79, 80]. Alternatively, voltage-dependent anion channels (VDAC) have been proposed as docking sites for Parkin in its recruitment to defective mitochondria [81]. p62 plays a role in linking ubiquitinated mitochondrial proteins to LC3 and the autophagosome, and may also facilitate the aggregation of defective mitochondria for mass clearance [82, 83]. The related Bcl-2 and adenovirus E1B 19 kDa-interacting protein 3 (BNIP) proteins BNIP3 and BNIP3L/Nix have also been implicated in the binding of autophagosome components to defective mitochondria [84]. In reticulocytes, BNIP3L/Nix has been shown to induce mitophagy by causing mitochondrial membrane depolarization [85, 86], while in yeast it directly interacted with LC3 [87].

Increased markers of mitophagy have been observed in atrophying skeletal muscle, as well as in myopathies [88]. During denervation atrophy, mitochondrial fission and clearance through mitophagy are upregulated [89]; mitochondrial fractions of denervated muscle showed increased levels of LC3II [90]. Parkin may play a key role in skeletal muscle, as it has recently been implicated in the activation of proteasomal degradation during denervation [91]. In fact, a murine model of congenital muscular dystrophy with mitochondrial structural abnormalities (CMDmt) has shown increased mitochondrial p62 tagging and accumulation of PINK1 and Parkin in mitochondrial fractions [92].

Degradative processes in skeletal muscle

Skeletal muscle is highly plastic and has an effective system to remove damaged cellular components in response to the stress of contraction [93]. Autophagy is required for the control of muscle mass under catabolic conditions, but is also active basally to maintain myofibre homeostasis [93, 94]. An excess of autophagic flux is detrimental to the muscle, as

Healthy mitochondrion



Damaged mitochondrion

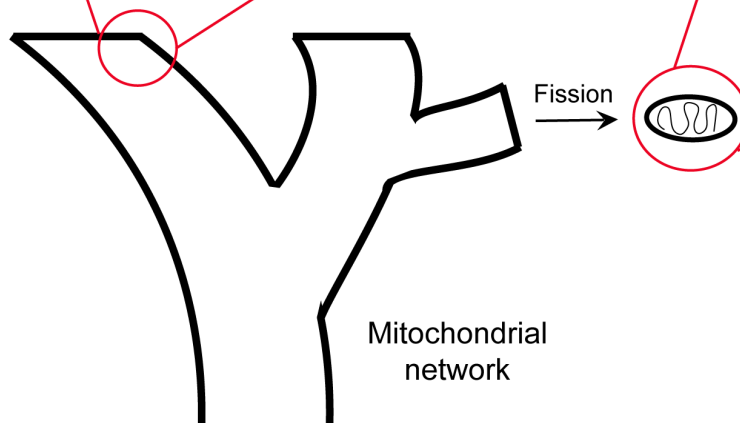
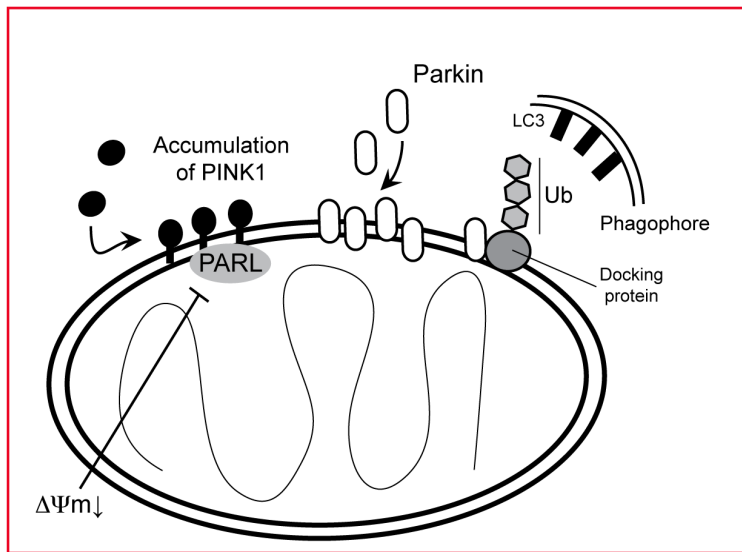


Figure 3. Mitophagy degrades dysfunctional mitochondria. In healthy mitochondria, the OMM protein PINK1 is rapidly degraded by PARL, preventing its accumulation. Damaged mitochondria are segregated from the mitochondrial network through fission and are tagged for degradation. When the mitochondrial membrane potential is lost ($\Delta\Psi_m\downarrow$), PARL is inhibited, resulting in the accumulation of PINK1 on the OMM. This recruits Parkin, which acts as a ubiquitin ligase, ubiquitinating a docking protein (e.g. VDAC, Nix) to tag the mitochondrion as an autophagic target. Adapted from Kawajiri et al., 2011, Narendra & Youle, 2011, and Twig et al., 2008 [75, 95, 96].

is seen in atrophy resulting from fasting, disease or disuse [97, 98]. Conversely, a lack of autophagy also leads to damage caused by the accumulation of dysfunctional organelles and proteins [99, 100]. In fact, several myopathies have been shown to be exacerbated by the inhibition of autophagy, due to the formation of protein aggregates [101, 102]. Autophagy also allows for skeletal protein turnover in response to exercise [103, 104].

Apoptosis is a key process in the regulation of skeletal muscle mass [105, 106]. Inhibition of apoptosis attenuates the progression of skeletal muscle deterioration and atrophy during damaging conditions [90, 107, 108]. For example, caspases have been found to play a necessary role in skeletal muscle atrophy resulting from immobilization [109, 110]. Caspases also contribute directly to protein degradation in wasting conditions by cleaving myofibrillar proteins [111]. Skeletal muscle is composed of terminally differentiated, multinucleated cells and, as such, cell death in this tissue is sometimes referred to as ‘myonuclear apoptosis’ [112]. In this process, a nucleus and its associated cytoplasmic domain are destroyed, rather than the entire cell [113]. With comparatively high levels of apoptosis inhibitors and other protective proteins, this process is tightly regulated in skeletal muscle [22]. Furthermore, skeletal muscle is a highly heterogeneous tissue and differences in apoptotic expression have been observed between muscles and fibre types [114].

In an effort to characterize the importance of autophagy in the maintenance of skeletal muscle health and structure, a number of groups have made use of skeletal muscle-specific autophagy-knockdown mice. Previous work using a constitutive skeletal muscle-specific *Atg7* knockdown mouse model has pointed to a need for autophagy in the maintenance of healthy muscle; however, many discrepancies remain to be addressed [115-118]. This model has shown degradative changes in the form of centralized myonuclei, muscle mass loss, decreased

force, and decreased muscle cross-sectional area [116-118]. In contrast to this, a study by Wu and colleagues found no phenotypic or degradative differences between skeletal muscle-specific *Atg7* knockdown mice and controls [115]. Apoptotic nuclei have been found to be increased in autophagy-deficient muscle, as have indicators of mitochondrial dysfunction. This suggests that these pathways may be mediating the phenotypic changes observed [115, 116]. Collectively, the data on this mouse model is ambiguous and further characterization is warranted.

Rationale

The role of autophagy in skeletal muscle has only recently begun to be elucidated and its role in the maintenance of muscle mass and physiology requires further investigation in order to characterize the biochemical and molecular pathways and interactions involved. While it is known that several forms of atrophy are associated with an upregulation of autophagy, the exact role of this process in the progression of muscle degradation remains unclear. The existing research is equivocal, suggesting that autophagy may drive the degradation of muscle [90, 119, 120], but it is also possible that the selective degradation of cellular components is a protective mechanism [99, 102, 121]. Varied responses to autophagy knockdown in muscle have been observed, an inconsistency that may be explained by the diverse muscle types used for analysis. Data on skeletal muscle-specific autophagy deficiency are further confounded by a disparity in the age of the animals examined. Furthermore, immunohistochemical analysis of fibre type-specific cross-sectional areas and fibre type distribution is required for a thorough understanding of the importance of autophagy in oxidative and glycolytic muscle. An increase in apoptotic nuclei has been found in *Atg7* knockdown mice [116], however a thorough characterization of apoptotic signalling in autophagy-deficient muscle is lacking. Skeletal muscle-specific autophagy-knockdown mice also display mitochondrial dysfunction, suggesting that mitochondrial signalling pathways involved in apoptosis may be modulated by the autophagic degradation of dysfunctional mitochondria (mitophagy).

Purpose and objectives

Several important questions persist in the characterization of autophagy deficiency in skeletal muscle. Therefore, the purpose of this thesis was to characterize the role of autophagy in the maintenance of skeletal muscle. Experiments were performed to examine basal differences in skeletal muscle morphology, as well as apoptotic, proteasomal, and mitochondrial signalling between skeletal muscle-specific autophagy-deficient (*mAtg7^{-/-}*) and control (*Flox/Flox*) mice at two ages, and in glycolytic and oxidative muscle. Specifically, this project was guided by the following objectives:

1. To describe any phenotypical and morphological differences between *mAtg7^{-/-}* and control animals
 - This was achieved by measuring body weight, muscle weights, muscle cross-sectional areas and analyzing microscopic images of muscle cross-sections for indications of damage
 - Morphological measures included immunohistochemical staining of muscle cross-sections to quantify fibre type distribution and fibre type-specific cross-sectional area
2. To measure the extent of autophagic impairment caused by the knockdown of *Atg7* in skeletal muscle
 - This included the measure of autophagosomal and lysosomal components, as well as markers of mitophagy
3. To determine whether the ubiquitin-proteasome system is upregulated in response to skeletal muscle-specific autophagy knockdown
 - This included measurement of muscle-specific ubiquitin ligases

4. To thoroughly characterize the apoptotic response in autophagy-deficient skeletal muscle
 - This will include measures of key apoptotic proteins, proteolytic enzymes, and ROS generation
5. To characterize any age-dependent differences in the extent of autophagy deficiency in skeletal muscle-specific autophagy knockdown animals
 - Previous work on this animal model has used animals at 8 weeks of age [115, 116]. In this study, animals were examined at 5 and 15 weeks of age to contribute 'before' and 'after' time points to the existing literature.
6. To characterize any differences in the effect of autophagy deficiency in glycolytic and oxidative *Atg7* knockdown muscle

Hypothesis

The hypotheses for this thesis were as follows:

1. Skeletal muscle of *mAtg7^{-/-}* animals will have altered autophagic protein expression
 - Expression of *Atg7* will be dramatically decreased in the muscles of *mAtg7^{-/-}* mice
 - *Atg7* knockdown will be associated with alterations to downstream markers of autophagic flux, namely the accumulation of p62 and LC3I
 - *mAtg7^{-/-}* muscle will show a downregulation of lysosomal markers, such as LAMP2
2. Skeletal muscle of *mAtg7^{-/-}* animals will have altered mitophagic protein expression
 - In *mAtg7^{-/-}* muscle, lack of mitochondrial clearance will result in lower cytosolic PINK1 levels
 - The mitochondrial-enriched fraction of *mAtg7^{-/-}* muscle will have increased levels the fission marker Drp1
3. Skeletal muscle of *mAtg7^{-/-}* animals will have upregulated apoptotic protein expression, protease activity, and reactive oxygen species (ROS) generation
4. *mAtg7^{-/-}* mice and their muscles will be morphologically different than the control littermates
 - Muscle weights, whole muscle cross-sectional areas, and individual fibre areas will be lower in *mAtg7^{-/-}* mice than in the control animals
 - *mAtg7^{-/-}* muscles will have a greater proportion of fast-twitch fibres than the control animals due a slow-to-fast fibre type shift [122]
 - *mAtg7^{-/-}* muscle fibres will have a greater proportion of centralized nuclei

5. The 15-week-old age groups will show morphological and apoptotic alterations compared to the 5-week-old animals
- The 15-week-old animals will have a higher body weight, individual muscle weight, muscle cross-sectional area, and fibre cross-sectional area compared to the 5-week-old animals
 - Muscle from 15-week-old animals will show upregulated apoptosis and proteolytic enzyme activity
 - The effects of *Atg7* knock-down will be exacerbated at 15 weeks compared to 5 weeks, resulting in increased accumulation of autophagosomal markers (LC3 and p62) in the 15-week-old *mAtg7^{-/-}* animals

Methods

The Cre-loxP system

The Cre protein (causes recombination) is a site-specific recombinase that acts on *loxP* (locus of crossover [x] in P1 bacteriophage) sites. When two *loxP* sequences in the same orientation flank a linear DNA sequence, the recombination event is resolved with the excision of the “floxed” sequence [123]. This characteristic is exploited in the Cre/*loxP* mouse model, in which the gene of interest is flanked by *loxP* sites and is removed following the expression of Cre recombinase under the control of a tissue-specific promoter, ultimately resulting in gene knockdown [123, 124]. Floxed copies of an allele are expressed normally in any tissue but are excised only in cells also expressing Cre.

Animals

C57Bl/6 mice heterozygous for the floxed *Atg7* (*Flox/Flox*) allele were obtained from Dr. Herbert Virgin (Washington University, St. Louis, Missouri). These were bred to carriers of a constitutive Cre recombinase allele (Cre) under the control of a skeletal muscle actin promoter (B6.Cg-Tg[*ACTA1*-cre]79Jme/J) (Jackson Laboratories). The resulting offspring were heterozygous for the floxed *Atg7* allele and carriers of the Cre allele (*Flox/Cre*). *Flox/Cre* females were bred to the original *Flox/Flox* males in order to obtain the double transgenic experimental animals homozygous for the floxed *Atg7* allele and carriers of Cre (*FloxFlox/Cre*). This breeding scheme generated *FloxFlox/Cre* animals, skeletal muscle-specific *Atg7*-null mouse (*mAtg7^{-/-}*). *Flox/Flox* littermates were used as controls (Appendix Figures 1 & 2). Mice were group-housed with access to water and standard lab rodent chow *ad libitum* (Harlan). *mAtg7^{-/-}* animals and *Flox/Flox* controls (n=8) were sacrificed by cervical dislocation at 5 and 15 weeks of age in order to characterize any age-dependent changes in

autophagy knockdown [115, 116]. All animal procedures were approved by the University of Waterloo Animal Care Committee.

Genotyping

To determine genotype, ear notches were collected from 4-week old mice. DNA was extracted and purified from the ear notches using the PureLink DNA Extraction Kit (Invitrogen) and DNA samples were stored at 4°C for no more than 48 hours. DNA samples were added to a mixture of 2X PCR Taq MasterMix (Applied Biological Materials), sterile water, and the appropriate forward and reverse primers for the *Atg7* Flox/WT, *Atg7* WT, and *ACTA1*-Cre alleles. The sequences of the *Atg7* Flox/WT forward and reverse primers are 5'TGGCTGCTACTTCTGCAATGATGT3' and 5'CAGGACAGAGACCATCAGCTCCAC3', respectively. The sequences of the *Atg7* WT forward and reverse primers are 5'TCTCCCAAGACAAGACAGGGTGAA3' and 5'AAGCCAAGGAAACCAAGGGAGTG3', respectively. Forward and reverse primers for the *ACTA1*-Cre allele are 5'GCGGTCTGGCAGTAAAACTATC3' and 5'GTGAAACAGCATTGCTGTCACTT3', respectively. Protocols for each primer pair were optimized (Table 1).

Table 1. *Atg7 loxP* genotyping thermocycler protocols

<i>Atg7</i> floxed allele (Flox/WT)	<i>Atg7</i> wild-type allele (WT)	ACTA1-Cre recombinase
94°C, 5 min 32 cycles: 94°C, 20 s 68°C, 30 s 72°C, 1.5 min 72°C, 10 min 4°C, ∞	94°C, 5 min 33 cycles: 94°C, 20 s 60°C, 15 s 72°C, 1 min 72°C, 10 min 4°C, ∞	94°C, 3 min 26 cycles: 94°C, 30 s 51.7°C, 1 min 72°C, 1 min 72°C, 2 min 10°C, ∞

Following amplification, samples were separated on a 1% agarose gel containing 0.01% ethidium bromide, then imaged using the ChemiGenius 2 Bio-Imaging System (Syngene).

Isolation of skeletal muscle

Extensor digitorum longus (EDL), soleus, gastrocnemius, and quadriceps were isolated and weighed. Cross-sections obtained from the EDL and soleus were frozen in optimal cutting temperature (OCT) embedding media for sectioning and histological and immunofluorescent analysis. The soleus and EDL were chosen as representative primarily red and primarily white muscles, respectively (Appendix Figure 5). The remainder of the muscles were snap-frozen in liquid nitrogen and stored at -80°C until analysis. The gastrocnemius and quadriceps were separated into red or white portions, containing oxidative and glycolytic muscle, respectively (Appendix Figure 3). These samples were also snap-frozen in liquid nitrogen and stored at -80°C . Total body weight, heart weight, as well as kidney weight were recorded.

Histological and immunofluorescent analyses

Samples were cut in $10\ \mu\text{m}$ cross-sections with a cryostat (Thermo Electronic) as previously described [114, 125]. Slides were stained with hematoxylin and eosin (H&E) to visualize markers of degradation and damage, specifically centrally located nuclei. Images were taken of the four quadrants of each H&E-stained section. The percentage of centrally-located nuclei was quantified as a percentage of the total number of fibres counted in these images.

Slides were stained for myosin heavy chain expression (MHC) as previously described [126] using antibodies against MHCI (BA-F8), MHCIIA (SC-71), and MHCIIB (BF-F3).

Slides were visualized using an Axio Observer Z1 microscope equipped with an AxioCam HRm camera and AxioVision software (Carl Zeiss). Individual images were taken across the entire cross-section and assembled into a composite image using AxioVision software (Carl Zeiss) and analyzed using ImageJ.

Fibre counts, fibre type percentages and individual fibre and full muscle cross-sectional area (CSA) were determined. For fiber type analysis, all fibres within the entire muscle/cross-section were characterized. Fibre CSA measurements included at least 30 fibres of each fibre type within a cross-section.

Preparation of whole muscle lysates and muscle subcellular fractions

Whole muscle lysates of white and red quadriceps were prepared as previously described [114]. Samples were homogenized with a glass mortar and pestle in ice-cold lysis buffer (20 mM HEPES, 10 mM NaCl, 1.5 mM MgCl₂, 1 mM DTT, 20% glycerol, and 0.1% Triton X100; pH 7.8), protease inhibitors (Complete Cocktail; Roche Diagnostics), and phosphatase inhibitors (Halt Phosphatase Inhibitor Cocktail; Thermo Scientific). Subsequently, samples were centrifuged at 1000 g for 10 minutes at 4°C, and the supernatant was collected. A BCA protein assay was used to determine the protein content of each sample.

Subcellular fractions were prepared as previously described [114, 127]. Briefly, muscle was gently homogenized on ice in a subcellular fractionation buffer (250 mM sucrose, 20 mM HEPES, 10 mM KCl, 1 mM EDTA, 1 mM EGTA, 1 mM DTT; pH 7.4) with protease (Complete Cocktail; Roche Diagnostics) and phosphatase inhibitors (Halt Phosphatase Inhibitor Cocktail; Thermo Scientific). The resulting homogenates were centrifuged at 800 g at 4°C for 10 min, yielding a pellet (P1) and supernatant (S1). The S1 fraction was then centrifuged at 800 g at 4°C for 10 min again, and the supernatant was transferred to a new tube

(S2). The S2 fraction was centrifuged at 20,800 g at 4°C for 20 min, yielding a pellet containing mitochondria (M1) and the cytosolic supernatant (C1). The M1 pellet was washed with subcellular fractionation buffer and centrifuged at 16,000 g at 4°C for 20 min. This pellet is the mitochondrial-enriched fraction. The cytosolic (C1) supernatant was centrifuged at 20,800 g at 4°C for 20 min to ensure that it contained no residual mitochondria. The resulting supernatant is the cytosolic-enriched fraction. The P1 pellet was washed and centrifuged three additional times at 800 g at 4°C for 10 min. Lysis buffer (200 µl) and 5 M NaCl (27.7 µl) was added to the resulting pellet and rotated for 1 h at 4°C, following which the samples were centrifuged at 20,800 g at 4°C for 15 min. The supernatant is the nuclear-enriched fraction. The protein concentration of each subcellular fraction was determined with a BCA protein assay. The purity of the subcellular fractions obtained was determined by immunoblotting (Appendix Figure 7).

Immunoblot analyses

SDS-PAGE gel electrophoresis and western blotting were performed as previously described [114]. Briefly, protein samples of equal amounts were loaded and separated on 10%, 12%, or 15% SDS-PAGE gels, transferred onto PVDF membranes (Bio-Rad), and blocked in 5% milk in TBS-T for 1 hour at room temperature. Membranes were incubated either overnight at 4°C or for 1 hour at room temperature in primary antibodies against: Atg7, LC3I/II, PINK1, Drp1 (Cell Signaling), AIF, ANT, Bcl-2, Beclin-1, cytochrome *c*, MAFbx, MuRF1, histone H2B (Santa Cruz Biotechnology), Bax (Sigma-Aldrich), CuZnSOD, Smac (Enzo Life Sciences), LAMP2 (Developmental Studies Hybridoma Bank), and p62 (ProGen Biotechnik).

Membranes were washed with TBS-T and incubated for 1 hour at room temperature in the appropriate horseradish peroxidase (HRP)-conjugated secondary antibody (Santa Cruz Biotechnology). Proteins were visualized using the Clarity Western ECL substrate (Bio-Rad) and the ChemiGenius 2 Bio-Imaging System (Syngene). Membranes were subsequently stained with Ponceau S (Sigma-Aldrich) to ensure quality of sample loading and protein transfer.

Enzyme and protease activity

Enzyme and protease activity were measured as previously described [114]. To determine calpain activity, white and red gastrocnemius muscle homogenates were prepared without protease inhibitors and were incubated in duplicate in the dark at 37°C with the substrate Suc-LLVY-AMC (Enzo Life Sciences), with or without the specific calpain inhibitor Z-LL-CHO (Enzo Life Sciences) [114]. Using excitation and emission wavelengths of 360 nm and 440 nm, respectively, fluorescence was measured using the SPECTRAmax Gemini XS microplate spectrofluorometer (Molecular Devices).

To assess cathepsin activity, muscle homogenates were prepared without protease inhibitors and incubated in duplicate in the dark at 30°C in reaction buffer (50 mM sodium acetate, 8 mM DTT, 4 mM EDTA, 1 mM Pefabloc; pH 5.0) with 50 µM of the fluorogenic substrate z-FR-AFC (Enzo Life Sciences). Using excitation and emission wavelengths of 400 nm and 489 nm, respectively, fluorescence was measured at 30°C using a SPECTRAmax Gemini XS microplate spectrofluorometer (Molecular Devices).

Caspase-3, 8, and 9 activity were determined in duplicate in muscle homogenates using Ac-DEVD-AMC, Ac-IETD-AMC, and Ac-LEHD-AMC caspase substrates, respectively (Enzo Life Sciences). Muscle homogenates were prepared without protease inhibitors and

incubated in the dark in the appropriate substrate at room temperature. Using a SPECTRAmax Gemini XS microplate spectrofluorometer (Molecular Devices), measures of fluorescence were made at 15-minute intervals for 2 hours with excitation and emission wavelengths of 360 nm and 440 nm, respectively.

All enzymatic activity fluorescence measurements were standardized to total protein content and expressed as AU per milligram of protein.

Measurement of reactive oxygen species generation

The generation of reactive oxygen species (ROS) was quantified as previously described [128]. Briefly, white and red gastrocnemius muscle ROS generation was determined using dichlorofluorescein-diacetate (DCFH-DA), a compound hydrolyzed by cellular esterases to form nonfluorescent DCFH, which can then be oxidized by a variety of ROS to the highly fluorescent DCF. Muscle was homogenized using a glass mortar and pestle in ice-cold subcellular fractionation buffer (250 mM sucrose, 20 mM HEPES, 10 mM KCl, 1 mM EDTA, 1 mM EGTA, 1 mM DTT; pH 7.4) along with protease inhibitors (Complete Cocktail, Roche Diagnostics). Muscle homogenates were incubated in duplicate. DCF fluorescence was detected with a SPECTRAmax Gemini XS microplate spectrofluorometer (Molecular Devices) with excitation and emission wavelengths of 490 nm and 525 nm, respectively. Fluorescence intensity was standardized to total protein content and expressed as AU per milligram of protein.

Statistical analysis

All results are given as means \pm SEM. Western blot and enzymatic activity assay data are standardized to the 5-week-old control group. Data were analyzed using two-way analyses

of variance (ANOVA), with $p < 0.05$ considered statistically significant and $p = 0.05$ to 0.09 considered a statistical trend. ANOVA interaction effects were assessed using the Tukey HSD post-hoc test. All statistical analyses were performed using Prism 5 statistical software.

Results

Generation of muscle-specific Atg7 knockdown animals

Transgenic mice were generated with copies of *Atg7* flanked by *loxP* sites, as well as copies of Cre recombinase (*FloxFlox/Cre*), resulting in skeletal-muscle specific knockdown of *Atg7* (*mAtg7^{-/-}*). These animals were identified through PCR analysis (Figure 4A). In *mAtg7^{-/-}* white quadriceps (WQ), protein expression of *Atg7* was reduced compared to *Flox/Flox* controls (CTRL) by 79% at 5 weeks of age, and 85% at 15 weeks ($p < 0.001$, Figure 4B). In the red quadriceps (RQ), *Atg7* expression was reduced by 71% at 5 weeks and 83% in the 15-week-old group ($p < 0.001$, Figure 4C). Cardiac muscle showed no significant decrease in *Atg7* expression ($p = 0.454$, Appendix Figure 4).

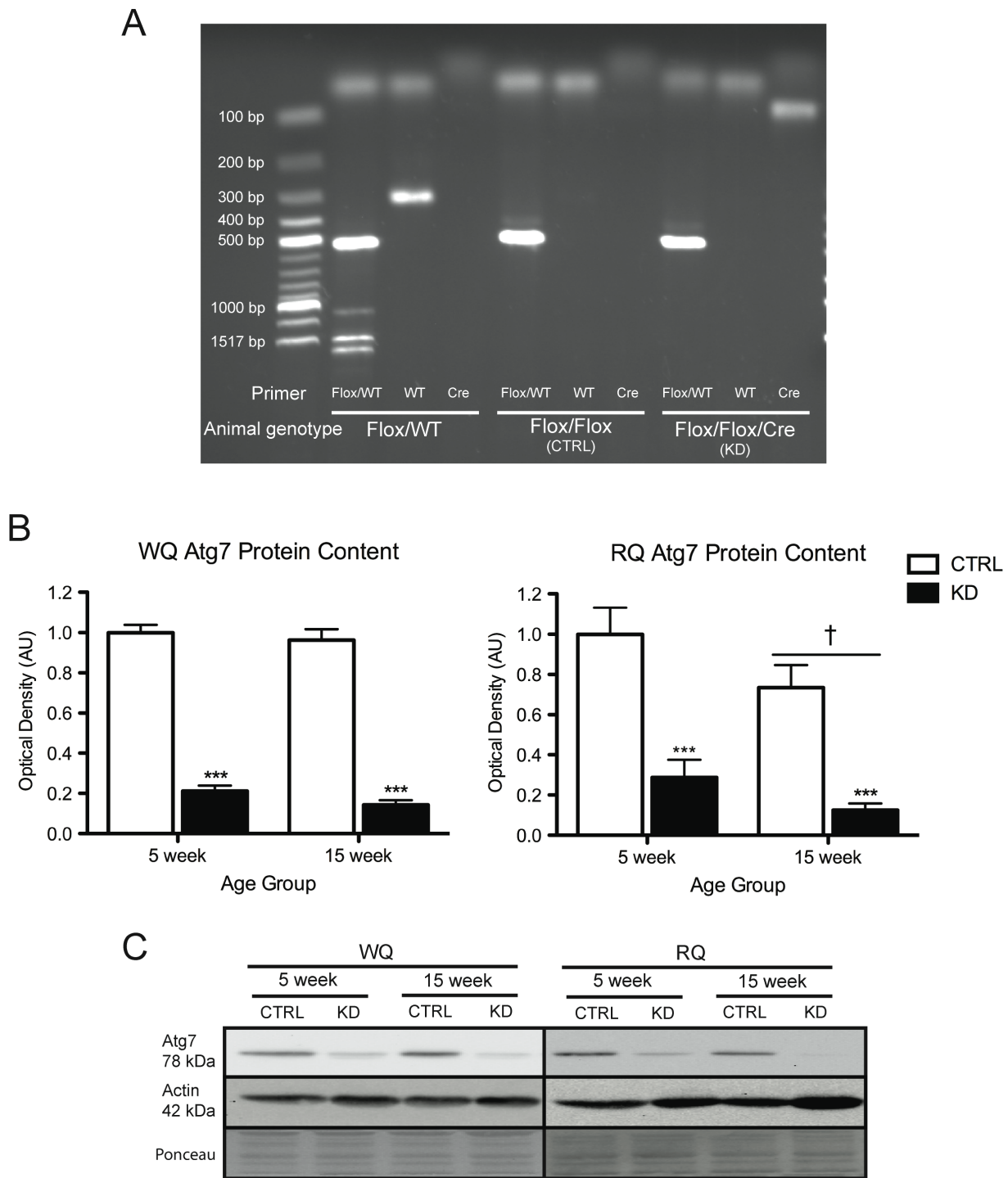


Figure 4. Generation of $mAtg7^{-/-}$ animals. A: PCR analysis of *Atg7* Flox (500bp), *Atg7* WT (300 bp), and *ACTA1*-Cre (100 bp) gene expression. B: Quantification of *Atg7* protein expression in the white quadriceps (WQ) and red quadriceps (RQ) of $mAtg7^{-/-}$ animals (KD) and *Flox/Flox* controls (CTRL). C: Representative immunoblots of *Atg7* protein expression in WQ and RQ of KD and CTRL animals. Actin immunoblots and ponceau-stained membranes are shown as an example of loading and transfer consistency (n = 8, *** main effect $p < 0.001$ vs. CTRL, † main effect $p < 0.05$ vs. 5-week group).

Morphological measures and histological observations

In both *mAtg7^{-/-}* and control animals, there was a main effect of age in body weight (Table 2, $p < 0.001$). While autophagy deficiency did not alter body weight ($p = 0.76$), control animals increased in body weight by 49% between 5 and 15 weeks, while *mAtg7^{-/-}* animals grew only by 33%. Similarly, the soleus weight of control animals increased by 53%, while autophagy-deficient soleus weight was only increased by 22%. The same trend was seen in EDL, with 46% and 33% growth in the control and knockdown animals, respectively. This effect was not seen to the same extent in quadriceps, with 71% and 72% growth in the control and knockdown animals, respectively. There was also an effect of age in wet muscle weights for soleus (SOL), EDL, and quadriceps ($p < 0.001$). Normalizing SOL and EDL wet muscle weights to heart or kidney weight negated the age-based differences; however, the effect persisted in the quadriceps ($p < 0.001$).

Table 2. Anthropomorphic characteristics of control and *mAtg7^{-/-}* animals. Data are expressed as means \pm SEM (n=8, ††† main effect p<0.001 vs. 5-week group).

		5 weeks		15 weeks	
		CTRL	KD	CTRL	KD
Body weight (g)		18.84 \pm 0.774	19.90 \pm 0.730	28.04 \pm 0.550	26.54 \pm 0.694 †††
Muscle weight (mg)	SOL	5.88 \pm 0.385	7.36 \pm 0.510	8.98 \pm 0.218	9.00 \pm 0.402 †††
	EDL	6.12 \pm 0.360	6.46 \pm 0.428	8.92 \pm 0.331	8.60 \pm 0.477 †††
	QUAD	105.73 \pm 5.615	108.34 \pm 7.254	181.08 \pm 5.695	186.65 \pm 6.446 †††
Muscle weight/heart weight (mg)	SOL	0.066 \pm 0.004	0.080 \pm 0.004	0.077 \pm 0.003	0.072 \pm 0.004
	EDL	0.069 \pm 0.003	0.073 \pm 0.004	0.077 \pm 0.003	0.069 \pm 0.005
	QUAD	1.180 \pm 0.030	1.169 \pm 0.048	1.553 \pm 0.039	1.486 \pm 0.040 †††
Muscle weight/kidney weight (mg)	SOL	0.054 \pm 0.004	0.062 \pm 0.003	0.060 \pm 0.003	0.060 \pm 0.003
	EDL	0.056 \pm 0.004	0.057 \pm 0.002	0.060 \pm 0.004	0.057 \pm 0.003
	QUAD	0.945 \pm 0.026	0.910 \pm 0.034	1.201 \pm 0.047	1.246 \pm 0.067 †††

Histological examination of soleus and EDL cross-sections revealed no significant differences in total cross-sectional area (CSA) in either soleus or EDL (Figure 5). In the soleus, fibre type-specific cross-sectional area measurements showed a significant effect of age in type I (p<0.05), type IIA and hybrid type IIX/IIB (p<0.001), as well as hybrid type IIA/IIX and type IIX (p<0.01). There was a trend to significance in fibre type I/IIA CSA (p=0.05). Type IIX CSA was also larger in *mAtg7^{-/-}* animals compared to controls (p<0.05) (Figure 6 and 7A). In the EDL, type IIA (p<0.05), IIA/IIX, IIX, IIX/IIB, and IIB (p<0.001) fibres were larger in 15-week-old animals compared to the 5-week age group. Type I/IIA fibres also tended to have a larger CSA in the older group (p=0.07). Type IIA fibre CSA tended to be higher in *mAtg7^{-/-}*

animals compared to controls ($p=0.07$) and type IIX fibre CSA was significantly higher in the knockdown animals ($p<0.05$) (Figure 8 and 9A).

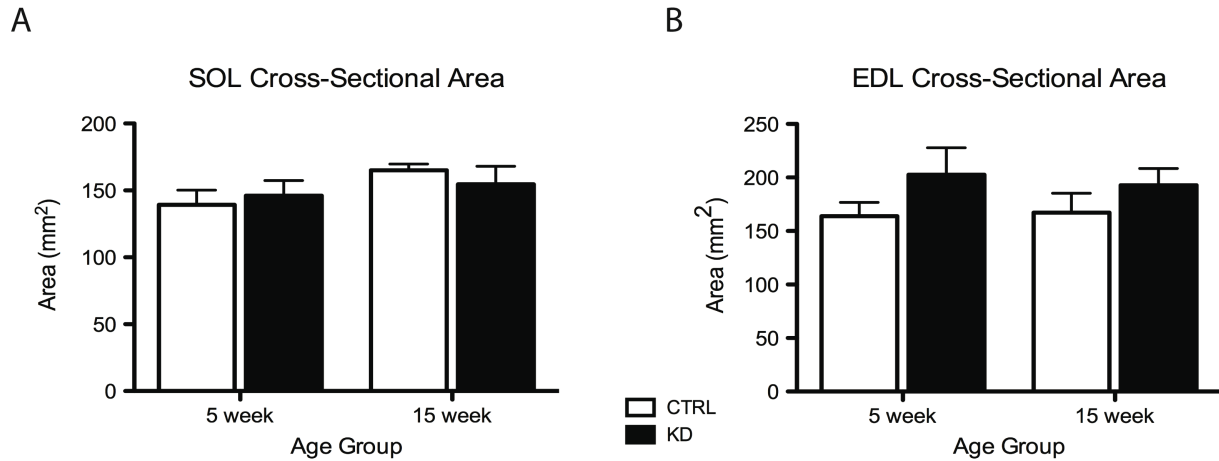
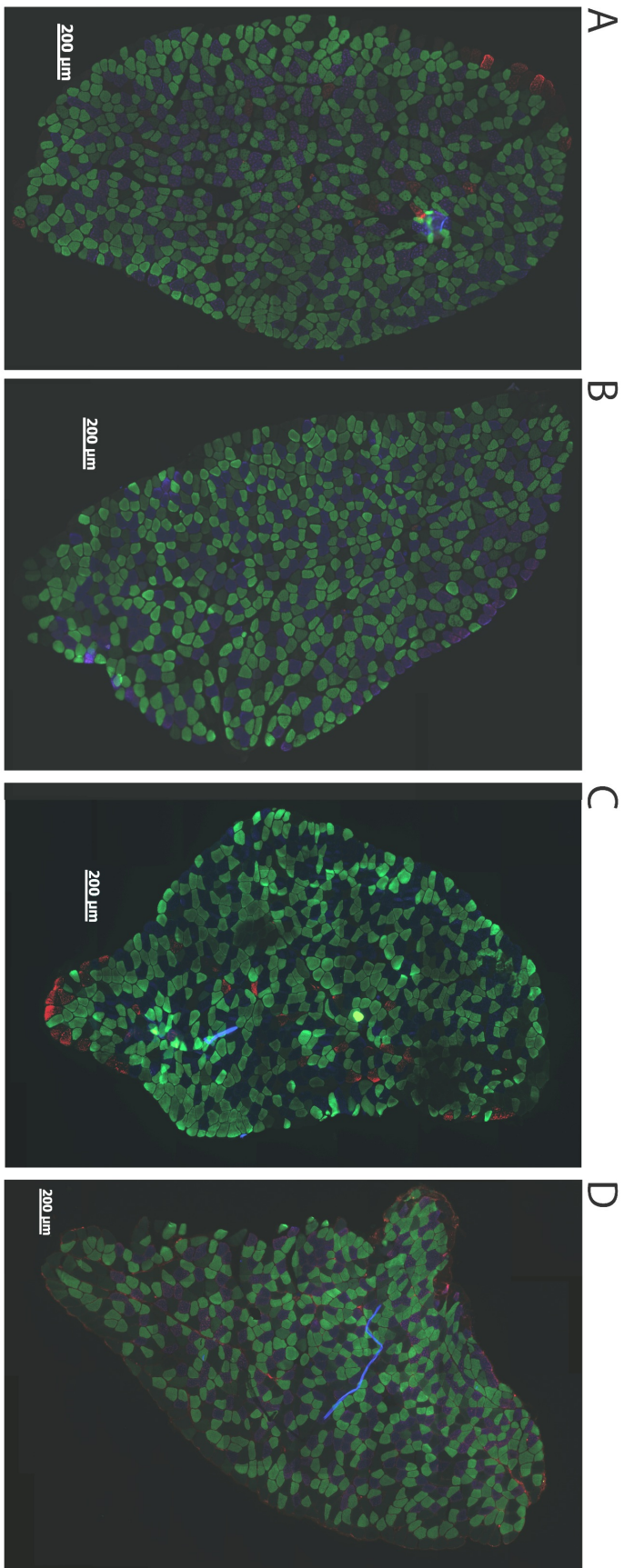


Figure 5. Total cross-sectional area of *mAtg7^{-/-}* muscle. A: Total muscle cross-sectional area in soleus (SOL) of *mAtg7^{-/-}* animals (KD) and *Flox/Flox* controls (CTRL). B: Total muscle cross-sectional area in extensor digitorum longus (EDL) in KD and CTRL animals. (n=6-8).

Total fibre number and fibre type distribution were also quantified. In the soleus, 15-week-old had a higher percentage of type I fibres and a lower percentage of type IIA/IIX fibres compared to their 5-week-old counterparts ($p<0.05$). Knockdown animals had a lower proportion of I and I/IIA fibres and a higher proportion of type IIX fibres compared to controls ($p<0.05$) (Figure 7B). 15-week-old animals had a higher percentage of EDL type IIA fibres ($p<0.05$) and tended to have a lower percentage of hybrid type I/IIA fibres ($p=0.08$) (Figure 9B).

(Next page) Figure 6. Representative immunohistochemical images of *mAtg7^{-/-}* soleus muscle. A-D: Representative images of soleus whole muscle cross-sections from *Flox/Flox* controls (CTRL) and *mAtg7^{-/-}* (KD) animals stained with antibodies specific for the individual myosin heavy chain isoforms: type I (blue), type IIA (green), type IIB (red), type IIX (unstained). Left to right: 5 week CTRL, 5 week KD, 15 week CTRL, 15 week KD. Scale bars indicate 200 μ m. E: Magnified images of EDL muscle cross-sections from CTRL and KD animals. Scale bar indicates 50 μ m.



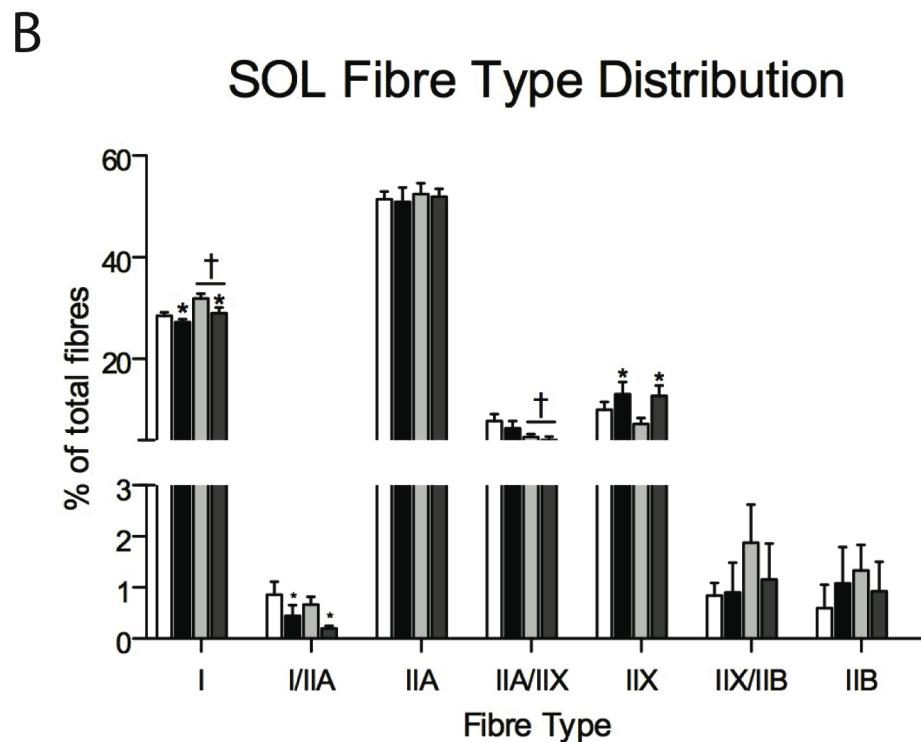
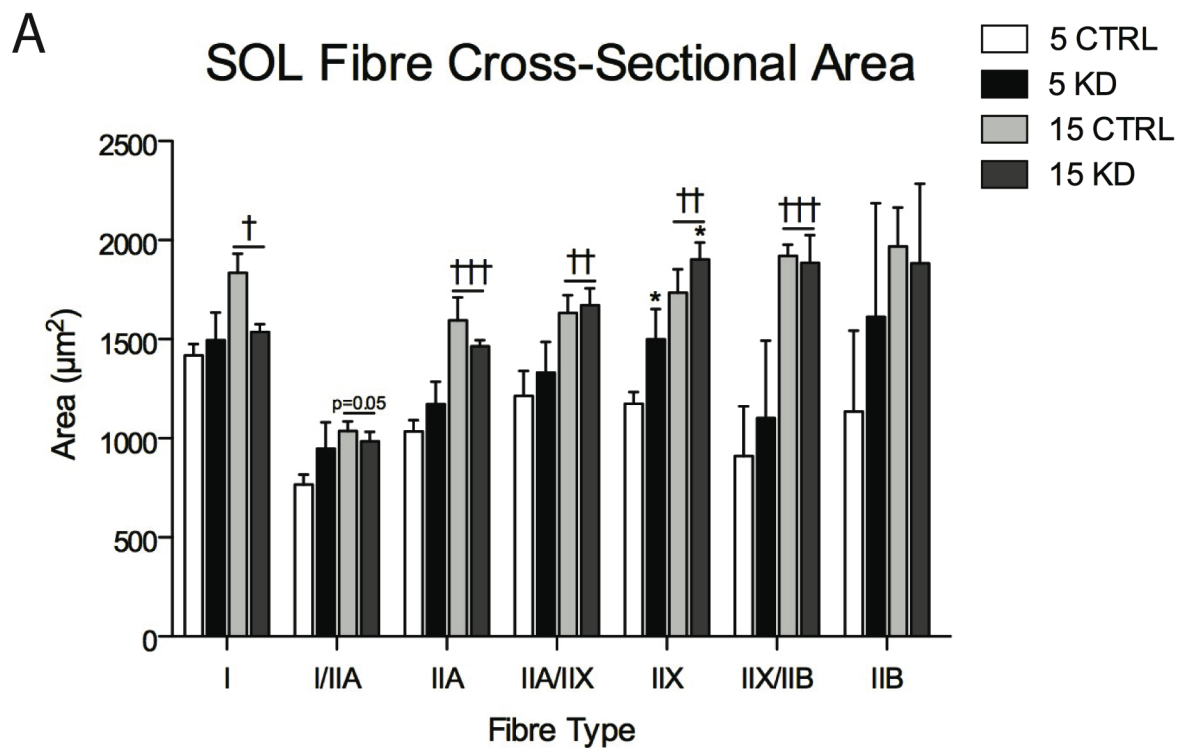
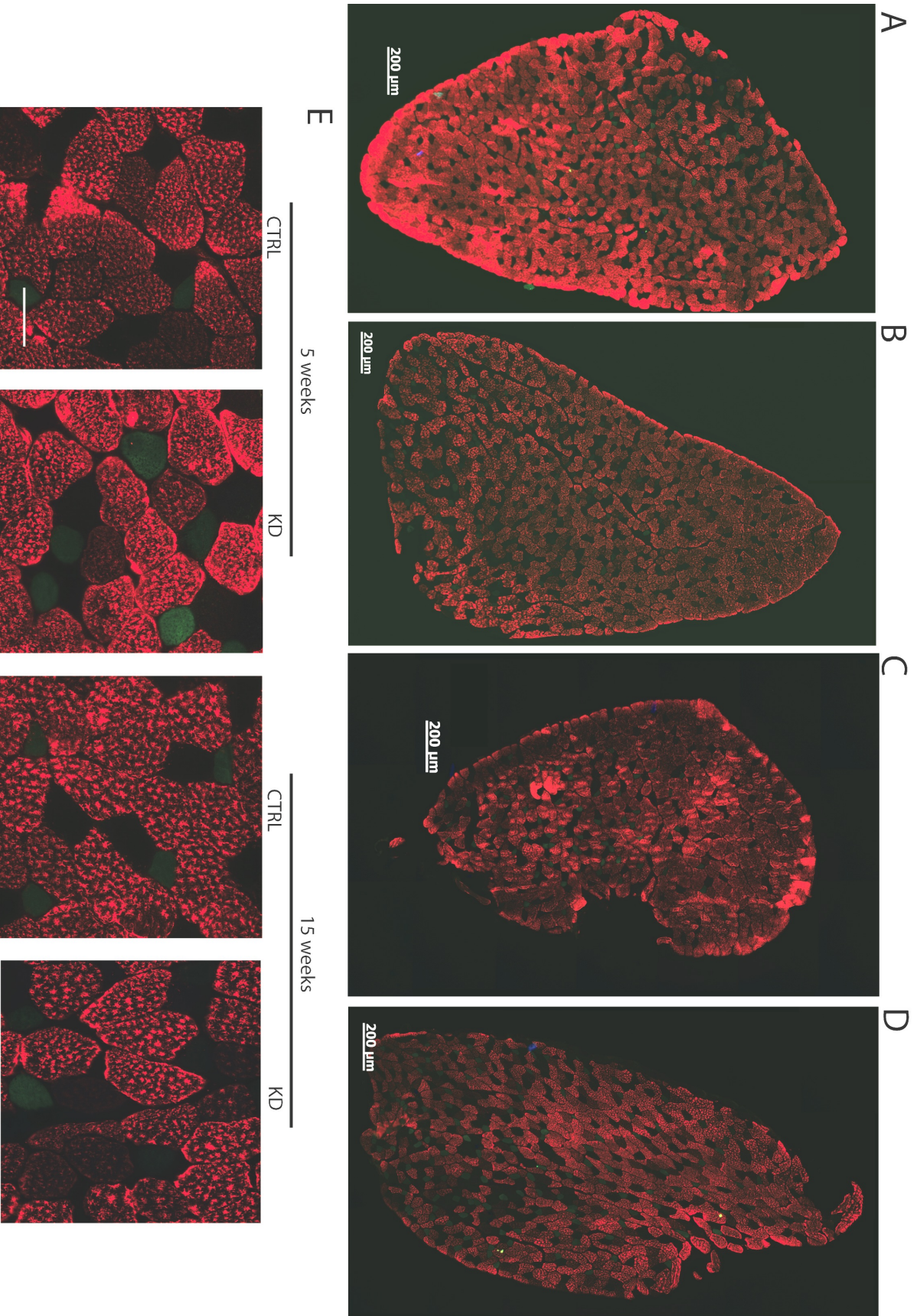


Figure 7. Immunohistochemical analyses of *mAtg7^{-/-}* soleus muscle. A: Fibre type-specific cross-sectional area in soleus (SOL) muscle of *mAtg7^{-/-}* animals (KD) and *Flox/Flox* controls (CTRL). B: Fibre type distribution (percentage of total fibres) in the SOL of KD and CTRL animals (n=6-8, * main effect $p < 0.05$ vs. CTRL, † main effect $p < 0.05$ vs. 5 week group, †† main effect $p < 0.01$ vs. 5-week group, ††† main effect $p < 0.001$ vs. 5-week group).

H&E staining of soleus and EDL cross-sections allowed for the quantification of centralized myonuclei, a hallmark of fibres recovering from muscle damage [129] (Figure 10A). *mAtg7^{-/-}* soleus showed 0.4% and 0.5% more centralized nuclei compared to control muscle at 5 and 15 weeks respectively; however, these findings were not statistically significant (Figure 10B). In the EDL at 5 weeks of age, *mAtg7^{-/-}* had 0.6% more centralized nuclei compared to controls. With an increase of 2.0% compared to controls, 15-week-old EDL muscle had higher percentage of centrally located nuclei than all other groups ($p < 0.001$, Figure 10C).

(Next page) Figure 8. Representative immunohistochemical images of *mAtg7^{-/-}* EDL muscle. A-D: Representative images of extensor digitorum longus (EDL) whole muscle cross-sections from *Flox/Flox* controls (CTRL) and *mAtg7^{-/-}* (KD) animals stained with antibodies specific for the individual myosin heavy chain isoforms: type I (blue), type IIA (green), type IIB (red), type IIX (unstained). Left to right: 5 week CTRL, 5 week KD, 15 week CTRL, 15 week KD. Scale bars indicate 200 μm . E: Magnified images of EDL muscle cross-sections from CTRL and KD animals. Scale bar indicates 50 μm .



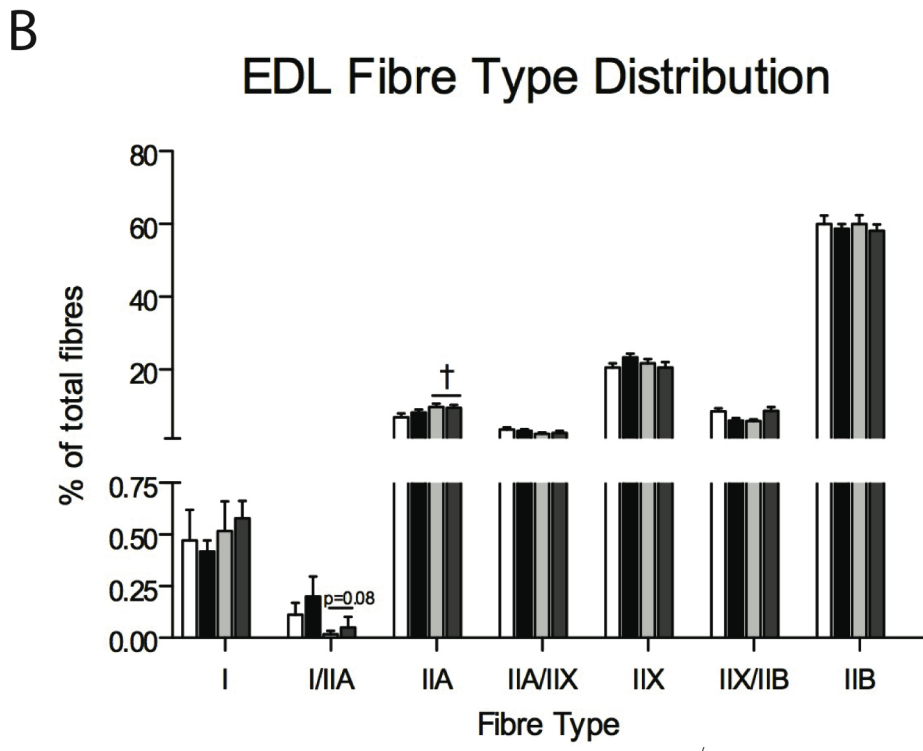
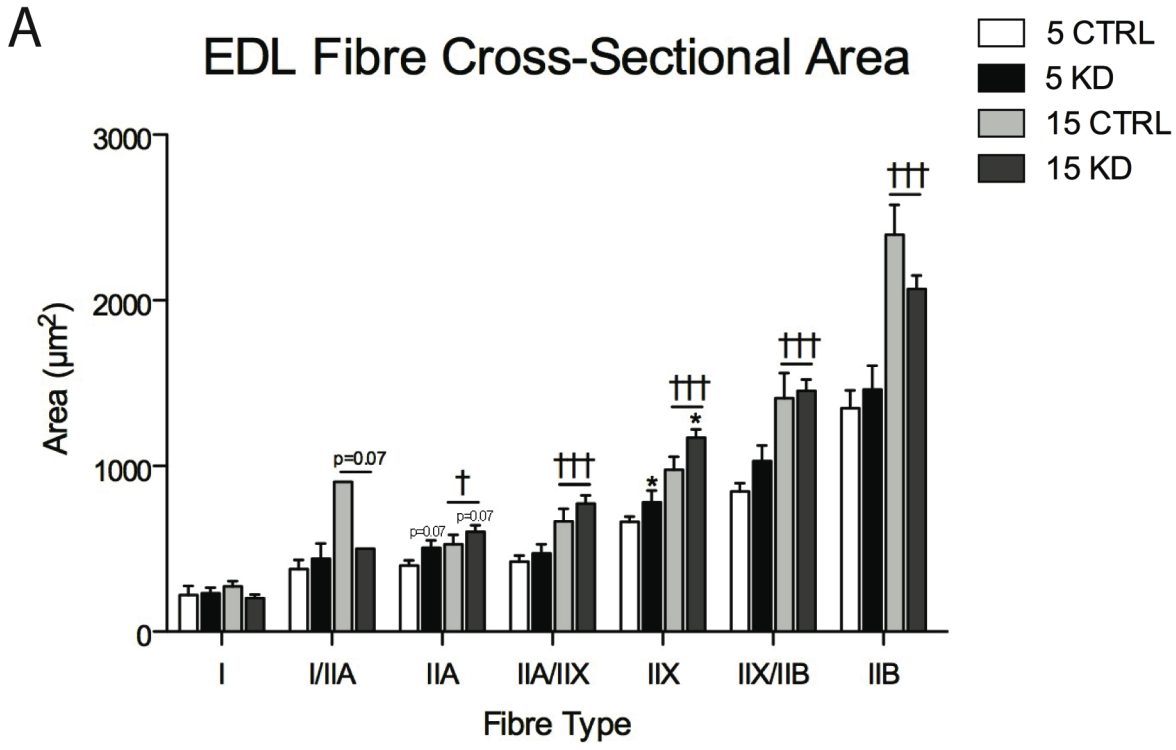


Figure 9. Immunohistochemical analyses of *mAtg7^{-/-}* EDL muscle. A: Fibre type-specific cross-sectional area in extensor digitorum longus muscle (EDL) of *mAtg7^{-/-}* animals (KD) and *Flox/Flox* controls (CTRL). B: Fibre type distribution (percentage of total fibres) in the EDL of KD and CTRL animals (n=6-8, * main effect p<0.05 vs. CTRL, † main effect p<0.05 vs. 5-week group, ††† main effect p<0.001 vs. 5-week group).

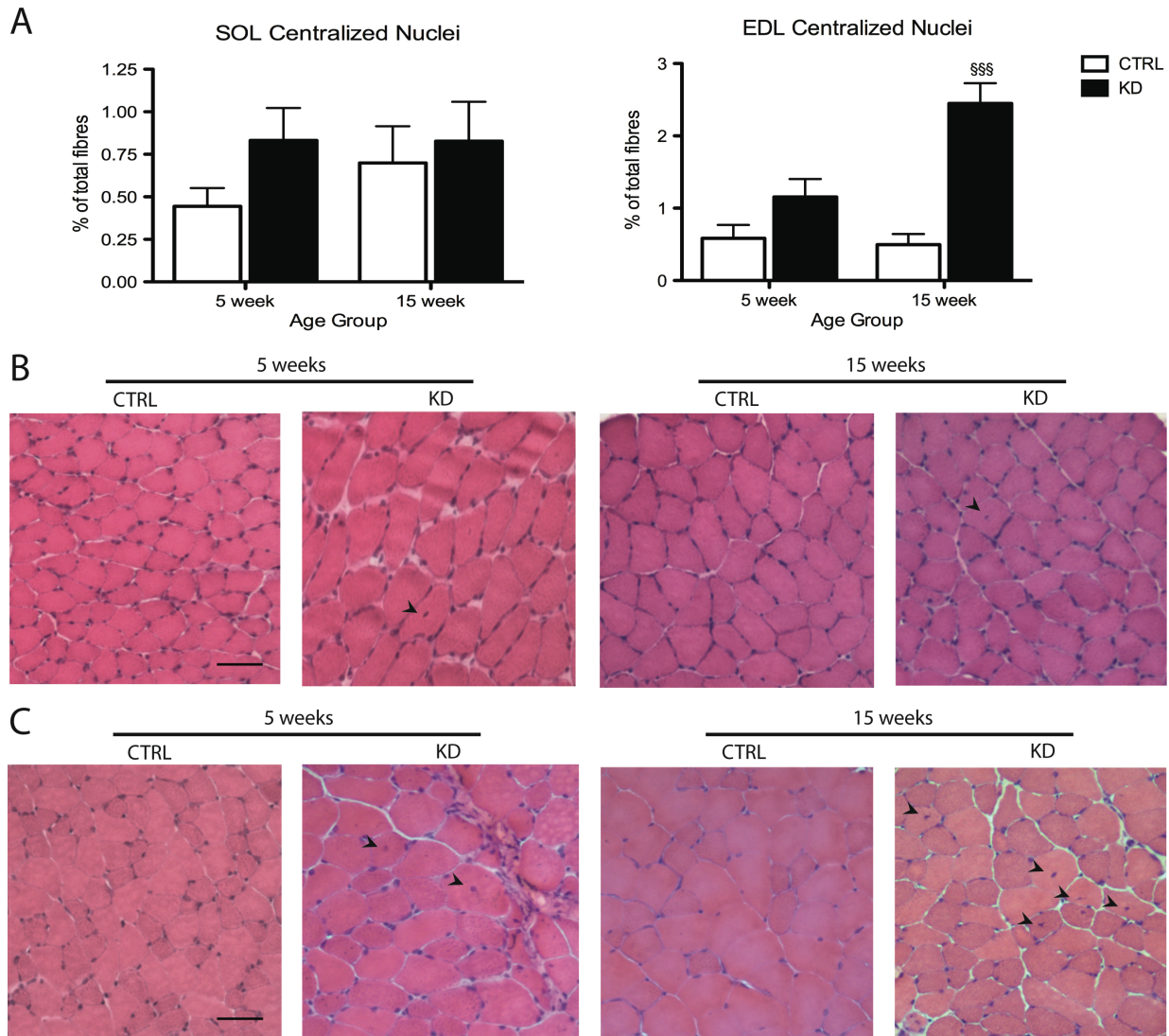


Figure 10. Analysis of H&E-stained cross-sections of *mAtg7^{-/-}* muscle. A: Semi-quantitative measure of centralized myonuclei in control (CTRL) and *mAtg7^{-/-}* (KD) soleus and EDL, expressed as the percentage of the fibres counted showing a central nuclei. B: Representative H&E stained soleus cross-sections. C: Representative H&E stained EDL cross-sections. Arrowheads indicate centralized myonuclei. Scale bar indicates 50 μ m (n=7-8, \$\$\$ interaction effect $p < 0.001$ vs. all).

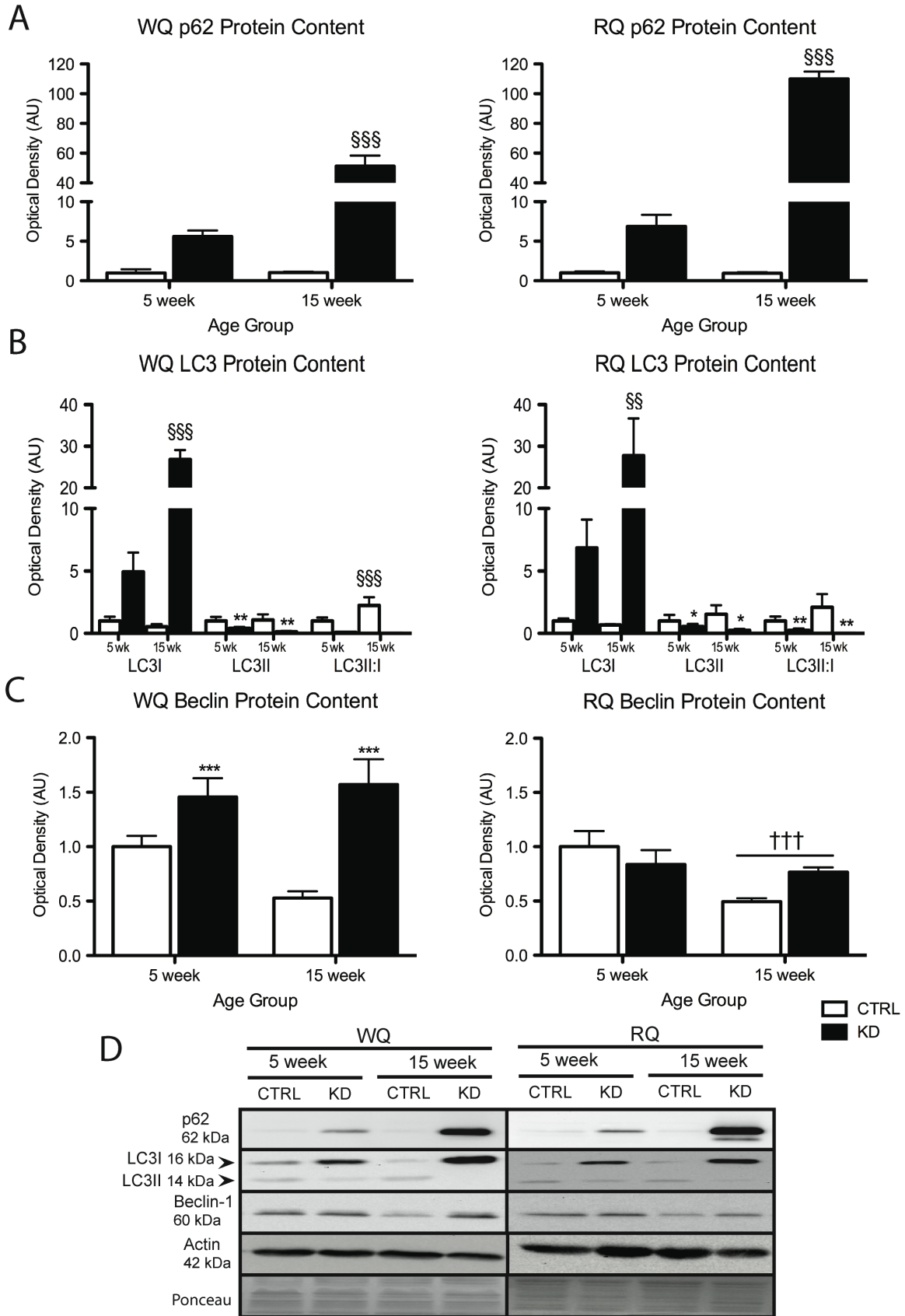
Autophagic and mitophagic protein expression

In order to characterize the effect of *Atg7* knockdown in oxidative and glycolytic muscle, the expression of downstream components of the autophagic machinery was quantified in whole muscle homogenate. The ubiquitin-binding protein p62 accumulated in the

autophagy-deficient animals, with the 15-week-old knockdown animals having significantly higher levels compared to all other groups in both WQ and RQ muscle ($p < 0.001$, Figure 11A). The 15-week-old knockdown animals also had significantly higher expression of the unbound cytosolic isoform of LC3, LC3I, compared to all other groups in the WQ ($p < 0.001$) and RQ ($p < 0.01$). Knockdown muscle had significantly lower levels of the autophagosome-associated lipidated isoform, LC3II, in the WQ ($p < 0.01$) and RQ ($p < 0.05$). Expressed as a ratio of autophagosomal-to-cytosolic LC3 (LC3II:I), the WQ of 15-week-old control animals had a higher ratio compared to all other groups ($p < 0.001$). The RQ LC3II:I ratio was significantly decreased in the knockdown animals compared to controls ($p < 0.01$, Figure 11B).

The expression of Beclin-1, a key regulator of autophagosome formation, was measured. WQ Beclin-1 expression was significantly elevated in knockdown animals ($p < 0.001$). In the RQ, 15-week-old animals showed reduced Beclin-1 expression compared to their 5-week-old counterparts ($p < 0.001$, Figure 11C).

(Next page) Figure 11. Expression of autophagic markers in *mAtg7^{-/-}* muscle. A: Quantification of p62 protein expression in the white quadriceps (WQ) and red quadriceps (RQ) of *mAtg7^{-/-}* animals (KD) and *Flox/Flox* controls (CTRL). B: Quantification of LC3I and LC3II protein expression in the WQ and RQ of KD and CTRL animals. The calculated LC3II:I ratio is also shown. C: Quantification of Beclin-1 protein expression in the WQ and RQ of KD and CTRL animals. D: Representative immunoblots of p62, LC3, and Beclin-1 expression in the WQ and RQ of KD and CTRL animals. Actin immunoblots and ponceau-stained membranes are shown as an example of loading and transfer consistency (n=4-8, §§§ interaction effect $p < 0.001$ vs. all, §§ interaction effect $p < 0.01$ vs. all, * main effect $p < 0.05$ vs. CTRL, ** main effect $p < 0.01$ vs. CTRL, *** main effect $p < 0.001$ vs. CTRL, ††† main effect $p < 0.001$ vs. 5-week group).



The effect of autophagy knockdown on autophagolysosomal fusion and subsequent cargo degradation was assessed through quantification of LAMP2 protein expression and the enzymatic activity of lysosomal cathepsins. While there were no significant differences across the groups in the expression of LAMP2 in the WQ, expression in the RQ of 15-week-old animals was significantly reduced compared to the 5-week group ($p < 0.05$, Figure 12A). In both the white gastrocnemius (WG) and red gastrocnemius (RG), 15-week-old animals showed lower maximal cathepsin activity compared to the 5-week-old age group ($p < 0.001$, Figure 12C).

Mitophagic degradation was characterized by quantifying the level of cleaved PINK1 in the cytosolic fraction. There were no significant differences in cytosolic PINK1 levels in either muscle type (Figure 13A). While there were no differences between groups in the levels of the GTPase Drp1 in the mitochondrial-enriched fractions of WQ, mitochondrial Drp1 was elevated in the RQ of 15-week-old animals compared to the 5-week-old age group ($p < 0.001$, Figure 13C).

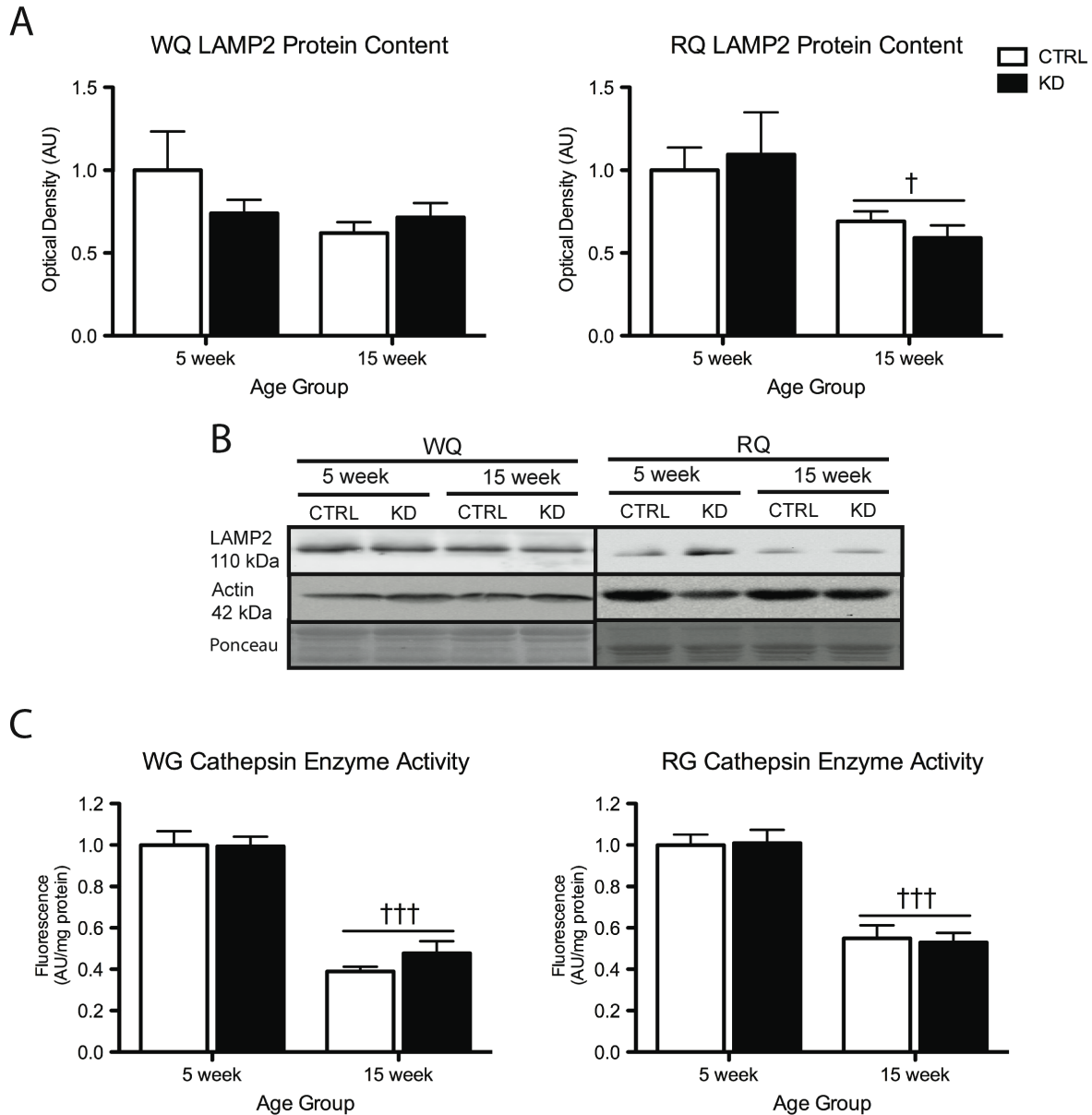


Figure 12. Expression of lysosomal markers in *mAtg7^{-/-}* muscle. A: Quantification of LAMP2 protein expression in the white quadriceps (WQ) and red quadriceps (RQ) of *mAtg7^{-/-}* animals (KD) and *Flox/Flox* controls (CTRL). B: Representative immunoblots of LAMP2 expression in the WQ and RQ of KD and CTRL animals. Actin immunoblots and ponceau-stained membranes are shown as an example of loading and transfer consistency. C: Quantitative analysis of maximal cathepsin enzymatic activity in the white gastrocnemius (WG) and red gastrocnemius (RG) of KD and CTRL animals (n=6-8, † main effect $p < 0.05$ vs. 5-week group, ††† main effect $p < 0.001$ vs. 5-week group).

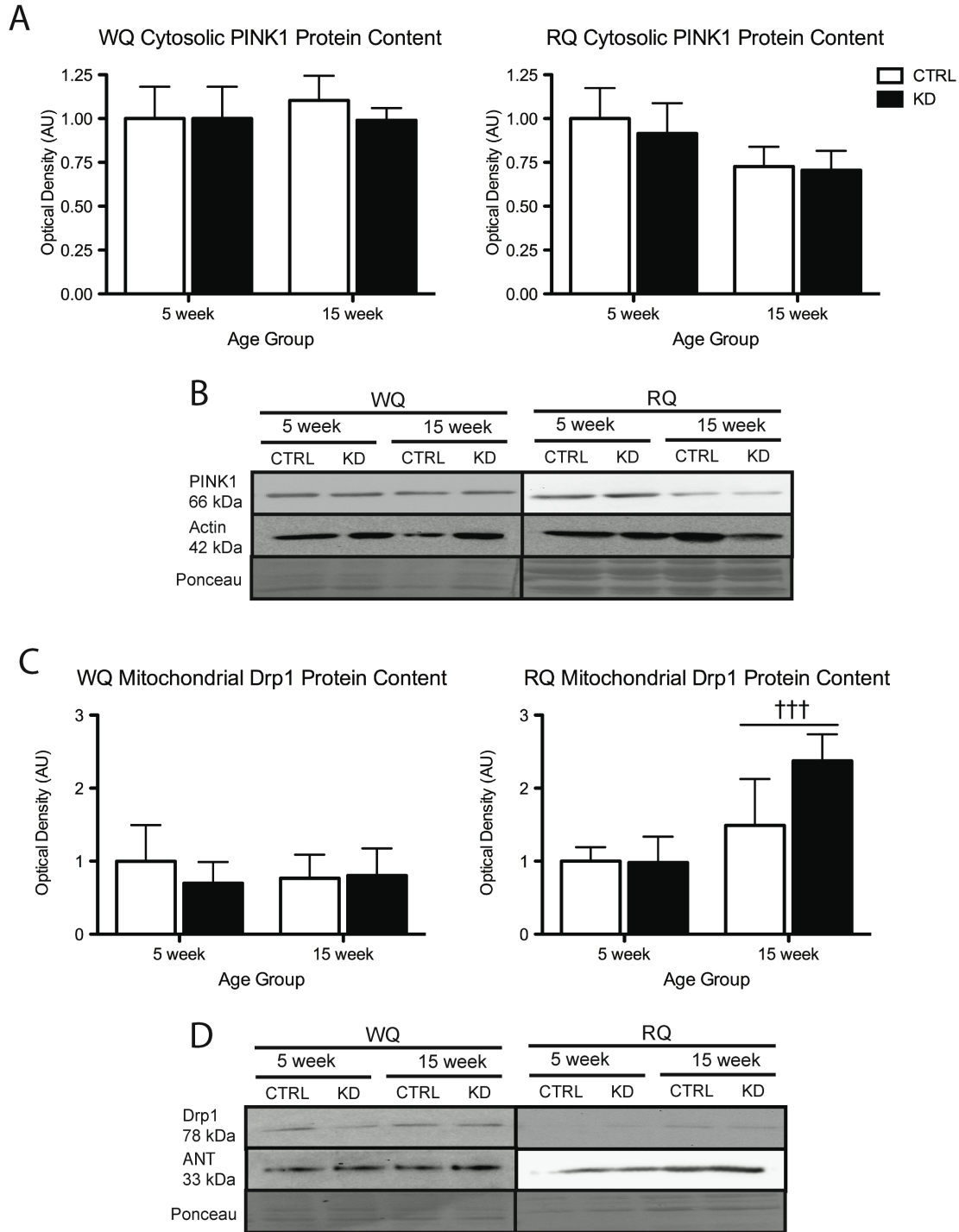


Figure 13. Expression of mitophagic markers in *mAtg7^{-/-}* muscle. A: Quantification and representative immunoblot of PINK1 protein expression in the cytosolic fraction of the white quadriceps (WQ) and red quadriceps (RQ) of *mAtg7^{-/-}* animals (KD) and *Flox/Flox* controls (CTRL). B: Quantification and representative immunoblot of Drp1 protein expression in the mitochondrial-enriched fraction of the WQ and RQ of KD and CTRL animals. Actin and ANT immunoblots and ponceau-stained membranes are shown as an example of loading and transfer consistency (n=4-8, *** main effect p<0.001 vs. 5-week group).

UPS signalling and proteolytic activity

The activity of the UPS was assessed by measuring the expression of the muscle-specific ubiquitin ligases MuRF1 and MAFbx. WQ MuRF1 expression was significantly higher in 15-week-old animals compared to their 5-week-old counterparts ($p < 0.01$). There were no differences between groups in the RQ expression of MuRF1 (Figure 14A). MAFbx levels were elevated in the WQ of 15-old-animals compared to the 5-week-old group ($p < 0.05$), and RQ levels tended to be higher in the 15-week-old age group ($p = 0.08$, Figure 14B).

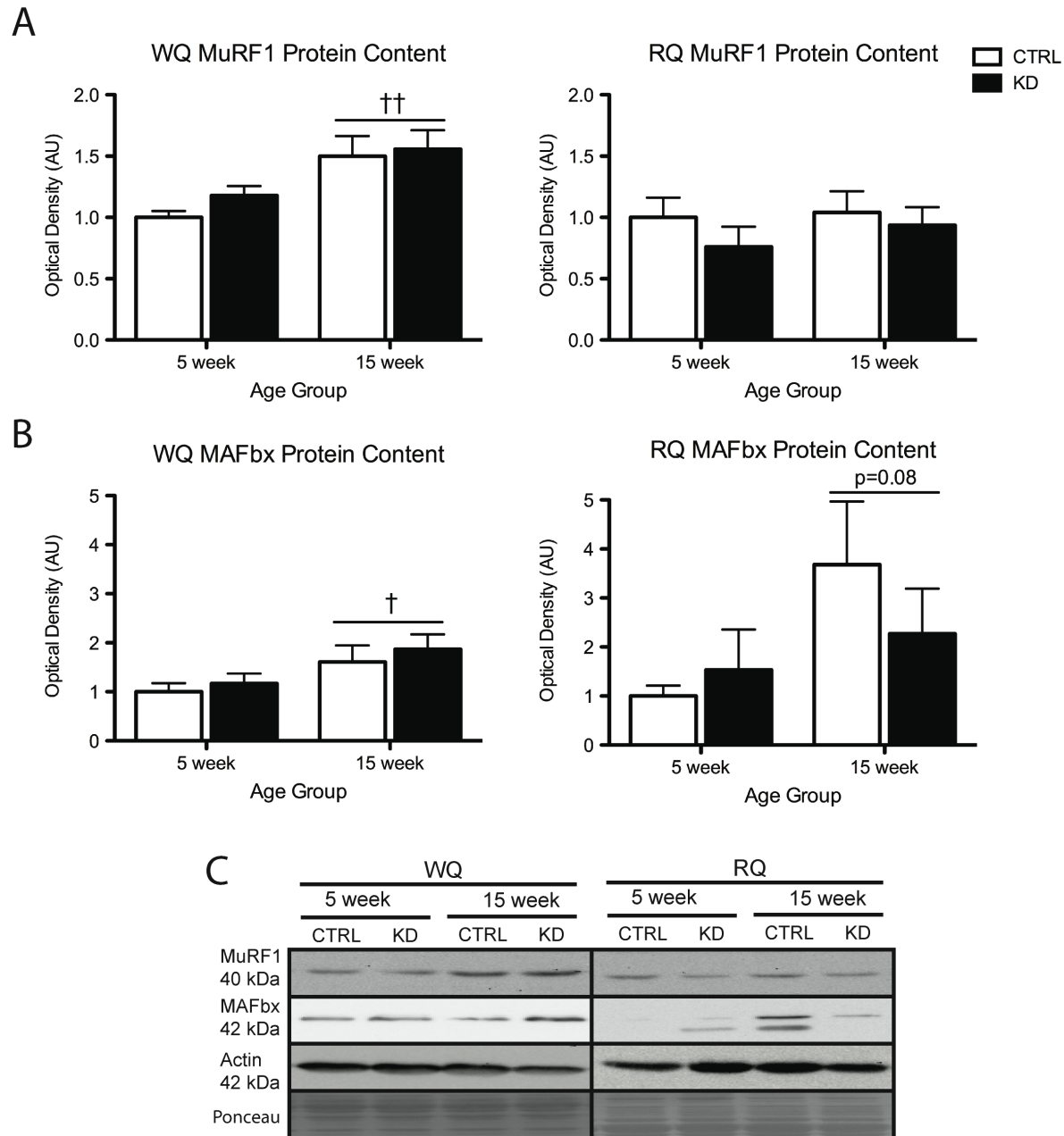


Figure 14. Expression of markers of the ubiquitin-proteasome system in *mAtg7^{-/-}* muscle. A: Quantification of MuRF1 protein expression in the white quadriceps (WQ) and red quadriceps (RQ) of *mAtg7^{-/-}* animals (KD) and *Flox/Flox* controls (CTRL). B: Quantification of MAFbx protein expression in the WQ and RQ of KD and CTRL animals. C: Representative immunoblots of MuRF1 and MAFbx expression in the WQ and RQ of KD and CTRL animals. Actin immunoblots and ponceau-stained membranes are shown as an example of loading and transfer consistency (n=5-8, † main effect p<0.05 vs. 5-week group, †† main effect p<0.01 vs. 5-week group).

Apoptotic protein expression and enzyme activity

To determine whether autophagy knockdown affects apoptotic signaling in skeletal muscle, the expression of pro- and anti-apoptotic proteins was measured. The pro-apoptotic marker Bax was significantly higher in the WQ of knockdown animals compared to controls ($p < 0.05$). In both the WQ and RQ, Bax expression was reduced in the 15-week age group compared to the 5-week-old animals ($p < 0.05$, $p < 0.001$; Figure 15A). Bcl-2, an important anti-apoptotic regulator, was significantly lower in the RQ of 15-week-old animals compared to the 5-week-old age group ($p < 0.01$). There were no differences across groups in the WQ expression of Bcl-2 (Figure 15B). The calculated Bax:Bcl-2 ratio in WQ tended to be significantly higher in knockdown animals compared to controls ($p = 0.086$) and lower in 15-week-old animals compared to the 5-week-old group ($p = 0.066$). In the RQ, the Bax:Bcl-2 ratio was not different between groups (Figure 15C).

The release of the mitochondrial protein cytochrome *c* into the cytosol is an important step in the execution of apoptosis [22]. WQ cytosolic levels of cytochrome *c* were 28% and 39% higher in the knockdown animals at 5 weeks and 15 weeks, respectively; however, these differences were not statistically significant ($p = 0.21$). In the RQ, 15-week-old animals showed elevated cytosolic cytochrome *c* that trended towards significance ($p = 0.05$, Figure 16A).

AIF acts in a caspase-independent manner by translocating to the nucleus to cause DNA fragmentation and chromatin condensation during apoptosis [22]. There were no differences across groups in the expression of AIF in the nuclear fraction of WQ. In the RQ, the 15-week-old knockdown animals had significantly higher levels of nuclear AIF compared to all other groups ($p < 0.01$, Figure 16C).

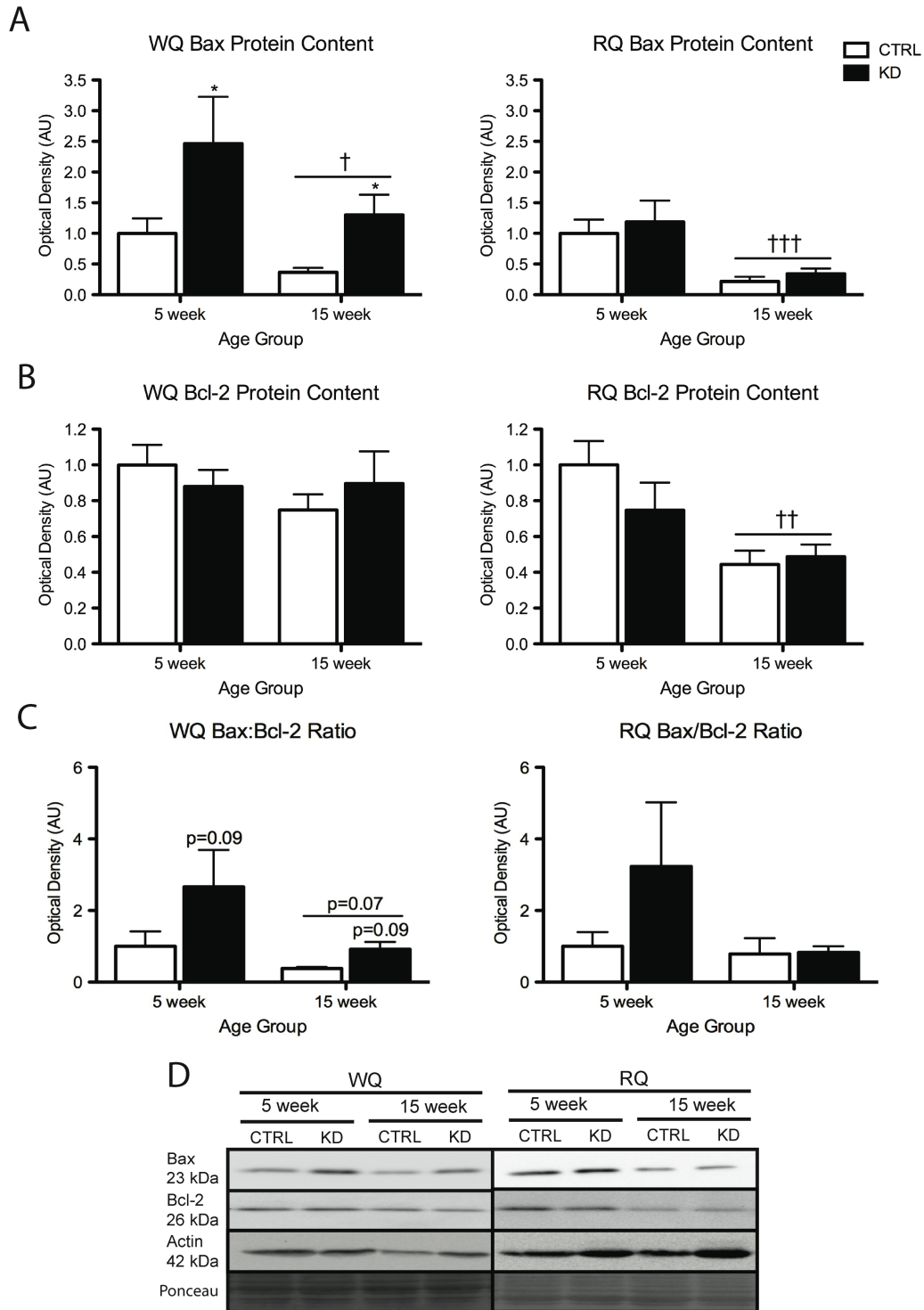


Figure 15. Expression of apoptotic markers in *mAtg7^{-/-}* muscle. A: Quantification of Bax protein expression in the white quadriceps (WQ) and red quadriceps (RQ) of *mAtg7^{-/-}* animals (KD) and *Flox/Flox* controls (CTRL). B: Quantification of Bcl-2 protein expression in the WQ and RQ of KD and CTRL animals. C: Representative immunoblots of Bax and Bcl-2 expression in the WQ and RQ of KD and CTRL animals. Actin immunoblots and ponceau-stained membranes are shown as an example of loading and transfer consistency (n=5-8, * main effect p<0.05 vs. CTRL, † main effect p<0.05 vs. 5-week group, †† main effect p<0.01 vs. 5-week group, ††† main effect p<0.001 vs. 5-week group).

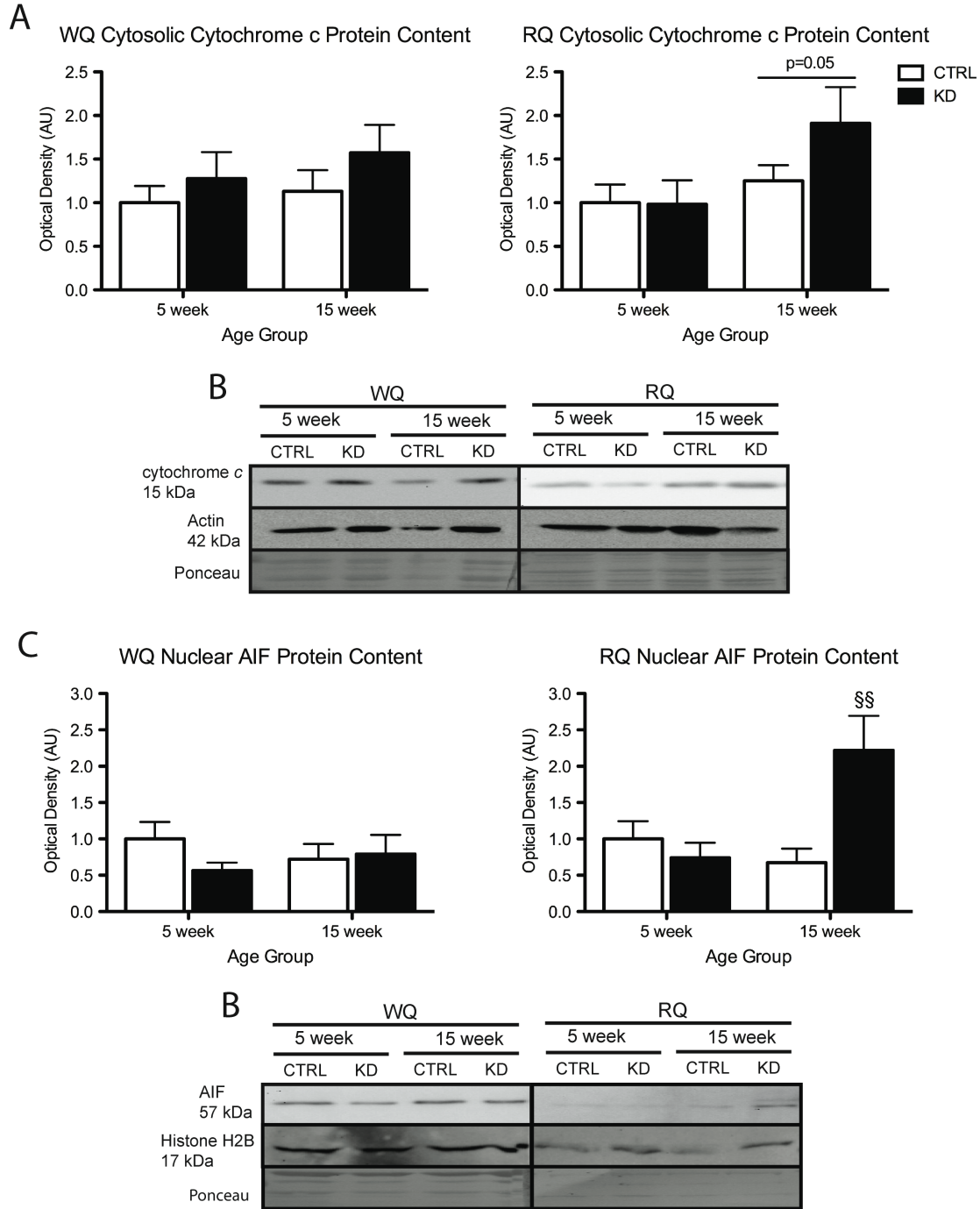
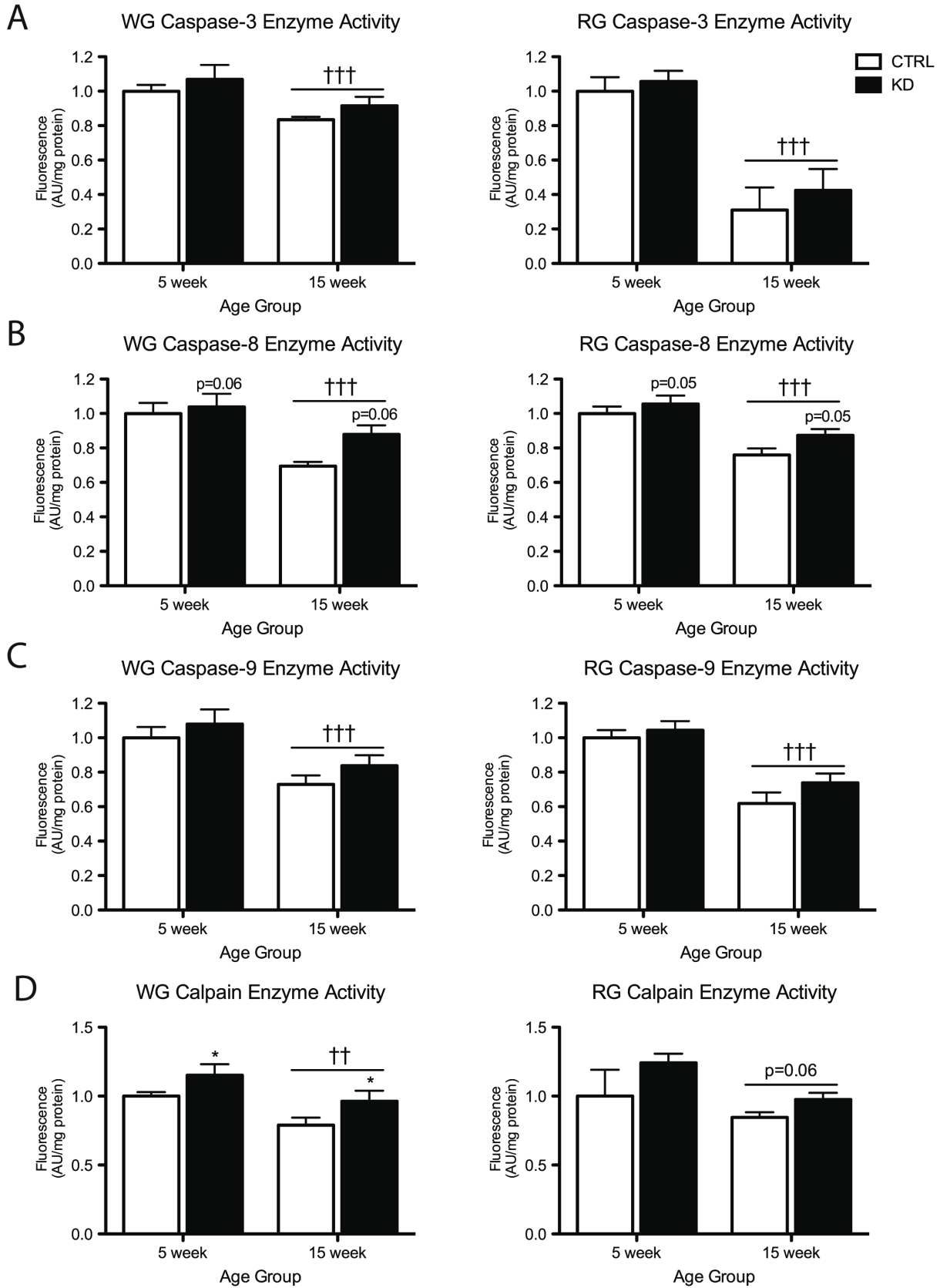


Figure 16. Expression of apoptotic markers in *mAtg7^{-/-}* muscle subcellular fractions. A: Quantification of cytochrome *c* protein expression in the cytosolic fractions of the white quadriceps (WQ) and red quadriceps (RQ) of *mAtg7^{-/-}* animals (KD) and *Flox/Flox* controls (CTRL). B: Representative immunoblots of cytochrome *c* expression in the WQ and RQ of KD and CTRL animals. C: Quantification of AIF protein expression in the nuclear fractions of the WQ and RQ of KD and CTRL animals. D: Representative immunoblots of AIF expression in the WQ and RQ of KD and CTRL animals. Actin and histone H2B immunoblots and ponceau-stained membranes are shown as an example of loading and transfer consistency (n=7-8, §§ interaction p<0.01 vs. all).

Caspases play instrumental roles during the initiation and execution of apoptosis, both by cleaving downstream targets and by directly degrading cellular components [26]. Caspase-3 activity was reduced in the 15-week-old animals compared to the 5-week-old age group, in both the WG and the RG ($p < 0.001$, Figure 17A). WG and RG caspase-8 activity trended towards being significantly elevated in the autophagy-ablated animals compared to controls ($p = 0.06$ and $p = 0.05$, respectively). In addition, caspase-8 activity was significantly lower in the older age group across both muscle types ($p < 0.001$, Figure 17B). Similarly, caspase-9 activity was reduced in the 15-week-old group compared to their 5-week-old counterparts, in both the WG and RG ($p < 0.001$, Figure 17C). In the WG, the activity of calcium-dependent proteases calpains was significantly higher in the knockdown animals compared to controls ($p < 0.05$), but was reduced in the 15-week-old age group compared to the 5-week-old animals ($p < 0.01$). RG calpain activity tended to be lower in the 15-week group ($p = 0.06$, Figure 17D).

(Next page) Figure 17. Proteolytic enzyme activity in *mAtg7^{-/-}* muscle. A: Quantitative analysis of maximal caspase-3 enzymatic activity in the white gastrocnemius (WG) and red gastrocnemius (RG) of *mAtg7^{-/-}* animals (KD) and *Flox/Flox* controls (CTRL). B: Quantitative analysis of maximal caspase-8 enzymatic activity in the WG and RG of KD and CTRL animals. C: Quantitative analysis of maximal caspase-9 enzymatic activity in the WG and RG of KD and CTRL animals. D: Quantitative analysis of maximal calpain enzymatic activity in the WG and RG of KD and CTRL animals (n=6-8, * main effect $p < 0.05$ vs. CTRL, †† main effect $p < 0.01$ vs. 5-week group, ††† main effect $p < 0.001$ vs. 5-week group).



Reactive oxygen species generation

To determine whether the redox environment of autophagy-deficient skeletal muscle was altered, reactive oxygen species (ROS) generation was quantified using the DCF assay. There were no significant differences in ROS generation between the four groups, across both WQ and RQ (Figure 18).

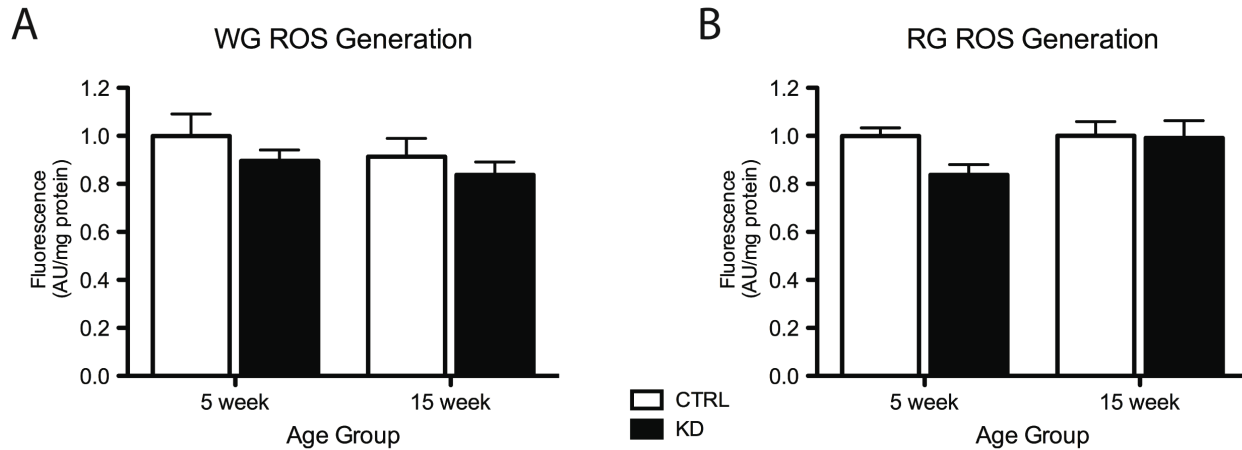


Figure 18. ROS generation in *mAtg7^{-/-}* muscle. A: Quantitative analysis of ROS generation (as determined by dichlorofluorescein fluorescence) in the white gastrocnemius (WG) of *mAtg7^{-/-}* animals (KD) and *Flox/Flox* controls (CTRL). B: Quantitative analysis of ROS generation in the red gastrocnemius (RG) of KD and CTRL animals (n=7-8).

Discussion

The purpose of this project was to characterize the role of autophagy in the maintenance of skeletal muscle health at a cellular level. To determine this, morphological, proteolytic, and apoptotic measures were performed in a skeletal muscle-specific *Atg7* knockdown mouse model. As autophagy is a key regulator of muscle size and function, it was hypothesized that *mAtg7^{-/-}* animals would display smaller muscles and muscle fibres, signs of muscle damage, as well as upregulated apoptotic and proteolytic markers. The role of mitochondrial signalling was of particular interest as a potential mediator of skeletal muscle degradation.

Muscle-specific autophagy knockdown did not affect whole body or isolated muscle weights; however, the 15-week-old animals predictably had larger muscles and muscle fibres than the 5-week-old animals. At the fibre level, the *mAtg7^{-/-}* animals exhibited differences in fibre type-specific cross-sectional area and fibre type distribution, as well as structural changes. As expected, *Atg7* knockdown resulted in profound alterations to downstream autophagic markers, such as LC3 lipidation and p62 accumulation. Indicators of lysosomal activity remained unchanged with autophagy knockdown, likely because lysosomes are necessary for a number of other degradative processes independent of autophagy [130]. While none of the measures of mitochondrial stress were affected by autophagy knockdown, there is evidence of increased apoptotic signalling in *mAtg7^{-/-}* muscle. Together, these findings point towards modest but accumulative damage in autophagy-ablated skeletal muscle. Interestingly, decreased proteolytic activity with a concurrent upregulation of proteasomal markers was observed, highlighting a role for degradative and cell death processes in skeletal muscle growth and development.

The role of autophagy in the maintenance of skeletal muscle morphology

Autophagy is a necessary cellular process in the development and maintenance of tissues [131]. Accordingly, early studies using autophagy-deficient mice found that they do not survive past the neonatal stage, once access to maternal nutrients is terminated [132]. In skeletal muscle, autophagic dysregulation results in pathology, either through excess degradation [97, 98], or conversely, the accumulation of damaged proteins and organelles [101, 102]. Evidence on the effect of autophagy disruption in skeletal muscle is equivocal. Using a similar constitutive *Atg7* knockdown mouse model, Masiero and colleagues showed abated growth, degenerative muscle fibre alterations in tibialis anterior, and reduced isolated muscle force in gastrocnemius [116]. Using the same animal model, Kim and colleagues observed muscle fibre damage and atrophy in the gastrocnemius [117]. Reduced psoas fibre diameter has also been reported using this model [118]. These investigations used a *Cre-loxP* construct with Cre expression driven by the myosin light chain 1 fast (*MLC1f*) promoter. In contrast, in an *Atg7* knockdown model using a muscle creatine kinase (*MCK*) promoter to drive Cre expression, no phenotypic differences were observed, and the soleus was free of histological muscle fibre abnormalities [115]. In the present work, *Atg7* knockdown driven by the alpha 1 actin promoter (*ACTA1*) did not result in any significant differences in body weight or isolated muscle weights. The genetic constructs used to knock down skeletal muscle autophagy may have contributed to the disparity in the results obtained with this model. While all the models of *Atg7* deficiency studied to date made use of *Cre-loxP* recombination to target skeletal muscle autophagy, differing skeletal muscle-specific promoters were used to drive Cre expression. As its name indicates, *MLC1f* is the light chain isoform expressed in fast muscle fibres; similarly, *MCK* is expressed at a much higher level in fast-twitch fibres [133]. Skeletal

muscle actin 1, the protein product of the *ACTA1* gene, is ubiquitously expressed in all skeletal muscle fibre types [133]. In the *MLC1f* and *MCK* Cre models, higher expression of Cre in fast fibres may have exacerbated the effect of autophagy knockdown, as these fibre types have a greater level of basal autophagy [134]. However, as murine muscle is primarily composed of fast muscle fibres, this effect is unlikely to explain the extent of the differences between the existing studies and this thesis [122, 135]. The expression of these promoters may nevertheless vary with the age of the mice used, as creatine kinase and proteins of the contractile apparatus are differentially expressed throughout development [136-138]. Unfortunately, the existing work on *Atg7* knockdown mice did not include a quantification of the reduction in *Atg7* protein expression, making comparison to the extent of the knockout impossible. Furthermore, while the majority of existing data on *mAtg7^{-/-}* mice was compared to *Flox/Flox* control littermates, one study used *Flox/WT/Cre* controls [115], potentially adding to the disparity between studies.

The present project demonstrated muscle fibre damage at a histological level in glycolytic muscle, with no significant effects seen in oxidative muscle. This is in agreement with previous characterization of muscle-specific autophagy knockdown mice: examinations of glycolytic muscle show increases in centralized nuclei [116, 117], while oxidative muscle appears to be spared [115]. Specifically, Masiero and colleagues found a 1.5% increase in centralized nuclei in the tibialis anterior muscle of 8-week-old *mAtg7^{-/-}* mice [116], a comparable figure to that observed in EDL in this thesis. Wu and colleagues' observations of lack of atrophy and damage in autophagy-deficient soleus were also corroborated [115]. Glycolytic muscle displays higher levels of basal autophagy [134], and is more responsive to the induction of autophagy through exercise [139]. It is possible that compared to oxidative

muscle, glycolytic muscle is more reliant on autophagy to maintain the cellular environment, both basally and in response to a stressor [140].

This work is the first to quantify fibre type distribution and fibre type-specific CSA in autophagy-deficient muscle. Unexpectedly, there were no differences in total muscle cross-sectional area in either muscle type; in fact, fibre type-specific CSA of type IIX fibres was increased in the knockdown animals in both muscle types. While these findings are paradoxical, a number of well-characterized myopathies and dystrophies present with fibre and whole-muscle hypertrophy, such as Duchenne muscular dystrophy [141, 142]. In the case of autophagy-deficient mice, it is possible that the lack of autophagic degradation is contributing to the larger fibre size through the accumulation of protein aggregates. Alternatively, repair by satellite cells may be mitigating atrophy, an effect that has been observed in *mdx* mice, a murine model of human muscular dystrophy [143]. The atrophy characteristic of this condition is greatly delayed in these mice, partly due to an excellent regeneration capacity of satellite cells [144]. In the present study, protective regeneration is supported by the presence of centrally located nuclei in the knockdown glycolytic muscle. In the soleus, autophagy knockdown resulted in a decrease in the proportion of slow oxidative type I and I/IIA fibres with a concurrent increase in the percentage of type IIX fast glycolytic fibres. Mouse muscle is composed predominantly of fast fibres, with a small proportion of slow oxidative fibres found mainly in the soleus [122, 135]. The small shift of slower fibre types to faster, glycolytic types may be an early response to damage caused by autophagy deficiency [145].

The relationship between apoptosis and autophagy

The closely related degradative processes of apoptosis and autophagy have been the subject of much investigation in a number of cell and physiological models. In cell culture

models – especially tumorigenesis studies – contrasting relationships between autophagy and apoptosis have been observed. Some reports indicate that autophagic degradation prevents apoptosis by clearing harmful cellular debris, a connection shown through tumor cell apoptosis in response to autophagy inhibition [146, 147], or alternatively through the protection of cells from cell death following the induction of autophagy [148, 149]. In contrast, enhanced autophagy in HeLa cells through overexpression of *Atg5* resulted in heightened susceptibility to apoptosis [150].

Murine models of whole-body and tissue-specific autophagy ablation have shown a variety of deleterious effects [151-153], including evidence of increased apoptotic signalling. The seminal global *Atg7* ablation work by Masaaki Komatsu's group showed increased TUNEL-positive staining in the liver, a marker of apoptotic DNA fragmentation [125]. Similarly, inducible cardiomyocyte-specific *Atg5* knockdown increased TUNEL-positive cells [154]. Targeted *Atg7* knockdown in erythroid cells resulted in increased cell death, measured by flow cytometry analysis of Annexin V staining [155]. The only measure of apoptosis that has been performed in skeletal muscle-specific *Atg7* knockdown mice is the quantification of apoptotic nuclei through terminal deoxynucleotidyltransferase-mediated dUTP nick end labelling (TUNEL), which were increased in autophagy-deficient gastrocnemius muscle [116]. However, the localization of these apoptotic nuclei was not indicated, leaving unanswered the question of whether myonuclear or interstitial nuclei are responsible for this increase. Additionally, the significance of myonuclear apoptosis has been contested, pointing rather to alternate apoptotic signalling responsible for muscle mass loss [112]. As such, a more exhaustive characterization of these pathways was warranted.

As the first characterization of apoptotic signalling in autophagy-deficient skeletal muscle, the present work contributes to existing knowledge of apoptotic signalling in response to autophagy disruption. Glycolytic muscle of knockdown animals had increased expression of the pro-apoptotic protein Bax, while oxidative muscle of the 15-week-old knockdown animals showed elevated translocation of AIF to the nucleus. Beclin-1 was also elevated in the glycolytic muscle of knockdown animals. This protein is known to regulate both apoptosis and autophagy, and may represent a futile effort by the cell to upregulate autophagy [11]. Together with the marked increase in autophagic byproducts such as p62 and LC3I, these findings point towards a moderate induction of apoptosis, potentially in response to autophagy knockdown. The accumulation of proteins and organelles tagged for degradation presents a stress to the cell that can result in apoptosis [41, 100]. This corroborates the theory that autophagy plays a protective role in skeletal muscle [42].

This study also examined the activity of a number of proteolytic enzymes in autophagy-deficient muscle. In both oxidative and glycolytic muscle, caspase-8 activity was elevated, trending towards significance. The relationship between caspase-8 and autophagic degradation has been studied in apoptosis-deficient cancer cells. These colon carcinoma cells are resistant to cell death receptor-mediated activation of caspase-8 due to a cytoprotective autophagic response [156]. Inhibition of autophagy in these cells results in heightened caspase-8 activity [157]. Caspases also directly cleave proteins independent of myonuclear apoptosis, specifically targeting actin [111]. These large molecules are broken down into smaller fragments suitable for degradation by the proteasome, contributing to this pathway of muscle degradation [109, 110].

mAtg7^{-/-} glycolytic muscle showed increased activity of calpains, proteolytic enzymes activated by increased cytosolic calcium to cleave a number of protein targets [158]. In the absence of autophagy, an accumulation of misfolded proteins may be responsible for the release of calcium from the ER to the cytosol and subsequent calpain activation [38]. There was no effect of the knockdown on calpain activity in oxidative muscle, but AIF translocation to the nucleus was increased, further suggesting the involvement of ER stress and caspase-independent apoptosis in this model. Calpains may also play a role in autophagic signalling and its cross-talk with apoptosis. Calpain-deficient cells have demonstrated a reduced autophagic response, indicating an alternate role for these enzymes [159]. Calpains have further been implicated in the cellular switch between autophagy and apoptosis through the cleavage of Atg5 [150, 160]. Together, the caspase-8 and calpain responses seen in autophagy-deficient muscle may point towards a compensatory mechanism of proteolysis in the absence of autophagic degradation.

The mitochondrial response to skeletal muscle-specific autophagy knockdown

Mitochondrial signalling was examined as a potential pathway contributing to the upregulation of some apoptotic markers observed in this study. Mitochondria are well established as an integral part of skeletal muscle health and function [161]. However, in a ‘chicken and egg’ type of problem, it remains unclear if damage-inducing stimuli causes mitochondrial dysfunction, or whether apoptotic and oxidative factors released by the mitochondria contribute to muscle damage [88, 89]. Electron microscopy evidence of the accumulation of abnormal mitochondria has been observed in autophagy-deficient tibialis anterior and soleus [115-117]. A further characterization of mitochondrial dysfunction in muscle-specific *Atg7* knockdown mice revealed changes in the expression of oxidative

phosphorylation components and a reduction in ATP content [115]. ROS generation was also found to be elevated in *Atg7*-null mouse embryonic fibroblasts (MEF) [115]. Nonetheless, this thesis' experiments did not show the increased ROS generation expected based on the existing literature. The DCF assay used to ascertain this reflects changes in the overall oxidative environment in the cell; a mitochondrial-targeted measure of oxidative stress may reveal differences associated with autophagy knockdown.

Mitophagy is a mechanism by which the cell can protect itself from the effects of dysfunctional or damaged mitochondria. Global *Atg7* knockdown manifested in the liver with cellular abnormalities, including deformed mitochondria [125]. Damaged mitochondria also accumulated in autophagy-null erythroid cells [155]. In a model of cells exposed to toxic metabolites, the mitophagic elimination of damaged mitochondria reduced oxidative stress [162]. Similarly, neuronal cells were protected from neurodegenerative cell death following the induction of autophagy and mitophagy by staurosporine [163]. The present study showed a moderate increase in apoptotic signalling, but it is difficult to discern whether this stress originates from the accumulation of dysfunctional mitochondria. Markers of mitochondrial-mediated apoptosis, such as cytosolic cytochrome *c* release and caspase-9 activation, were non-significantly elevated in knockdown animals, possibly indicating mitochondrial stress. Investigations using mitochondrial respirometry and electron microscopy will be able to further elucidate the effect of autophagy disruption on mitochondrial signalling.

While mitophagy and autophagy share key effectors and upstream activators, there is evidence that these processes are differentially modulated. In yeast, mitophagic degradation has been shown to be a separate event from bulk autophagy in response to starvation [164], and involves specific mitochondrial tagging proteins [165, 166]. Distinct ubiquitin-conjugating

enzymes have also been associated with the induction of mitophagy [167]. This may also include effectors specific to the mitophagic machinery. PINK1 was first identified as having a role in a mitophagic response mitochondrial membrane potential loss [74, 168], but it has also been shown to inhibit mitophagy once cleaved from healthy mitochondria by binding Parkin in the cytosol and preventing its translocation to the OMM [169]. Quantification of PINK1 in the cytosol of autophagy-deficient mice did not show any differences compared to control animals, suggesting that mitophagic signalling may not be contributing to the upregulated markers of apoptosis and structural alterations observed in the present model.

Muscle-specific ubiquitin ligases as an alternative degradative pathway

In conditions of cellular stress, the ubiquitin-proteasome system (UPS) is activated in concert with the autophagy-lysosome system [170, 171]. While there is extensive evidence of the compensatory upregulation autophagy following the proteasomal inhibition [172, 173], the reverse is not as clearly determined. In colon cancer cells, RNA interference and pharmacological inhibition of autophagy caused the upregulation of proteasomal degradation [174]. Evidence from previous work in autophagy-deficient muscle shows increased mRNA expression of MuRF1 and MAFbx in tibialis anterior [116]. Conversely, inhibition of autophagy has also been shown to inhibit the clearance of proteasomal substrates, a phenomenon thought to be caused by p62 accumulation [175]. The results of this study serve only to add to the debate; MuRF1 and MAFbx expression were not different between autophagy-deficient animals and controls. Further investigation into the crosstalk taking place between autophagic machinery and the UPS will help to elucidate whether varying types of muscle damage differentially activate these degradative pathways.

Developmental modulation of skeletal muscle degradative pathways

While the effects of *Atg7* knockdown in skeletal muscle were varied, there were clear differences between the 5-week and the 15-week-old groups in several measures. This included a logical increase in whole-body weight, isolated muscle weights, and fibre CSA associated with growth. Existing data on muscle-specific autophagy-deficient mice shows an age-dependent increase in structural abnormalities and accumulation of autophagic markers. Specifically, the reduction in gastrocnemius force was greater in 5-month-old mice compared to 2-month-old mice, as was the proportion of centralized nuclei in the tibialis anterior [116]. The present work was in agreement with these findings: the accumulation of p62 and LC3 was exacerbated in the 15-week-old group, as was the presence of centralized myonuclei in glycolytic muscle. Furthermore, while body weight did not differ significantly with autophagy deficiency, growth from 5 weeks to 15 weeks was abated in *mAtg7^{-/-}* animals. It remains to be determined whether *mAtg7^{-/-}* muscle is eventually able to adapt to this accumulative effect of autophagy deficiency.

The age groups used in the present study represent two distinct stages in postnatal muscle development. In developing murine muscle, growth is a result of the addition of new myonuclei and the expansion of the cytoplasmic domains associated with them. These new myonuclei are provided by satellite cells, muscle progenitor cells [176]. In mice, proliferation of satellite cells peaks during the first 3 weeks postnatally. Following a decline, the majority of satellite cells become quiescent by 6 to 8 weeks of age [177]. Thus, animals in the 5-week age group are still increasing myofibre size, while the 15-week-old mice are considered to have fully developed adult muscle. Interestingly, while growth was evident in increased isolated muscle weights and fibre CSA measurements in the 15-week age group, the overall muscle

CSA was unchanged with age. The increases in isolated muscle weights are likely driven by longitudinal growth, which would not be observed in the cross-sectional area measurements.

Multiple markers of proteolytic degradation were downregulated in the 15-week-old age group compared to the 5-week-old animals, including the activity of all measured caspases, calpain, and cathepsin. Caspases are critical in the development of a number of tissues [178, 179], and the action of caspases is required for cellular proliferation and the control of tissue growth [180]. In fact, generalized inhibition of caspases disrupts development and can cause embryonic death [179]. The differentiation of skeletal muscle from muscle progenitor cells to myofibres requires caspase-3 to cleave protein kinase targets, thereby activating them. A more modest, but similar, increase in caspase-8 activity is also seen during differentiation [181]. Muscle-specific ubiquitin ligases MuRF1 and MAFbx are known to be upregulated in aging animals [182, 183]. While the 15-week-old age group in this project are not considered to be 'aging', it is possible that adult muscle undergoes higher levels of basal proteasomal degradation than that of young animals. Research into the developmental role of muscle-specific ubiquitin ligases is limited, but suggests modulation in the embryonic and postnatal periods [184]. The downregulation of proteolytic enzymes and concurrent upregulation of proteasomal markers in the 15-week-old group may also indicate a counterbalance between these processes over the course of development.

It is clear that autophagy also plays many important roles during embryonic development and post-natal growth [125]. Knockdown of a variety of autophagic regulators in transgenic mouse models shows diverse defects and developmental problems, from embryonic lethality to specific health problems in adulthood [185]. Beclin-1 and LAMP2 were found to be downregulated in the 15-week-old animals in the present study. In the case of Beclin-1,

there is evidence that its interaction with other autophagic and apoptotic regulatory proteins may be altered during development. Similarly, apoptosis is regulated over the course of the mammalian lifespan [186]. In this characterization, the Bax:Bcl-2 ratio was decreased in the 15-week-old age group. Together with the variation in proteasomal and proteolytic markers, these results point to differential regulation of degradative processes throughout development.

Study limitations

While tissue-specific autophagy knockdown models have been used extensively to circumvent the lethality of global autophagy knockout, it remains that *Cre-loxP* constructs do not achieve complete ablation of the target gene [123]. The remaining *Atg7* expression in this mouse model may have contributed to the modest effect of the knockdown seen in many of the measures performed. Residual *Atg7* expression has been noted in all the existing studies using this model, but the extent of this has not been quantified. Complete autophagy inhibition could potentially be achieved by administering chemical inhibitors of autophagy to *mAtg7^{-/-}* mice (e.g. 3-methyladenine, bafilomycin); however, these compounds would achieve whole-body autophagy inhibition, negating the skeletal muscle specificity of this model [187].

Quadriceps, gastrocnemius, soleus, and EDL were used in the study as representative oxidative and glycolytic muscle. Due to the relatively small size of these tissues, immunoblots, enzymatic measures, and histological analyses were performed on different muscle. This may have led to some disparity in the comparisons between muscle types. Similarly, some specific measures were not possible due to lack of sample. In the future, pooled muscle samples would help resolve this problem.

Obstacles in the measurement of autophagic flux remain, particularly regarding LC3 immunoblotting. The study of autophagy using single-timepoint measures, such as the ones in

this project, only provide a snapshot of a constantly ongoing process. For example, while a decreased LC3II:I ratio is generally accepted as an indication of autophagic impairment, it can also be an indication of decreased LC3II degradation caused by rapid lysosomal turnover [188]. LC3 has also been found associated with non-autophagosomal structures, and may be a less specific measure than was previously thought [189]. In the present project, LC3 measures were interpreted in conjunction with Atg7 and p62 data in order to strengthen the analysis. Furthermore, previous investigations using the *mAtg7^{-/-}* model corroborate this autophagy deficiency with evidence of p62 and LC3I accumulation [115-117], as well as fluorescent microscopy measures of autophagic flux using GFP-tagged LC3 [116].

Future directions

While it has been established that autophagy deficiency affects the morphology and maintenance of skeletal muscle, further examination of this model would be beneficial. The growth of *mAtg7^{-/-}* mice has been tracked for the first 40 days of life [116], but a characterization of the aging process in these animals remains to be examined. Autophagy is known to decline in aging skeletal muscle, therefore a characterization of aged autophagy-deficient skeletal muscle may reveal the mechanisms behind this change [190]. Similarly, some measures of force have been reported in skeletal muscle-specific autophagy deficient mice [116, 118], but a complete set of force measurements is needed to further our understanding of the functional effect of the knockdown.

mAtg7^{-/-} mice have been subjected to denervation in the study by Masiero and colleagues, showing a increased atrophy and degradation in the knockdown muscle [116]. However, the effect of other known muscle stressors should be examined. Chemical inducers of muscle damage such as doxorubicin will reveal how autophagy-deficient muscle will

contend with this type of stress [97]. Exercise is known to induce autophagy in skeletal muscle [101, 104, 191], and is another challenge to autophagy-deficient animals that has yet to be fully explored. Autophagy may play a protective or adaptive role in response to exercise [140], possibly by contributing to protein turnover. These experiments will broaden our understanding of the role of autophagy in the plasticity of skeletal muscle.

Conclusion

The purpose of this thesis was to characterize the role of autophagy in the maintenance of skeletal muscle health. Using a skeletal muscle-specific *Atg7* knockdown mouse model, autophagic, mitophagic, apoptotic, and proteosomal pathways were investigated in order to ascertain their role in mediating muscle morphology. While overt phenotypic differences were absent between the knockdown animals and the controls, structural alterations were observed at the fibre level indicating moderate damage. A coinciding upregulation of some markers of apoptotic signalling suggests that autophagy ablation is detrimental to skeletal muscle. Several age-based alterations, specifically in the proteolytic and proteosomal pathways, emphasize the varying role of degradative processes over the course of the lifespan. Collectively, the present work contributes to the existing literature demonstrating the importance of autophagy in the maintenance of skeletal muscle health.

References

1. Murton AJP & Greenhaff PL. (2010). Physiological control of muscle mass in humans during resistance exercise, disuse and rehabilitation. *Curr Opin Clin Nutr*, 13(6), 249-255.
2. Lecker SH, Jagoe RT, Gilbert A, Gomes M, Baracos V, Bailey J, Price SR, Mitch WE, Goldberg AL. (2004). Multiple types of skeletal muscle atrophy involve a common program of changes in gene expression. *FASEB J*, 18, 39-51.
3. Welle S (1999) *Human Protein Metabolism*, (Springer, New York).
4. Marimuthu K, Murton AJ, Greenhaff PL. (2011). Mechanisms regulating muscle mass during disuse atrophy and rehabilitation in humans. *J Appl Physiol*, 110, 555-560.
5. Ravikumar B, Sarkar S, Davies JE, Futter M, Garcia-Arencibia M, Green-Thompson ZW, Jimenez-Sanchez M, Korolchuk VI, Lichtenberg M, Luo S, Massey DCO, Menzies FM, Moreau K, Narayanan U, Renna M, Siddiqi FH, Underwood BR, Winslow AR, Rubinsztein DC. (2010). Regulation of mammalian autophagy in physiology and pathophysiology. *Physiol Rev*, 90, 1383-1435.
6. Kovsan J, Bluher M, Tarnovscki T, Kloting N, Kirshtein B, Madar L, Shai I, Golan R, Harman-Boehm I, Schon MR, Greenberg AS, Elazar Z, Bashan N, Rudich A. (2011). Altered autophagy in human adipose tissue in obesity. *J Clin Endocrinol Metab*, 96(2), E268-E277.
7. Glick D, Barth S, Macleod KF. (2010). Autophagy: Cellular and molecular mechanisms. *J Pathol*, 221(1), 3-12.
8. Mizushima N & Komatsu M. (2011). Autophagy: Renovation of cells and tissues. *Cell*, 147(4), 728-741.
9. Tanida I. (2011). Autophagy basics. *Microbiol Immunol*, 55(1), 1-11.

10. Young ARJ, Chan EYW, Hu XW, Köchl R, Crawshaw SG, High S, Hailey DW, Lippincott-Schwartz J, Tooze SA. (2006). Starvation and ULK1-dependent cycling of mammalian Atg9 between the TGN and endosomes. *J Cell Sci*, 119(18), 3888-3900.
11. Kang R, Zeh HJ, Lotze MT, Tang D. (2011). The beclin 1 network regulates autophagy and apoptosis. *Cell Death Differ*, 18(4), 571-580.
12. Zhou F, Yang Y, Xing D. (2011). Bcl-2 and bcl-xL play important roles in the crosstalk between autophagy and apoptosis. *FEBS J*, 278, 403-413.
13. Vasquez CL & Colombo MI. (2010). Beclin 1 modulates the anti-apoptotic activity of bcl-2: Insights from a pathogen infection system. *Autophagy*, 6(1), 177-178.
14. Xie Z & Klionsky DJ. (2007). Autophagosome formation; core machinery and adaptations. *Nat Cell Biol*, 9, 1107-1109.
15. Nakatogawa H, Ishii J, Asai E, Ohsumi Y. (2012). Atg4 recycles inappropriately lipidated Atg8 to promote autophagosome biogenesis. *Autophagy*, 8(2), 177-186.
16. Romanov J, Walczak M, Ibricic I, Schüchner S, Ogris E, Kraft C, Martens S. (2012). Mechanisms and functions of membrane binding by the Atg5-Atg12/Atg16 complex during autophagosome formation. *EMBO J*, 31, 4304-4317.
17. Mizushima N & Yoshimori T. (2007). How to interpret LC3 immunoblotting. *Autophagy*, 3(6), 542-545.
18. Shaid S, Brandts CH, Serve H, Dikic I. (2013). Ubiquitination and selective autophagy. *Cell Death Differ*, 20, 21-30.

19. Shvets E & Elazar Z. (2008). Autophagy-independent incorporation of GFP-LC3 into protein aggregates is dependent on its interaction with p62/SQSTM1. *Autophagy*, 4(8), 1054-1056.
20. Shvets E, Fass E, Scherz-Shouval R, Elazar Z. (2008). The N-terminus and Phe52 residue of LC3 recruit p62/SQSTM1 into autophagosomes. *J Cell Sci*, 121, 2685-2695.
21. Komatsu M & Ichimura Y. (2010). Physiological significance of selective degradation of p62 by autophagy. *FEBS Lett*, 584, 1374-1378.
22. Quadrilatero J, Alway SE, Dupont-Versteegden E. (2011). Skeletal muscle apoptotic response to physical activity: Potential mechanisms for protection. *Appl Physiol Nutr Metab*, 36, 608-617.
23. Taylor RC, Cullen SP, Martin SJ. (2008). Apoptosis: Controlled demolition at the cellular level. *Nat Rev Mol Cell Bio*, 9, 231-241.
24. Budihardjo I, Oliver H, Lutter M, Luo X, Wang X. (1999). Biochemical pathways of caspase activation during apoptosis. *Annu Rev Cell Biol*, 15, 269-290.
25. Bao Q & Shi Y. (2007). Apoptosome: A platform for the activation of initiator caspases. *Cell Death Differ*, 14, 56-65.
26. Stroh C & Schulze-Osthoff K. (1998). Death by a thousand cuts: An ever increasing list of caspase substrates. *Cell Death Differ*, 5, 997-1000.
27. Pinton P, Giorgi C, Siviero R, Zecchini E, Rizzuto R. (2008). Calcium and apoptosis: ER-mitochondria Ca²⁺ transfer in the control of apoptosis. *Oncogene*, 27(50), 6407-6418.
28. Dremina ES, Sharov VS, Schöneich C. (2012). Heat-shock proteins attenuate SERCA inactivation by the anti-apoptotic protein bcl-2: Possible implications for the ER Ca²⁺-mediated apoptosis. *Biochem J*, 444, 127-139.

29. Alberts B, *et al* (2008) *Molecular Biology of the Cell*, (Garland Science, New York).
30. Landes T & Martinou JC. (2011). Mitochondrial outer membrane permeabilization during apoptosis: The role of mitochondrial fission. *Biochim Biophys Acta*, 1813, 540-545.
31. Antignani A & Youle RJ. (2006). How do bax and bak lead to permeabilization of the outer mitochondrial membrane?. *Curr Opin Cell Biol*, 18, 685-689.
32. Brooks C & Dong Z. (2007). Regulation of mitochondrial morphological dynamics during apoptosis by bcl-2 family proteins. *Cell Cycle*, 6(24), 3043-3047.
33. Westphal D, Dewson G, Czabotar PE, Kluck RM. (2011). Molecular biology of bax and bak activation and action. *Biochim Biophys Acta*, 1813, 521-531.
34. Martinou JC & Youle RJ. (2011). Mitochondria in apoptosis: Bcl-2 family members and mitochondrial dynamics. *Dev Cell*, 21(1), 92-101.
35. Dupont-Versteegden E. (2005). Apoptosis in muscle atrophy: Relevance to sarcopenia. *Exp Gerontol*, 40, 473-481.
36. Armand AS, Laziz I, Djeghloul D, Lécolle S, Bertrand AT, Biondi O, De Windt LJ, Chanoine C. (2011). Apoptosis-inducing factor regulates skeletal muscle progenitor cell number and muscle phenotype. *PLoS One*, 6(11), e27283.
37. Norberg E, Orrenius S, Zhivotovsky B. (2010). Mitochondrial regulation of cell death: Processing of apoptosis-inducing factor (AIF). *Biochem Biophys Res Co*, 396, 95-100.
38. Candé C, Cecconi F, Dessen P, Kroemer G. (2002). Apoptosis-inducing factor (AIF): Key to the conserved caspase-independent pathways of cell death. *J Cell Sci*, 115, 4727-4734.

39. Zhang R, Humphreys I, Sahu RP, Shi Y, Srivastava SK. (2008). In vitro and in vivo induction of apoptosis by capsaicin in pancreatic cancer cells is mediated through ROS generation and mitochondrial death pathway. *Apoptosis*, 13, 1465-1478.
40. Seiler A, Schneider M, Förster H, Roth S, Wirth EK, Culmsee C, Plesnila N, Kremmer E, Radmark O, Wurst W, Bornkamm GW, Schweizer U, Conrad M. (2008). Glutathione peroxidase 4 senses and translates oxidative stress into 12/15-lipoxygenase dependent- and AIF-mediated cell death. *Cell Metab*, 8, 237-248.
41. Eisenberg-Lerner A, Bialik S, Simon HU, Kimchi A. (2009). Life and death partners: Apoptosis, autophagy and the cross-talk between them. *Cell Death Differ*, 16, 966-975.
42. Shen HM & Codogno P. (2012). Autophagy is a survival force via suppression of necrotic cell death. *Exp Cell Res*, 318, 1304-1308.
43. Boya P, Gonzalez-Polo A, Casares N, Perfettini JL, Dessen P, Larochette N, Métivier D, Meley D, Souquere S, Yoshimori T, Pierron G, Codogno P, Kroemer G. (2005). Inhibition of autophagy triggers apoptosis. *Mol Cell Biol*, 25(3), 1025-1040.
44. Xu HD, Wu D, Gu JH, Ge JB, Wu JC, Han R, Liang ZQ, Qin ZH. (2013). The pro-survival role of autophagy depends on bcl-2 under nutrition stress conditions. *PLoS One*, 8(5), e63232.
45. Pattingre S, Tassa A, Qu X, Garuti R, Liang XH, Mizushima N, Packer M, Schneider MD, Levine B. (2005). Bcl-2 antiapoptotic proteins inhibit beclin 1-dependent autophagy. *Cell*, 122(6), 927-939.
46. Bialik S & Kimchi A (2008). Autophagy and tumor suppression: recent advances in understanding the link between autophagic cell death pathways and tumor development in *Programmed Cell Death in Cancer Progression*, eds Khosravi-Far R & White E (Springer, pp 177-200.

47. Buytaert E, Callewaert G, Vandenheede JR, Agostinis P. (2006). Deficiency in apoptotic effectors bax and bak reveals an autophagic cell death pathway initiated by photodamage to the endoplasmic reticulum. *Autophagy*, 2(3), 238-240.
48. Buytaert E, Callewaert G, Hendrickx N, Scorrano L, Hartmann D, Missiaen L, Vandenheede JR, Heirman I, Grooten J, Agostinis P. (2006). Role of endoplasmic reticulum depletion and multidomain proapoptotic BAX and BAK proteins in shaping cell death after hypericin-mediated photodynamic therapy. *FASEB J*, 20(6), 756-758.
49. Shen HM & Codogno P. (2011). Autophagic cell death: Loch ness monster or endangered species?. *Autophagy*, 7(5), 457-465.
50. Shen S, Kepp O, Kroemer G. (2012). The end of autophagic cell death?. *Autophagy*, 8(1), 1-3.
51. Clarke PGH & Puyal J. (2012). Autophagic cell death exists. *Autophagy*, 8(6), 867-869.
52. Bassaglia Y, Cebrian J, Covan S, Garcia M, Foucrier J. (2005). Proteasomes are tightly associated to myofibrils in mature skeletal muscle. *Exp Cell Res*, 302, 221-232.
53. Murton AJ, Constantin D, Greenhaff PL. (2008). The involvement of the ubiquitin proteasome system in human skeletal muscle remodelling and atrophy. *Biochim Biophys Acta*, 1782, 730-743.
54. Passmore LA & Barford D. (2004). Getting into position: The catalytic mechanisms of protein ubiquitylation. *Biochem J*, 379, 513-525.
55. Thrower JS, Hoffman L, Rechsteiner M, Pickart CM. (2000). Recognition of the polyubiquitin signal. *EMBO J*, 19(1), 94-102.
56. Xie Y & Varshavsky A. (2000). Physical association of ubiquitin ligases and the 26S proteasome. *PNAS*, 97(6), 2497-2502.

57. Schreiber A & Peter M. (2014). Substrate recognition in selective autophagy and the ubiquitin-proteasome system. *Biochim Biophys Acta*, 1843(1), 163-181.
58. Bodine SC, Latres E, Baumhuetr S, Lai VKM, Nunez L, Clarke BA, Poueymirou WT, Panaro FJ, Na E, Dharmarajan K, Pan ZQ, Valenzuela DM, DeChiara TM, Stitt TN, Yancopoulos GD, Glass DJ. (2001). Identification of ubiquitin ligases required for skeletal muscle atrophy. *Science*, 294, 1704-1708.
59. Clarke BA, Drujan D, Willis MS, Murphy LO, Corpina RA, Burova E, Rakhilin SV, Stitt TN, Patterson C, Latres E, Glass DJ. (2007). The E3 ligase MuRF1 degrades myosin heavy chain protein in dexamethasone-treated skeletal muscle. *Cell Metab*, 6, 376-385.
60. Fielitz J, Kim MS, Shelton JM, Latif S, Spencer JA, Glass DJ, Richardson JA, Bassel-Duby R, Olson EN. (2007). Myosin accumulation and striated muscle myopathy result from the loss of muscle RING finger 1 and 3. *J Clin Invest*, 117(9), 2486-2495.
61. Lokireddy S, Wijesoma IW, Bonala S, Wei M, Sze SK, McFarlane C, Kambadur R, Sharma M. (2012). Myostatin is a novel tumoral factor that induces cancer cachexia. *Biochem J*, 446, 23-36.
62. Gomes MD, Lecker SH, Jagoe RT, Navon A, Goldberg AL. (2001). Atrogin-1, a muscle-specific F-box protein highly expressed during muscle atrophy. *PNAS*, 98(25), 14440-14445.
63. Sandri M, Sandri C, Gilbert A, Skurk C, Calabria E, Picard A, Wash K, Schiaffino S, Lecker SH, Goldberg AL. (2004). Foxo transcription factors induce the atrophy-related ubiquitin ligase atrogin-1 and cause skeletal muscle atrophy. *Cell*, 117(3), 399-412.
64. Ashrafi G & Schwartz TL. (2013). The pathways of mitophagy for quality control and clearance of mitochondria. *Cell Death Differ*, 20, 31-42.

65. Youle RJ & Narendra DP. (2011). Mechanisms of mitophagy. *Nat Rev Mol Cell Bio*, 12, 9-24.
66. Ding WX & Yin XM. (2012). Mitophagy: Mechanisms, pathophysiological roles, and analysis. *Biol Chem*, 393(7), 547-564.
67. Frank M, Duvezin-Caubet S, Koob S, Occhipinti A, Jagasia R, Petcherski A, Ruonala MO, Priault M, Salin B, Salin B, Reichert AS. (2012). Mitophagy is triggered by mild oxidative stress in mitochondrial fission dependent manner. *Biochim Biophys Acta*, 1823, 2297-2310.
68. MacVicar TD & Lane JD. (2014). Impaired OMA1-dependent cleavage of OPA1 and reduced Drp1 fission activity combine to prevent mitophagy in cells that are dependent on oxidative phosphorylation. *J Cell Sci*, 127(10), 2313-2325.
69. Jin SM & Youle RJ. (2012). PINK1- and parkin-mediated mitophagy at a glance. *J Cell Sci*, 125, 4-795.
70. Deas E, Plun-Favreau H, Gandhi S, Desmond H, Kjaer S, Loh SHY, Renton AEM, Harvey RJ, Whitworth AJ, Martins LM, Abramov AY, Wood NW. (2011). PINK1 cleavage at position A103 by the mitochondrial protease PARL. *Hum Mol Genet*, 20(5), 867-879.
71. Lin W & Kang UJ. (2008). Characterization of PINK1 processing, stability, and subcellular localization. *J Neurochem*, 106(1), 464-474.
72. Jin SM, Lazarou M, Wang C, Kane LA, Narendra DP, Youle RJ. (2010). Mitochondrial membrane potential regulates PINK1 import and proteolytic destabilization by PARL. *J Cell Biol*, 191(5), 933-942.

73. Narendra DP, Jin SM, Tanaka A, Suen DF, Gautier CA, Shen J, Cookson MR, Youle RJ. (2010). PINK1 is selectively stabilized on impaired mitochondria to activate parkin. *PLoS One*, 8(1), e1000298.
74. Matsuda N, Sato S, Shiba K, Okatsu K, Saisho K, Gautier CA, Sou Y, Saiki S, Kawajiri S, Sato F, Kimura M, Komatsu M, Hattori N, Tanaka K. (2010). PINK1 stabilized by mitochondrial depolarization recruits parkin to damaged mitochondria and activates latent parkin for mitophagy. *J Cell Biol*, 189(2), 211-221.
75. Narendra DP & Youle RJ. (2011). Targeting mitochondrial dysfunction: Role for PINK1 and parkin in mitochondrial quality control. *Antioxid Redox Signal*, 14(10), 1929-1938.
76. Kawajiri S, Saiki S, Sato S, Sato F, Hatano T, Eguchi H, Hattori N. (2010). PINK1 is recruited to mitochondria with parkin and associates with LC3 in mitophagy. *FEBS Lett*, 584, 1073-1079.
77. Shiba K, Arai T, Sato S, Kubo S, Ohba Y, Mizuno Y, Hattori N. (2009). Parkin stabilizes PINK1 through direct interaction. *Biochem Biophys Res Commun*, 383, 331-335.
78. Vives-Bauza C, Zhou C, Huang Y, Cui M, de Vries RLA, Kim J, May J, Tocilescu MA, Liu W, Ko HS, Magrané J, Moore DJ, Dawson VL, Grailhe R, Dawson TM, Li C, Tieu K, Przedborski S. (2010). PINK1-dependent recruitment of parkin to mitochondria in mitophagy. *PNAS*, 107(1), 378-383.
79. Shiba-Fukushima K, Inoshita T, Hattori N, Imai Y. (2014). PINK1-mediated phosphorylation of parkin boosts parkin activity in drosophila. *PLoS Genet*, 10(6), e1004391.
80. Kim Y, Park J, Kim S, Song S, Kwon SK, Lee SH, Kitada T, Kim JM, Chung J. (2008). PINK1 controls mitochondrial localization of parkin through direct phosphorylation. *Biochem Biophys Res Commun*, 377(3), 975-980.

81. Sun Y, Vashisht AA, Tchiew J, Wohlschlegel JA, Dreier L. (2012). Voltage-dependent anion channels (VDACs) recruit parkin to defective mitochondria to promote mitochondrial autophagy. *J Biol Chem*, 287, 40652-40660.
82. Narendra DP, Kane LA, Hauser DN, Fearnley IM, Youle RJ. (2010). p62/SQSTM1 is required for parkin-induced mitochondrial clustering but not mitophagy; VDAC1 is dispensable for both. *Autophagy*, 6(8), 1090-1106.
83. Geisler S, Holmström KM, Skujat D, Fiesel FC, Rothfuss OC, Kahle PJ, Springer W. (2010). PINK1/parkin-mediated mitophagy is dependent on VDAC1 and p62/SQSTM1. *Nat Cell Biol*, 12(2), 119-131.
84. Zhang J & Ney PA. (2009). Role of BNIP3 and NIX in cell death, autophagy, and mitophagy. *Cell Death Differ*, 16(7), 939-946.
85. Schweers RL, Zhang L, Randall MS, Loyd MR, Li W, Dorsey FC, Kundu M, Opferman JT, Cleveland JL, Miller JL, Ney PA. (2007). NIX is required for programmed mitochondrial clearance during reticulocyte maturation. *PNAS*, 104(49), 19500-19505.
86. Zhang J & Ney PA. (2008). NIX induces mitochondrial autophagy in reticulocytes. *Autophagy*, 4(3), 354-356.
87. Novak I, Kirkin V, McEwan DG, Zhang J, Wild P, Rozenknop A, Rogov V, Löhr F, Popovic D, Occhipinti A, Reichert AS, Terzic J, Dötsch V, Ney PA, Dikic I. (2010). Nix is a selective autophagy receptor for mitochondrial clearance. *EMBO Rep*, 11(1), 45-51.
88. Powers SK, Wiggs MP, Duarte JA, Zergeroglu AM, Dmirel HA. (2012). Mitochondrial signaling contributes to disuse muscle atrophy. *Am J Physiol Endocrinol Metab*, 303, E31-E39.

89. Romanello V, Guadagnin E, Gomes L, Roder I, Sandri C, Petersen Y, Milan G, Masiero E, Del Piccolo P, Foretz M, Scorrano L, Rudolf R, Sandri M. (2010). Mitochondrial fission and remodelling contributes to muscle atrophy. *EMBO J*, 29, 1774-1785.
90. O'Leary MFN, Vainshtein A, Carter HN, Zhang Y, Hood DA. (2012). Denervation-induced mitochondrial dysfunction and autophagy in skeletal muscle of apoptosis-deficient animals. *Am J Physiol Cell Physiol*, 303, C447-C454.
91. Furuya N, Ikeda SI, Sato S, Soma S, Ezaki J, Trejo JAO, Takeda-Ezaki M, Fujimura T, Arikawa-Hirasawa E, Tada N, Komatsu M, Tanaka K, Kominami E, Hattori N, Ueno T. (2014). PARK2/parkin-mediated mitochondrial clearance contributes to proteasome activation during slow-twitch muscle atrophy via NFE2L1 nuclear translocation. *Autophagy*, 10(4), 631-641.
92. Mitsuhashi S & Nishino I. (2011). Phospholipid synthetic defect and mitophagy in muscle disease. *Autophagy*, 7(12), 1559-1562.
93. Sandri M. (2010). Autophagy in skeletal muscle. *FEBS Lett*, 584(7), 1411-1416.
94. Mammucari C, Milan G, Romanello V, Masiero E, Rudolf R, Del Piccolo P, Burden SJ, Di Lisi R, Sandri C, Zhao J, Goldberg AL, Schiaffino S, Sandri M. (2007). FoxO3 controls autophagy in skeletal muscle in vivo. *Cell Metab*, 6, 458-471.
95. Kawajiri S, Saiki S, Sato S, Hattori N. (2011). Genetic mutations and functions of PINK1. *Trends Pharmacol Sci*, 32(10), 573-580.
96. Twig G, Elorza A, Molina AJA, Mohamed H, Wikstrom J, Walzer G, Stiles L, Haigh SE, Katz S, Las G, Alroy J, Wu M, Py BF, Yuan J, Deeney JT, Corkey BE, Shirihai OS. (2008). Fission and selective fusion govern mitochondrial segregation and elimination by autophagy. *EMBO J*, 27, 433-446.

97. Smuder AJ, Kavazis AN, Min K, Powers SK. (2011). Exercise protects against doxorubicin-induced markers of autophagy signaling in skeletal muscle. *J Appl Physiol*, *111*, 1190-1198.
98. Bhatnagar S, Mittal A, Gupta SK, Kumar A. (2012). TWEAK causes myotube atrophy through coordinated activation of ubiquitin-proteasome system, autophagy, and caspases. *J Cell Physiol*, *227*(3), 1042-1051.
99. Masiero E & Sandri M. (2010). Autophagy inhibition induces atrophy and myopathy in adult skeletal muscles. *Autophagy*, *6*(2), 307-310.
100. Vanhorebeek I, Gunst J, Derde S, Derese I, Boussemaere M, Güiza F, Martinet W, Timmermans JP, D'Hoore A, Wouters PJ, Van den Berghe G. (2011). Insufficient activation of autophagy allows cellular damage to accumulate in critically ill patients. *J Clin Endocrinol Metab*, *96*(4), E633-E645.
101. Grumati P, Coletto L, Schiavinato S, Castagnaro S, Bertaggia E, Sandri M, Bonaldo P. (2011). Physical exercise stimulates autophagy in normal skeletal muscles but is detrimental for collagen VI-deficient muscles. *Autophagy*, *7*(12), 1415-1423.
102. Grumati P, Coletto L, Sandri M, Bonaldo P. (2011). Autophagy induction rescues muscular dystrophy. *Autophagy*, *7*(4), 426-428.
103. Pagano AF, Py G, Bernardi H, Candau RB, Sanchez AMJ. (2014). Autophagy and protein turnover signaling in slow-twitch muscle during exercise. *Med Sci Sport Exer*, *46*(7), 1314-1325.
104. Jamart C, Naslain D, Gilson H, Francaux M. (2013). Higher activation of autophagy in skeletal muscle of mice during endurance exercise in the fasted state. *Am J Physiol Endocrinol Metab*, *305*, E964-E974.

105. Argilés JM, Lopez-Soriano FJ, Busquets S. (2008). Apoptosis signalling is essential and precedes protein degradation in wasting skeletal muscle during catabolic conditions. *Int J Biochem Cell B*, 40(9), 1674-1678.
106. Allen DL, Linderman JK, Roy RR, Bigbee AJ, Grindeland RE, Mukku V, Edgerton VR. (1997). Apoptosis: A mechanism contributing to remodeling of skeletal muscle in response to hindlimb unweighting. *Am J Physiol*, 273(2 Pt 1), C579-C587.
107. Teng BT, Tam EW, Benzie IF, Siu PM. (2011). Protective effect of caspase inhibition on compression-induced muscle damage. *J Physiol*, 589(13), 3349-3369.
108. Stratos I, Li Z, Rotter R, Herlyn P, Mittlmeier T, Vollmar B. (2012). Inhibition of caspase mediated apoptosis restores muscle function after crush injury in rat skeletal muscle. *Apoptosis*, 17, 269-277.
109. Talbert EE, Smuder AJ, Min K, Kwon OS, Powers SK. (2013). Calpain and caspase-3 play required roles in immobilization-induced muscle atrophy. *J Appl Physiol*, 114, 1482-1489.
110. Plant PJ, Bain JR, Correa JE, Woo M, Batt J. (2009). Absence of caspase-3 protects against denervation-induced skeletal muscle atrophy. *J Appl Physiol*, 107(1), 224-234.
111. Du J, Wang X, Miereles C, Bailey JL, Debigare R, Zheng B, Price SR, Mitch WE. (2004). Activation of caspase-3 is an initial step triggering accelerated muscle proteolysis in catabolic conditions. *J Clin Invest*, 113(1), 115-123.
112. Gundersen K & Bruusgaard JC. (2008). Nuclear domains during muscle atrophy: Nuclei lost or paradigm lost?. *J Physiol*, 586, 2675-2681.

113. Alway SE & Siu PM. (2008). Nuclear apoptosis contributes to sarcopenia. *Exerc Sport Sci Rev*, 36(2), 51-57.
114. McMillan EM & Quadrilatero J. (2011). Differential apoptosis-related protein expression, mitochondrial properties, proteolytic enzyme activity, and DNA fragmentation between skeletal muscles. *Am J Physiol Reg I*, 300(3), R531-R543.
115. Wu JJ, Quijano C, Chen E, Liu H, Cao L, Fergusson MM, Rovira II, Gutkind S, Daniels MP, Komatsu M, Finkel T. (2009). Mitochondrial dysfunction and oxidative stress mediate the physiological impairment induced by the disruption of autophagy. *Aging*, 1(4), 425-437.
116. Masiero E, Agatea L, Mammucari C, Blaauw B, Loro E, Komatsu M, Metzger D, Reggiani C, Schiaffino S, Sandri M. (2009). Autophagy is required to maintain muscle mass. *Cell Metab*, 10(6), 507-515.
117. Kim KH, Jeong YT, Oh H, Kim SH, Cho JM, Kim YN, Kim SS, Kim DH, Hut KY, Kim HK, Ko T, Han J, Kim HL, Kim J, Back SH, Komatsu M, Chen H, Chan DC, Konishi M, Itoh N, Choi CS, Lee MS. (2013). Autophagy deficiency leads to protection from obesity and insulin resistance by inducing Fgf21 as a mitokine. *Nat Med*, 19(1), 83-93.
118. Raben N, Schreiner C, Baum R, Takikita S, Xu S, Xie T, Myerowitz R, Komatsu M, Van der Meulen JH, Nagaraju K, Ralston E, Plotz PH. (2010). Suppression of autophagy permits successful enzyme replacement therapy in a lysosomal storage disorder--murine pompe disease. *Autophagy*, 6(8), 1078-1089.
119. Fry CS, Drummond MJ, Lujan HL, Di Carlo SE, Rasmussen BB. (2012). Paraplegia increases skeletal muscle autophagy. *Muscle Nerve*, 46(5), 793-798.

120. Hussain SN, Mofarrahi M, Sigala I, Kim HC, Vassilakopoulos T, Maltais F, Bellenis I, Chaturvedi R, Gottfried SB, Metrakos P, Danialou G, Matecki S, Jaber S, Petrof BJ, Goldberg P. (2010). Mechanical ventilation-induced diaphragm disuse in humans triggers autophagy. *Am J Resp Crit Care*, 182(11), 1377-1386.
121. Nascimbeni AC, Fanin M, Masiero E, Angelini C, Sandri M. (2012). Impaired autophagy contributes to muscle atrophy in glycogen storage disease type II patients. *Autophagy*, 8(11), 1697-1700.
122. Pette D & Staron RS. (2001). Transitions of muscle fiber phenotypic profiles. *Histochem Cell Biol*, 115, 359-372.
123. Kuhn R & Torres RM. (2002). Cre/loxP recombination system and gene targeting. *Method Mol Cell Biol*, 180, 175-204.
124. Rao P & Monks DA. (2009). A tetracycline-inducible and skeletal muscle-specific cre recombinase transgenic mouse. *Dev Neurobiol*, 69(6), 401-406.
125. Komatsu M, Waguri S, Ueno T, Iwata J, Murata S, Tanida I, Ezaki J, Mizushima N, Ohsumi Y, Uchiyama Y, Kominami E, Tanaka K, Chiba T. (2005). Impairment of starvation-induced and constitutive autophagy in Atg7-deficient mice. *J Cell Biol*, 169(3), 425-434.
126. Bloemberg D & Quadrilatero J. (2012). Rapid determination of myosin heavy chain expression in rat, mouse, and human skeletal muscle using multicolor immunofluorescence analysis. *PLoS One*, 7(4), e35273.
127. Quadrilatero J & Bloemberg D. (2010). Apoptosis repressor with caspase recruitment domain is dramatically reduced in cardiac, skeletal, and vascular smooth muscle during hypertension. *Biochem Bioph Res Co*, 391, 1437-1452.

128. McMillan EM, Graham DA, Rush JW, Quadrilatero J. (2012). Decreased DNA fragmentation and apoptotic signaling in soleus muscle of hypertensive rats following 6 weeks of treadmill training. *J Appl Physiol*, 113, 1048-1057.
129. Young B & Heath JW (2000) *Wheater's Functional Histology, 4th ed.* (Churchill Livingstone, Toronto).
130. Luzio JP, Pryor PR, Bright NA. (2007). Lysosomes: Fusion and function. *Nat Rev Mol Cell Biol*, 8(8), 622-632.
131. Mizushima N & Komatsu M. (2011). Autophagy: Renovation of cells and tissues. *Cell*, 147(4), 728-741.
132. Kuma A, Hatano M, Matsui M, Yamamoto A, Nakaya H, Yoshimori T, Ohsumi Y, Tokuhiisa T, Mizushima N. (2004). The role of autophagy during the early neonatal starvation period. *Nature*, 432(7020), 1032-1036.
133. Schiaffino S & Reggiani C. (1996). Molecular diversity of myofibrillar proteins: Gene regulation and functional significance. *Physiol Rev*, 76(2), 371-423.
134. Mofarrahi M, Guo Y, Haspel JA, Choi AMK, Davis EC, Gouspillou G, Hepple RT, Godin R, Burelle Y, Hussain SNA. (2013). Autophagic flux and oxidative capacity of skeletal muscles during acute starvation. *Autophagy*, 9(10), 1604-1620.
135. Wigston DJ & English AW. (1991). Fibre-type proportions in mammalian soleus muscle during postnatal development. *J Neurobiol*, 23(1), 61-70.
136. Watchko JF, Daood MJ, Labella JJ. (1996). Creatine kinase activity in rat skeletal muscle relates to myosin phenotype during development. *Pediatr Res*, 40, 53-58.

137. Cox RD & Buckingham ME. (1992). Actin and myosin genes are transcriptionally regulated during mouse skeletal muscle development. *Dev Biol*, 149(1), 228-234.
138. Tondelair D, Vandamme D, Vandekerckhove J, Ampe C, Lambrechts A. (2009). Actin isoform expression patterns during mammalian development and in pathology: Insights from mouse models. *Cell Motil Cytoskel*, 66, 798-815.
139. Lira VA, Okutsu M, Zhang M, Greene NP, Laker RC, Breen DS, Hoehn KL, Yan Z. (2013). Autophagy is required for exercise training-induced skeletal muscle adaptation and improvement of physical performance. *FASEB J*, 27(10), 4184-4193.
140. Sanchez AMJ, Bernardi H, Py G, Candau R. (2014). Autophagy is essential to support skeletal muscle plasticity in response to endurance exercise. *Am J Physiol Regul Integr Comp Physiol*, in press
141. Sasaoka T, Imamura M, Araishi K, Noguchi S, Mizuno Y, Takagoshi N, Hama H, Wakabayashi-Takai E, Yoshimoto-Matsuda Y, Nonaka I, Kaneko K, Yoshida M, Ozawa E. (2003). Pathological analysis of muscle hypertrophy and degeneration in muscular dystrophy in γ -sarcoglycan-deficient mice. *Neuromuscular Disord*, 13, 193-206.
142. Faber RM, Hall JK, Chamberlain JS, Banks GB. (2014). Myofiber branching rather than myofiber hyperplasia contributes to muscle hypertrophy in *mdx* mice. *Skeletal Muscle*, 4(10)
143. Pastoret C & Sebillé A. (1995). Mdx mice show progressive weakness and muscle deterioration with age. *J Neurol Sci*, 129, 97-105.
144. Fukada S, Morikawa D, Yamamoto Y, Yoshida T, Sumie N, Yamaguchi M, Ito Y, Miyagoe-Suzuki Y, Takeda S, Tsujikawa K, Yamamoto H. (2010). Genetic background affects properties of satellite cells and mdx phenotypes. *Am J Pathol*, 176(5), 2414-2424.

145. Ciciliot S, Rossi AC, Dyar KA, Blaauw B, Schiaffino S. (2013). Muscle type and fibre type specificity in muscle wasting. *Int J Biochem Cell B*, 45, 2191-2199.
146. Sasaki K, Tsuno NH, Sunami E, Tsurita G, Kawai K, Okaji Y, Nishikawa T, Shuno Y, Hongo K, Hiyoshi M, Kaneko M, Kitayama J, Takahashi K, Nagawa H. (2010). Chloroquine potentiates the anti-cancer effect of 5-fluorouracil on colon cancer cells. *BMC Cancer*, 10(370)
147. Kanematsu S, Uehara N, Miki H, Yoshizawa K, Kawanaka A, Yuri T, Tsubura A. (2010). Autophagy inhibition enhances sulforaphane-induced apoptosis in human breast cancer cells. *Anticancer Res*, 30(9), 3381-3390.
148. Fiorini C, Menegazzi M, Padroni C, Dando I, Dalla Pozza E, Gregorelli A, Costanzo C, Palmieri M, Donadelli M. (2013). Autophagy induced by p53-reactivating molecules protects pancreatic cancer cells from apoptosis. *Apoptosis*, 18(3), 337-346.
149. Cai N, Zhao X, Jing Y, Sun K, Jiao S, Chen X, Yang H, Zhou Y, Wei L. (2014). Autophagy protects against palmitate-induced apoptosis in hepatocytes. *Cell Biosci*, 4(28)
150. Yousefi S, Perozzo R, Schmid I, Ziemiecki A, Schaffner T, Scapozza L, Brunner T, Simon HU. (2006). Calpain-mediated cleavage of Atg5 switches autophagy to apoptosis. *Nat Cell Biol*, 8(10), 1124-1132.
151. Hara T, Nakamura K, Matsui M, Yamamoto A, Nakahara Y, Suzuki-Migishima R, Yokoyama M, Mishima K, Saito I, Okano H, Mizushima N. (2006). Suppression of basal autophagy in neural cells causes neurodegenerative disease in mice. *Nature*, 441(15), 885-889.
152. Onal M, Piemontese M, Xiong J, Wang Y, Han L, Ye S, Komatsu M, Selig M, Weinstein RS, Zhao H, Jilka RL, Almeida M, Manolagas SC, O'Brien CA. (2013). Suppression of autophagy in osteocytes mimics skeletal aging. *J Biol Chem*, 288(24), 17423-17440.

153. Jung HS, Chung KW, Kim JW, Kim J, Komatsu M, Tanaka K, Nguyen YH, Kang TM, Yoon KH, Kim JW, Jeong YT, Han MS, Lee MK, Kim KW, Shin J, Lee MS. (2008). Loss of autophagy diminishes pancreatic β cell mass and function with resultant hyperglycemia. *Cell Metab*, 8, 318-324.
154. Nakai A, Yamaguchi O, Takeda T, Higuchi Y, Hikoso S, Taniike M, Omiya S, Mizote I, Matsumura Y, Asahi M, Nishida K, Hori M, Mizushima N, Otsu K. (2007). The role of autophagy in cardiomyocytes in the basal state and in response to hemodynamic stress. *Nat Med*, 13(5), 619-624.
155. Mortensen M, Ferguson DJP, Edelmann M, Kessler B, Morten KJ, Komatsu M, Simon AK. (2010). Loss of autophagy in erythroid cells leads to defective removal of mitochondria and severe anemia in vivo. *PNAS*, 107(2), 832-837.
156. Han J, Hou W, Goldstein LA, Lu C, Stolz DB, Yin XM, Rabinowich H. (2008). Involvement of protective autophagy in TRAIL resistance of apoptosis-defective tumor cells. *J Biol Chem*, 283(28), 19665-19677.
157. Hou W, Han J, Lu C, Goldstein LA, Rabinowich H. (2010). Autophagic degradation of active caspase-8: A crosstalk mechanism between autophagy and apoptosis. *Autophagy*, 6(7), 891-900.
158. Demarchi F & Schneider C. (2007). The calpain system as a modulator of stress/damage response. *Cell Cycle*, 6(2), 136-138.
159. Demarchi F, Bertoli C, Copetti T, Tanida I, Brancolini C, Eskelinen EL, Schneider C. (2006). Calpain is required for macroautophagy in mammalian cells. *J Cell Biol*, 175(4), 595-605.
160. Lépine S, Allegood JC, Edmonds Y, Milstien S, Spiegel S. (2011). Autophagy induced by deficiency of sphingosine-1-phosphate phosphohydrolase 1 is switched to apoptosis by calpain-mediated autophagy-related gene 5 (Atg5) cleavage. *J Biol Chem*, 286(52), 44380-44390.

161. Russell AP, Foletta VC, Snow RJ, Wadley GD. (2014). Skeletal muscle mitochondria: A major player in exercise, health and disease. *Biochim Biophys Acta*, 1840, 1276-1284.
162. Bin-Umer MA, McLaughling JE, Butterly MS, McCormick S, Tumer NE. (2014). Elimination of damaged mitochondria through mitophagy reduces mitochondrial oxidative stress and increases tolerance to trichothecenes. *P Natl Acad Sci USA*, 111(32), 11798-11803.
163. Ha JY, Kim JS, Kim SE, Son JH. (2014). Simultaneous activation of mitophagy and autophagy by staurosporine protects against dopaminergic neuronal cell death. *Neurosci Lett*, 561, 101-106.
164. Eiyama A, Kondo-Okamoto N, Okamoto K. (2013). Mitochondrial degeneration during starvation is selective and temporally distinct from bulk autophagy in yeast. *FEBS Lett*, 587(12), 1787-1792.
165. Kanki T, Wang K, Cao Y, Baba M, Klionsky DJ. (2009). Atg32 is a mitochondrial protein that confers selectivity during mitophagy. *Dev Cell*, 17(1), 98-109.
166. Kissova I, Deffieu M, Manon S, Camougrand N. (2004). Uth1p is involved in the autophagic degradation of mitochondria. *J Biol Chem*, 279(37), 39068-39074.
167. Fiesel FC, Moussaud-Lamodière EL, Ando M, Spinger W. (2014). A specific subset of E2 ubiquitin-conjugating enzymes regulate parkin activation and mitophagy differently. *J Cell Sci*, 127(16), 3488-3504.
168. Okatsu K, Uno M, Koyano F, Go E, Kimura M, Oka T, Tanaka K, Matsuda N. (2013). A dimeric PINK1-containing complex on depolarized mitochondria stimulates parkin recruitment. *J Biol Chem*, 288, 36372-36384.

169. Fedorowicz MA, de Vries-Schneider RLA, Rüb C, Becker D, Huang Y, Zhou C, Alessi Wolken DM, Voos W, Liu Y, Przedborski S. (2014). Cytosolic cleaved PINK1 represses parkin translocation to mitochondria and mitophagy. *EMBO Rep*, 15(1), 86-93.
170. Paul PK & Kumar A. (2011). TRAF6 coordinates the activation of autophagy and ubiquitin-proteasome systems in atrophying skeletal muscle. *Autophagy*, 7(5), 555-556.
171. Driscoll JJ & Chowdhury RD. (2012). Molecular crosstalk between the proteasome, aggresomes and autophagy: Translational potential and clinical implications. *Cancer Lett*, 325(2), 147-154.
172. Selimovic D, Porzig BB, El-Khattouti A, Badura HE, Ahmad M, Ghanjati F, Santourlidis S, Haikel Y, Hassan M. (2013). Bortezomib/proteasome inhibitor triggers both apoptosis and autophagy-dependent pathways in melanoma cells. *Cell Signal*, 25(1), 308-318.
173. Kageyama S, Sou YS, Uemura T, Kametaka S, Saito T, Ishimura R, Kouno T, Bedford L, Mayer RJ, Lee MS, Yamamoto M, Waguri S, Tanaka K, Komatsu M. (2014). Proteasome dysfunction activates autophagy and the Keap1-Nrf2 pathway. *J Biol Chem*, in press
174. Wang XJ, Yu J, Wong SH, Cheng AS, Chan FK, Ng SS, Cho CH, Sung JJ, Wu WK. (2013). A novel crosstalk between two major protein degradation systems: Regulation of proteasomal activity by autophagy. *Autophagy*, 9(10), 1500-1508.
175. Korolchuk VI, Mansilla A, Menzies FM, Rubinsztein DC. (2009). Autophagy inhibition compromises degradation of ubiquitin-proteasome pathway substrates. *Mol Cell*, 33(4), 517-527.
176. Pallafacchina G, Blaauw B, Schiaffino S. (2013). Role of satellite cells in muscle growth and maintenance of muscle mass. *Nutr Metab Cardiovasc*, 23, S12-S18.

177. White RB, Biérinx AS, Gnocchi VF, Zammit PS. (2010). Dynamics of muscle fibre growth during postnatal mouse development. *BMC Dev Biol*, 10(21)
178. Kuranaga E. (2011). Caspase signaling in animal development. *Develop Growth Differ*, 53, 137-148.
179. Zakeri Z, Lockshin RA, Criado-Rodriguez LM, Martinez AC. (2005). A generalized caspase inhibitor disrupts early mammalian development. *Int J Dev Biol*, 49(1), 43-47.
180. Miura M. (2012). Apoptotic and nonapoptotic caspase functions in animal development. *Cold Spring Harb Perspect Biol*, 4, a008664.
181. Fernando P, Kelly JF, Balazsi K, Slack RS, Megeney LA. (2002). Caspase 3 is required for skeletal muscle differentiation. *Proc Natl Acad Sci U S A*, 99(17), 11025-11030.
182. Altun M, Besche HC, Overkleeft HS, Piccirillo R, Edelmann MJ, Kessler BM, Goldberg AL, Ulfhake B. (2010). Muscle wasting in aged, sarcopenic rats is associated with enhanced activity of the ubiquitin proteasome pathway. *J Biol Chem*, 285(51), 39597-39608.
183. Clavel S, Coldefy AS, Kurkdjian E, Salles J, Margaritis I, Derijard B. (2006). Atrophy-related ubiquitin ligases, atrogin-1 and MuRF1 are up-regulated in aged rat tibialis anterior muscle. *Mech Ageing Dev*, 127(10), 794-801.
184. Perera S, Mankoo B, Gautel M. (2012). Developmental regulation of MURF E3 ubiquitin ligases in skeletal muscle. *J Muscle Res Cell Motil*, 33(2), 107-122.
185. Hale AN, Ledbetter DJ, Gawriluk TR, Rucker EB, III. (2013). Autophagy: Regulation and role in development. *Autophagy*, 9(7), 951-972.

186. Pollack M, Phaneuf S, Dirks A, Leeuwenburgh C. (2002). The role of apoptosis in the normal aging brain, skeletal muscle, and heart. *Ann N Y Acad Sci*, 959, 93-107.
187. Yang Y, Hu L, Zheng H, Mao C, Hu W, Xiong K, Wang F, Liu C. (2013). Application and interpretation of current autophagy inhibitors and activators. *Acta Pharmacol Sin*, 34, 625-635.
188. Klionsky DJ, Abeliovitch H, Agostinis P, Agrawal DK, Aliev G, Askew DS, Baba M, Baehrecke EH, Bahr BA, Ballabio A, Bamber BA, Bassham DC, Bergamini E, Bi X, Biard-Piechaczyk M, Blum JS, Bredezen DE, Brodsky JL, Brumell JH, Brunk UT, Bursch W, Camougrand N, Cebollero E, Cecconi F, Chen Y, Chin LS, Choi A, Chu CT, Chung J, Clarke PGH, Clark RSB, Clarke SG, Clavé C, Cleveland JL, Codogno P, Colombo MI, Coto-Montes A, Cregg JM, Cuervo AM, Debnath J, Demarchi F, Dennis PB, Dennis PA, Deretic V, Devenish RJ, Di Sano F, Dice JF, DiFiglia M, Dinesh-Kumar S, Distelhorst CW, Djavaheri-Mergny M, Dorsey FC, Dröge W, Dron M, Dunn WAJ, Duszenko M, Eissa NT, Elazar Z, Esclatine A, Eskelinen EL, Fésüs L, Finley KD, Fuentes JM, Fueyo J, Fujisaki K, Gaillot B, Gao FB, Gewirtz DA, Gibson SB, Gohla A, Goldberg AL, Gonzalez R, González-Estévez C, Gorski S, Gottlieb RA, Häussinger D, He YW, Heidenreich K, Hill JA, Hoyer-Hansen M, Hu X, Huang WP, Iwasaki A, Jäätelä M, Jackson WT, Jiang X, Jin S, Johansen T, Jung JU, Kadowaki M, Kang C, Kelekar A, Kessel DH, Kiel JAKW, Kim HP, Kimchi A, Kinsella TJ, Kiselyov K, Kitamoto K, Knecht E, Komatsu M, Kominami E, Kondo S, Kovács AL, Kroemer G, Kuan CY, Kumar R, Kundu M, Landry J, Laporte M, Le W, Lei HY, Lenardo MJ, Levine B, Lieberman A, Lim KL, Lin FC, Liou W, Liu LF, Lopez-Berestein G, López-Otín C, Lu B, Macleod KF, Malorni W, Martinet W, Matsuoka K, Mautner J, Meijer AJ, Meléndez A, Michels P, Miotto G, Mistiaen WP, Mizushima N, Mograbi B, Monastyrska I, Moore MN, Moreira PI, Moriyasu Y, Motyl T, Münz C, Murphy LO, Naqvi NI, Neufeld TP, Nishino I, Nixon RA, Noda T, Nürnberg B, Ogawa M, Oleinick NL, Olsen LJ, Ozpolat B, Paglin S, Palmer GE, Papassideri I, Parkes M, Perlmutter DH, Perry G, Piacentini M, Pinkas-Kramarski R, Prescott M, Proikas-Cezanne T, Raben N, Rami A, Reggiori F, Rohrer B, Rubinsztein DC, Ryan

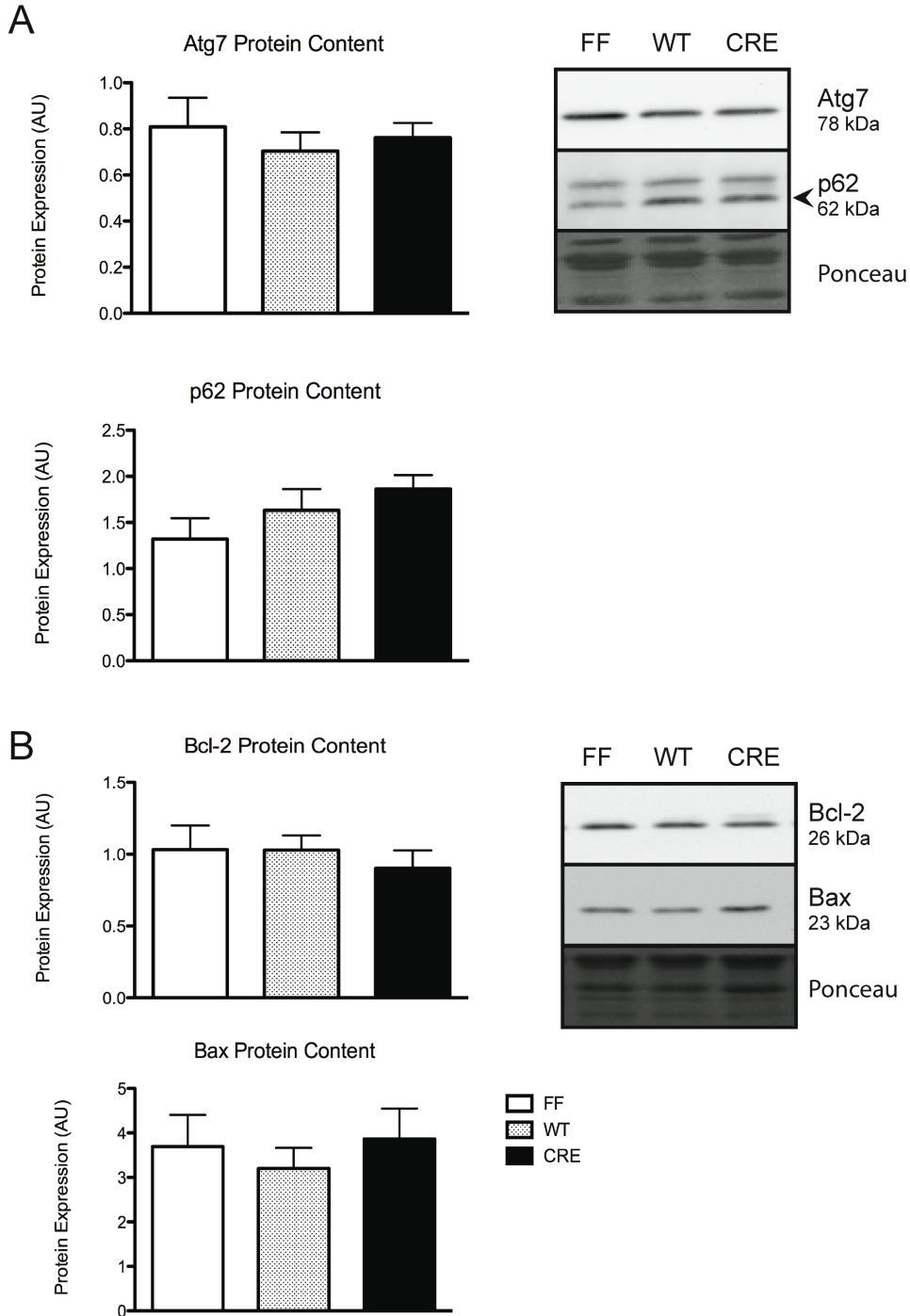
KM, Sadoshima J, Sakagami H, Sakai Y, Sandri M, Sasakawa C, Sass M, Schneider C, Seglen PO, Seleverstov O, Settleman J, Shacka JJ, Shapiro IM, Sibirny A, Silva-Zacarin ECM, Simon HU, Simone C, Simonsen A, Smith MA, Spanel-Boroski K, Srinivas V, Steeves M, Stenmark H, Stromhaug PE, Subauste CS, Sugimoto S, Sulzer D, Suzuki T, Swanson MS, Tabas I, Takeshita F, Talbot NJ, Tallóczy Z, Tanaka K, Tanaka K, Tanida I, Taylor GS, Taylor JP, Terman A, Tettamanti G, Thompson CB, Thumm M, Tolkovsky AM, Tooze SA, Truant R, Tumanovska LV, Uchiyama Y, Ueno T, Uzcátegui NL, van der Klei I, Vaquero EC, Vellai T, Vogel MW, Wang HG, Webster P, Yap G, Yin XM, Yoshimori T, Yu L, Yue Z, Yuzaki M, Zahirnyk O, Zheng X, Zhu X, Deter RL. (2008). Guidelines for the use and interpretation of assays for monitoring autophagy in higher eukaryotes. *Autophagy*, 4(2), 151-175.

189. Mizushima N & Yoshimori T. (2007). How to interpret LC3 immunoblotting. *Autophagy*, 3(6), 542-545.

190. Wohlgemuth SE, Seo AY, Marzetti E, Lees HA, Leeuwenburgh C. (2010). Skeletal muscle autophagy and apoptosis during aging: Effects of calorie restriction and life-long exercise. *Exp Gerontol*, 45(2), 138-148.

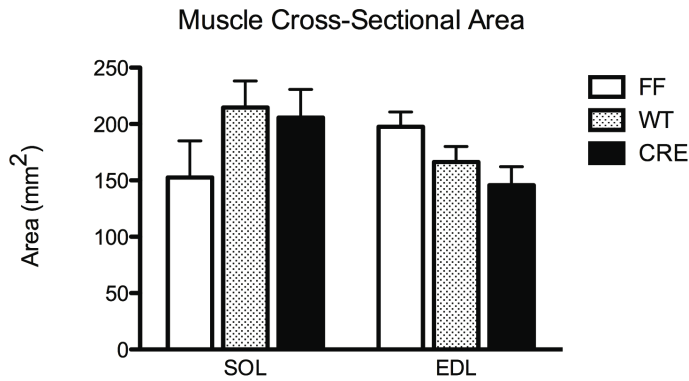
191. He C, Bassik MC, Moresi V, Sun K, Wei Y, Zou Z, An Z, Loh J, Fisher J, Sun Q, Korsmeyer S, Packer M, May HI, Hill JA, Virgin HW, Gilpin C, Xiao G, Bassel-Duby R, Scherer PE, Levine B. (2012). Exercise-induced BCL2-regulated autophagy is required for muscle glucose homeostasis. *Nature*, 481(7382), 511-515.

Appendix

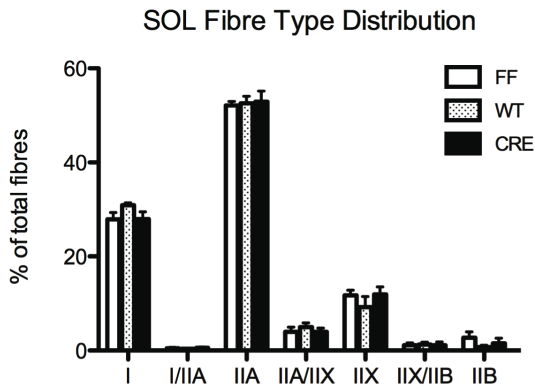


Appendix Figure 1. Use of *Flox/Flox* littermates as controls. White gastrocnemius samples were used to compare *Flox/Flox* control animals (FF) to Cre-negative (WT) and -positive (CRE) animals. A: Quantitative analysis and representative immunoblots of Atg7 and p62 protein expression in FF, WT, and CRE animals. The p62 blot is a reprobe of the Atg7 blot. B: Quantitative analysis and representative immunoblots of apoptotic proteins Bcl-2 and Bax expression in FF, WT, and CRE animals. Ponceau-stained membranes are shown as loading and transfer controls (n = 6).

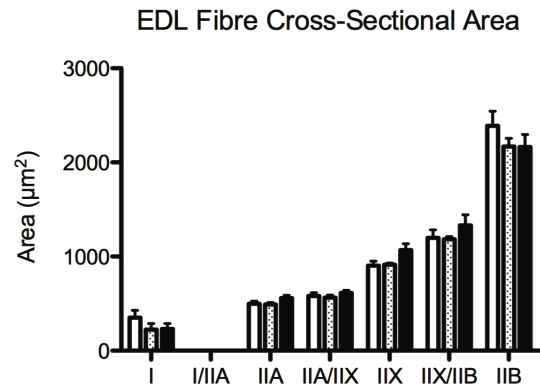
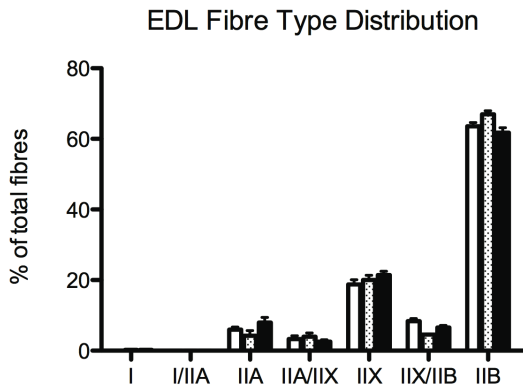
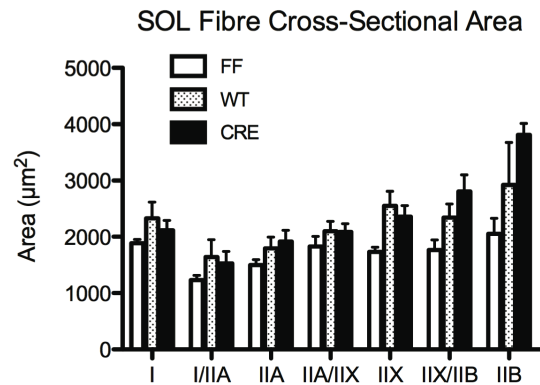
A



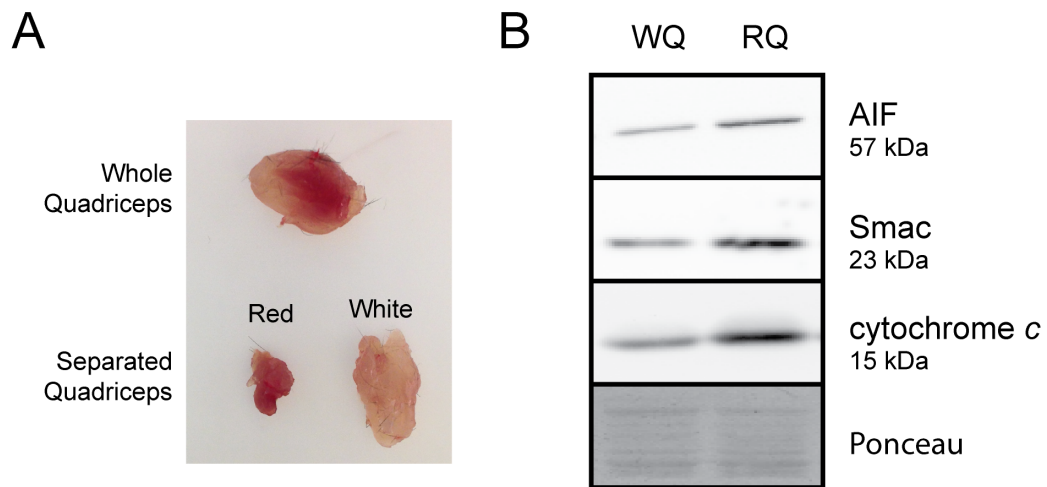
B



C

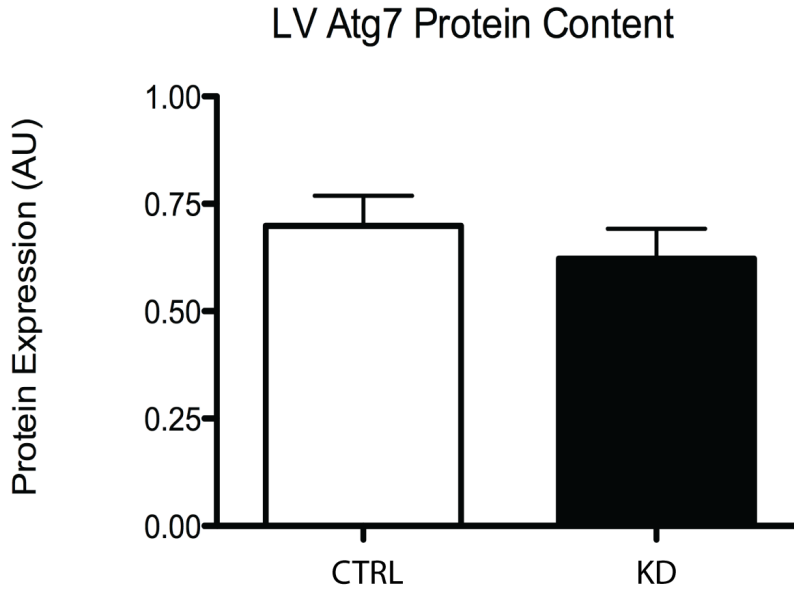


Appendix Figure 2. Immunohistological analyses of *Flox/Flox* control animals. Soleus (SOL) and extensor digitorum longus (EDL) cross-sections were used to compare morphological characteristics between *Flox/Flox* control animals (FF), Cre-negative (WT), and Cre-positive (CRE) animals. A: Total muscle cross-sectional area in SOL and EDL. B: Fibre type distribution in SOL and EDL as a percentage of total fibres. C: Fibre type-specific cross-sectional areas in SOL and EDL. (n = 4-6).

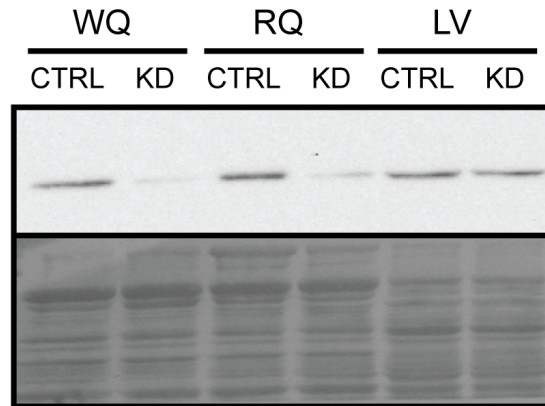


Appendix Figure 3. Validation of red and white muscle isolation procedure. Whole quadriceps muscles were visually separated into primarily red and primarily white sections. Mixed muscle was discarded. A: representative image of whole and separated quadriceps muscle, as well as isolated soleus and EDL. B: Representative immunoblots of mitochondrial markers in white quadriceps (WQ) and red quadriceps (RQ). A Ponceau-stained membrane is shown as a loading and transfer control.

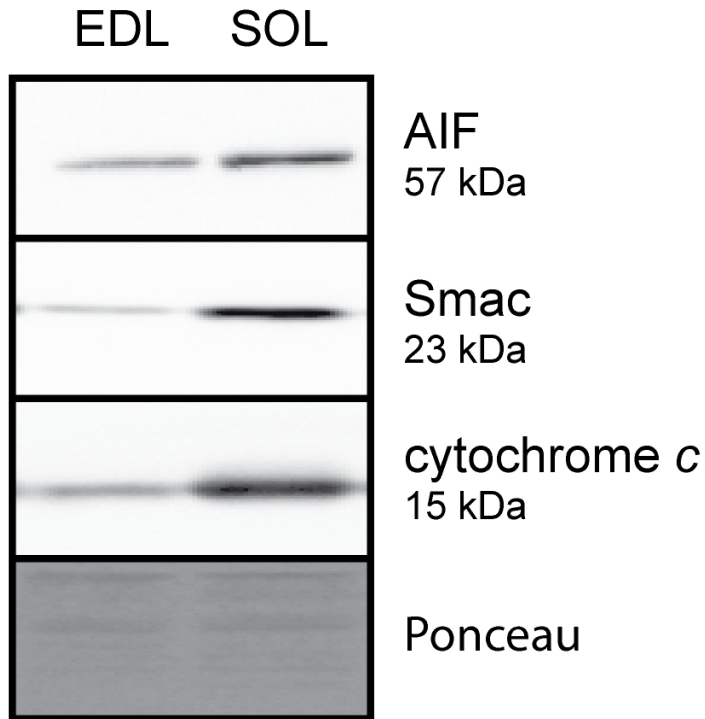
A



B

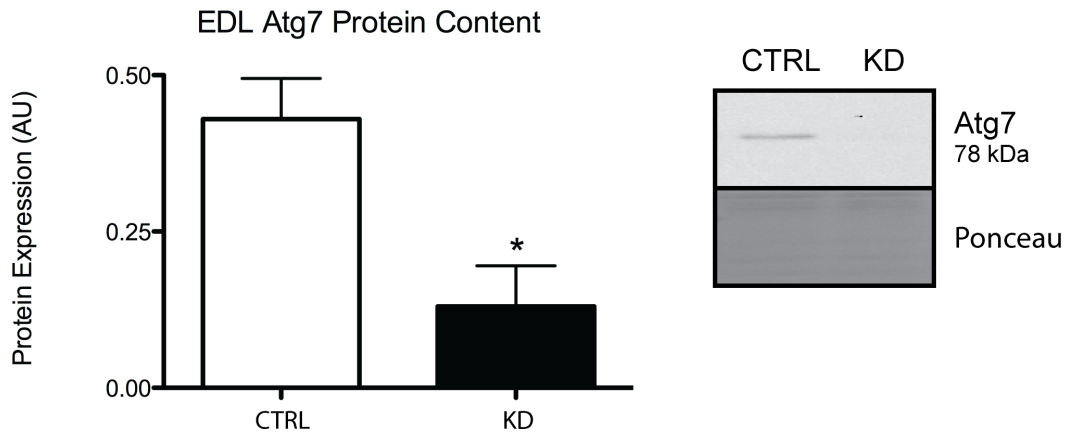


Appendix Figure 4. Skeletal muscle specificity of *Atg7* knockdown. Left ventricle (LV) samples were used to ensure that *Atg7* knockdown was limited to skeletal muscle. A: Quantification of *Atg7* protein expression in the white quadriceps (WQ), red quadriceps (RQ), and LV of control (CTRL) and *Atg7*-ablated animals (KD). B: Representative immunoblot of *Atg7* protein expression in the WQ, RQ, and LV of CTRL and KD animals. A Ponceau-stained membrane is shown as loading and transfer controls (n = 6)

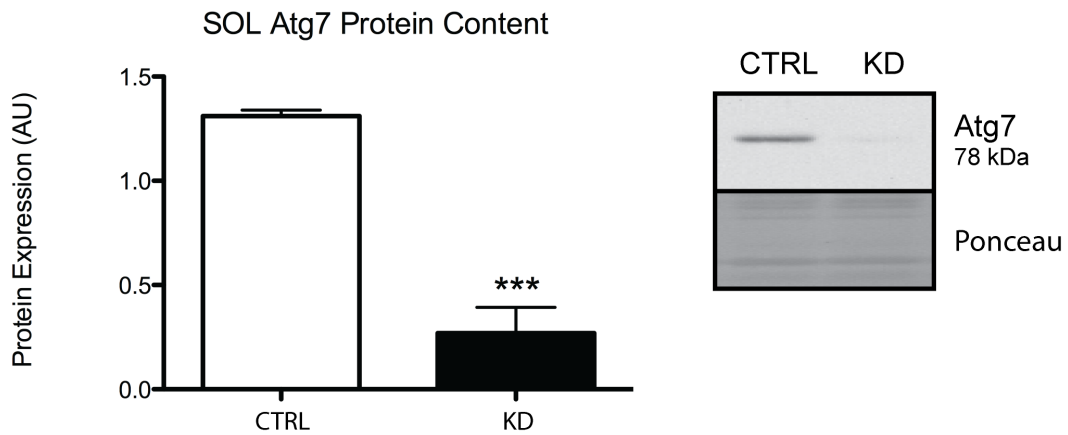


Appendix Figure 6. Use of extensor digitorum longus and soleus as representative white and red muscles. Extensor digitorum longus (EDL) and soleus (SOL) were used as white and red representative muscles, respectively, for cross-sectioning and histological examination. Representative immunoblots of mitochondrial markers in the SOL and EDL of control (CTRL) and Atg7-ablated animals (KD). Ponceau-stained membranes are shown as loading and transfer controls.

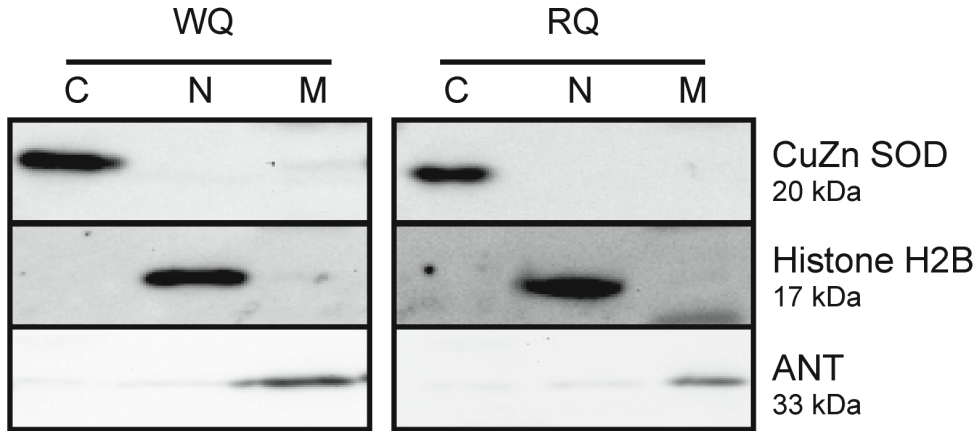
A



B



Appendix Figure 6. *Atg7* knockdown in extensor digitorum longus and soleus. Extensor digitorum longus (EDL) and soleus (SOL) were used for cross-sectioning and histological examination. A: Quantification of *Atg7* protein expression and representative immunoblots in the EDL of control (CTRL) and *Atg7*-ablated animals (KD). B: Quantification of *Atg7* protein expression and representative immunoblots in the SOL of control (CTRL) and *Atg7*-ablated animals (KD). Ponceau-stained membranes are shown as loading and transfer controls. (n = 2-4, * p<0.05, *** p<0.001).



Appendix Figure 7. Validity of the subcellular fractionation procedure. Fraction purity confirmation in white and red quadriceps. A: Representative immunoblots in white quadriceps (WQ) of CuZnSOD as a cytosolic marker, histone H2B as a nuclear marker, and ANT as a mitochondrial marker. B: Representative immunoblots in red quadriceps (RQ) of CuZn SOD, histone H2B, and ANT. Ponceau-stained membranes are shown as loading and transfer controls. Lanes are labeled C (cytosolic), N (nuclear), M (mitochondrial).